Crustal and (sub)lithospheric structure beneath the Iranian Plateau from geophysical modeling

Dissertation
zur Erlangung des akademischen Grades
eines Doktors der Naturwissenschaften (Dr. rer. nat.)
der Mathematisch-Naturwissenschaftlichen Fakultät
der Christian-Albrechts-Universität zu Kiel

vorgelegt von

Naeim Mousavi

Kiel, Juli 2019

Institut für Geowissenschaften
Abteilung Geophysik

Referent:	Prof. Dr. Jörg Ebbing
Korreferent:	Prof. Dr. Javier Fullea
Tag der mündlichen Prüfung:	11 Juli 2019
Zum Druck genehmigt:	----------
	Der Dekan

Abstract

The thesis presents a geophysical study of the Iranian Plateau and the surrounding regions in order to understand the crustal and upper mantle structure. First, I present a study on the depth to basement and magnetic crustal domains beneath the Iranian Plateau by modeling aeromagnetic and gravity data. First, field processing of the aeromagnetic data was undertaken to estimate the general characteristics of the magnetic basement. Afterwards, inverse modeling of aeromagnetic data was carried out to estimate the depth to basement. The obtained model of basement was refined using combined gravity and magnetic forward modeling. Hereby, different magnetic domains in the uppermost crust (10-20 km depths) could be identified, which influence the medium to long wavelength trends of the magnetic anomalies. Magnetic basement mapping shows that prominent shallow magnetic features are furthermore located in the volcanic areas, e.g. the Urumieh Dokhtar Magmatic Assemblage. The presence of ophiolite outcrops in SE Iran implies that shallow oceanic crust (with high magnetization) is the main source of one of the biggest magnetic anomalies in entire Iran area located north of the Makran.

Next, the 3D crustal and upper mantle structure of Iran is investigated through integrated geophysical-petrological modeling combining elevation, gravity potential field, seismic data and petrological data. While tectonics and mantle xenolith suggest composition heterogeneities in the lithospheric mantle beneath Iranian Plateau, distinct mantle compositions are also required to make the model predictions and geophysical observables compatible. For the first time, I hypothesize the 3D distribution of the mantle composition beneath the Iranian Plateau and surrounding areas. The fit of geophysical observables confirms the background Phanerozoic mantle (based on mantle xenolith of the northeast of Iran) for the entire area, in particular, in northwest and southeast of area. The results confirm a depleted Harzburgite-type composition in Zagros-Makran belt, extending to the Caspian Sea and Kopet-Dagh terrains. In contrast, the Arabian Plate and Turan platform are characterized by depleted Proterozoic Peridotite-type composition comparable to the suggested Proterozoic composition in Central Iran from xenolith samples.

In the next step, the inversion-based Moho and intra-crustal structure were modified to obtain the best fit mainly to the previous seismic studies and to some extent to geophysical modeling results. Fixing crustal effects allows us to focus on the thermochemical structure of the lithosphere and sensible mantle density. Results on the crustal modeling shows Moho boundary is deepest beneath the high Zagros Mountains (~65 km), but shallowing occurs in Central Iran and in the southeast of the Oman Sea. A relatively deep Moho boundary is modeled in the Alborz and Kopet-Dagh Mountains and at the onshore margin of the Makran subduction zone, where Moho depth reaches to ~55 km. In our preferred model, the lithosphere is ~220 km thick beneath the Persian Gulf and the Caspian Sea (Turan platform). In contrast, a comparatively thinner lithosphere is imaged beneath the high Zagros towards Central Iran (~120 km).

Sub-lithospheric sources have been disregarded in the initial model and I explore in the last step the effect of sub-lithospheric heterogeneities that might represent the remnants of a Neo-Tethys slab by adding a cold and fast body in the sub-lithosphere. With such an addition and the necessary modifications, the lithosphere thickness of central Iran is only ~100 km and thickens to ~200 km depth below the northern part of the Caspian Sea. An extreme thick

lithosphere of ~260 km is now modelled north of the Makran subduction zone in relation to the subducting slab. The best fitting (seismically and geophysically) model was selected by testing various sub-lithospheric thermochemical settings. The addition of the slab with depleted mantle composition and with appropriate thermal conditions results in a positive seismic velocity anomaly, similar to what is observed in seismic tomography models. Our (sub)lithospheric thermochemical and geometrical model structure provides synthetic seismic velocities and density anomalies comparable to model of Neo-Tethys slab break-off and the extensive Eocene magmatism in Iranian Plateau.

The geometry and depth of subducting slab varies in the study area. For instance the slab is shallower in the Makran subduction zone and can influence the density structure more than a deeper slab. For the location of slab I applied to approaches. First, I used geodynamic modeling to see what is the location of slab regarding the geodynamic scenario of the area. My geodynamic model was constrained by plate motions.

Zusammenfassung

Ich präsentiere eine Studie über die Tiefe der magnetischen Krustendomänen unter dem iranischen Plateau durch Modellierung von aeromagnetischen und Schweredaten. Zunächst wurde eine Feldverarbeitung der aeromagnetischen Daten vorgenommen, um die allgemeinen Eigenschaften des magnetischen Grundgesteins zu bestimmen. Anschließend wurde eine inverse Modellierung der aeromagnetischen Daten durchgeführt, um die Tiefe bis zum Grundgestein abzuschätzen. Das erhaltene Modell wurde mittels kombinierter Schwerkraft- und magnetischer Vorwärtsmodellierung verfeinert. Hierdurch konnte ich verschiedene magnetische Domänen in der obersten Kruste (10-20 km Tiefe) unterscheiden, die den mittleren bis langen Wellenlängenanteil der magnetischen Anomalien beeinflussen. Magnetische Kartierung zeigt, dass sich markante flache magnetische Merkmale weiterhin in den vulkanischen Gebieten befinden, z. die Urumieh Dokhtar Magmatic Assemblage. Das Vorhandensein von Ophiolit-Aufschlüssen im SE-Iran impliziert, dass die flache ozeanische Kruste (mit hoher Magnetisierung) die Hauptquelle für eine der größten magnetischen Anomalien im gesamten Iran-Gebiet nördlich des Makran ist.

Im weiteren, wird die 3D-Struktur der Kruste und des oberen Mantels des Irans durch integrierte geophysikalisch-petrologische Modellierung untersucht, die Topographie, Schwerefeld, seismische Daten und petrologische Daten kombiniert. Während Tektonik und Mantelxenolithe im lithosphärischen Mantel unter dem iranischen Plateau auf Heterogenitäten in der Zusammensetzung schließen lassen, sind auch verschiedene Mantelkompositionen erforderlich, um Modellvorhersagen und geophysikalische Beobachtungen kompatibel zu machen. Zum ersten Mal stelle ich die 3D-Verteilung der Mantelzusammensetzung unter dem iranischen Plateau und den umliegenden Gebieten in Frage. Die Anpassung geophysikalischer Beobachtungen bestätigt das Vorhandenseins eines phänozoischen Mantels (basierend auf dem Mantel-Xenolithen im Nordosten Irans) für das gesamte Gebiet, insbesondere im Nordwesten und Südosten des Gebiets. Die Ergebnisse bestätigen eine Harzburgit-artige Zusammensetzung im Zagros-Makran-Gürtel, die sich bis zum Kaspischen Meer und dem Kopet-Dagh-Terrain erstreckt. Im Gegensatz dazu sind die Arabische Platte und die Turan-Plattform durch eine abgereicherte proterozoische Peridotit-ähnliche Zusammensetzung gekennzeichnet, die mit der vorgeschlagenen proterozoischen Zusammensetzung in Zentral-Iran aus Xenolith-Proben vergleichbar ist. Im nächsten Schritt wurden die Inversionsbasierte Moho- und Intrakrustenstruktur modifiziert, um die beste Anpassung hauptsächlich an die früheren seismischen Studien und teilweise an geophysikalische Modellierungsergebnisse zu erhalten. Durch die Fixierung der Krusteneffekte konnte ich mich auf die thermochemische Struktur der Lithosphäre und die Dichte des sensiblen Mantels konzentrieren. Ergebnisse der Krustenmodellierung zeigen, dass die Moho-Grenze unterhalb des hohen Zagros-Gebirges (~ 65 km) am tiefsten ist, aber im Zentral-Iran und im Südosten des Oman-Meeres flach ist. Eine relativ tiefe Moho-Grenze wird in den Alborz- und Kopet-Dagh-Bergen und am Onshore-Rand der Makran-Subduktionszone modelliert, wo die Moho-Tiefe ~ 55 km erreicht. In dem bevorzugten Modell ist die Lithosphäre ~ 220 km dick unter dem Persischen Golf und dem Kaspischen Meer (Turan-Plattform). Im Gegensatz dazu wird eine vergleichsweise dünnere Lithosphäre unterhalb des hohen Zagros in Richtung Zentral-Iran (~ 120 km) abgebildet.

Sub-lithosphärische Quellen wurden im ursprünglichen Modell vernachlässigt, und ich untersuchen im nächsten Schritt den Effekt von sub-lithosphärischen Heterogenitäten, welche die Reste einer Neo-Tethys-Platte darstellen könnten, indem ich einen kalten und schnellen Körper in die Sub-Lithosphäre aufnehmen. Mit solch einer Struktur und den notwendigen

Modifikationen ist die lithosphärische Dicke des zentralen Iran nur ~ 100 km und verdickt sich auf ~ 200 km Tiefe unterhalb des nördlichen Teils des Kaspischen Meeres. Eine extrem dicke Lithosphäre von ~ 260 km wird jetzt nördlich der Subduktionszone Makran in Bezug auf die subduzierende Platte modelliert. Das Modell mit der besten Anpassung (seismisch und geophysikalisch) wurde ausgewählt, indem verschiedene sub-lithosphärische thermochemische Einstellungen getestet wurden. Die Ergänzung der Platte mit erschöpfter(depleted=abgereichert) Mantelzusammensetzung und mit geeigneten thermischen Bedingungen führt zu einer positiven seismischen Geschwindigkeitsanomalie, ähnlich derjenigen, die in seismischen Tomographie-Modellen beobachtet wird. Die (sub-) lithosphärische thermochemische und geometrische Modellstruktur liefert synthetische seismische Geschwindigkeiten und Dichteanomalien, die mit dem Modell des Neo-Tethys-Brammenbrechens und dem extensiven Eozän-Magmatismus im iranischen Plateau vergleichbar sind.

Contents

Chapter 1

1.1 Introduction

The area of interest in this thesis is the Iranian Plateau and its surroundings. The Iranian Plateau is located in the Alpine-Himalaya collision zone and it has been emplaced by convergence of Africa-Eurasia plates (e.g. Torsvik et al., 2010). The collision-subduction setting clearly makes an imprint on the lithospheric structure and the plate organization. The complexity of region increases with the interaction of collision and subduction processes. To give an example, in a short distance from Zagros collision, one can encounter the Makran accretionary prism which behaves differently to the adjacent tectonic province.

The main motivation for this study were:

1) The geology and tectonic of the Iranian Plateau are very dynamic and still the geophysical structure is underexplored. Further, the formation of the Iranian Plateau leads to potential reservoirs for mineral or hydrocarbon exploration.
2) I am targeting in general density. Density model incorporate implicitly in modeling of several geometrical parameters and materials in crustal, lithospheric and sub-lithospheric scales. The geophysical observables serve as testable data sets for the density model.
3) The density solution in geophysical modeling is determined with a high uncertainty. Therefore, density modeling was performed consistent with several model parameters like susceptibility, temperature, seismic velocities, and mantle composition, etc.
Several sources cause the density anomalies. In every step, the models include more details from deeper areas. Every model will be more sensible with respect geodynamic scenarios and more reliable regarding the completeness of gravity resources.
4) Most of the natural and hydrocarbon resources are buried in shallow crustal layers in particular sedimentary layers. Therefore, one motivation was to characterize the basement beneath the Iranian Plateau, which has a potential industrial application. Different parameters from top down to 410 km depth will be defined in this thesis through geophysical modeling.

The thesis is structured like this:

In chapter 2, a basement study is been shown. At the beginning of this thesis work, no robust basement model of Iran existed, even though some studies have been conducted to model the susceptibility structure of the crust (e.g. Namaki et al., 2011; Oskooi and Abedi, 2015; Abedi and Bahroudi, 2016; Mousavi and Ebbing, 2017). Later, Teknik and Ghods (2017) published the first 3D basement of the area, but their model is not capable to describe some magmatic features due to difficulties in addressing such features with spectral analysis. In addition, it is important to constrain the bottom of magnetization, which can be interpreted as the Curie isotherm depth. The bottom of magnetization in susceptibility model should coincide with the Curie isotherm depth in order to address the long wavelength magnetic anomalies (Mousavi and Ebbing, 2018). Otherwise, all information in magnetic data: i) will be projected to shallow structures by applying artificially high susceptibility to shallow structures, or ii) very deep structures which cannot be magnetized due to high temperature can be recognized as magnetization sources. The crust of Iran has been explored by a number of seismic studies (Gök et al., 2008; Gritto et al., 2008; Nasrabadi et al., 2008; Paul et al., 2006, 2010; Radjaee et al., 2010; Shad-Manaman et al.,

2011) and potential field modeling (e.g. Dehghani and Makris, 1984; Tunini et al., 2015). Interestingly, the crustal structure of Iran has been formed in a convergence regime (Berberian and King, 1981; Talebian and Jackson, 2004). This tectonic condition causes that one expects shortening in crustal architecture appearing by crustal decollement or faulting. Here, a unique aeromagnetic data set is used in combination with terrestrial gravity data which have been rarely used before for modeling the complete crustal structure. The novel data sets helped me in modeling the Iranian crust with its enigmatic geophysical heritage.

In chapter 3, the challenge of lithospheric structure beneath Iranian Plateau motivated me to review available geophysical models (e.g. Molinaro et al., 2005; Motavalli-Anbaran et al., 2011; Jiménez-Munt et al., 2012; Mousavi et al., 2016; Mousavi et al., 2017). Most of the geophysical studies on Iranian Plateau at lithosphere scale are performed by pure thermal approaches. However, the effect of composition on the density structure of the mantle should not be disregarded (e.g., Griffin et al., 2009 and references therein). Therefore, I model the 3D thermochemical structure of the lithosphere and asthenosphere (i.e. subducting slab) down to 400 km depth by an integrated geophysical-petrological methodology. Using thermochemical dependent density model allows us to constrain the model by best knowledge of mantle chemical composition. The accuracy of the density model is examined by comparing the preferred model with multiple geophysical datasets with complementary sensitivity. It is important at which depth Moho depth and Lithosphere-Asthenosphere Boundary (LAB) are set. On the one hand, seismically derived Moho depths do not always coincide with a sharp density contrast between crust and upper mantle. On the other hand, the base of the lithosphere is important because of the abrupt changes in the thermal regime and composition between the lithosphere and the rheologically weaker asthenosphere. This transition at the LAB can be defined by change in mineral oxides; but, like the Curie isotherm depth, the LAB is defined as a thermal boundary. Temperature is a key parameter to characterize the stable mineral phases with varying type of chemical compositions. The densities of the upper mantle are calculated based on the characteristics of minerals in each pressure-temperature (P-T) condition. The results from this chapter are used in the next chapter as regional constraints. As the introduction of basement structure needs a reliable setting of deep structures which is my second challenge in this thesis.

In chapter 4, a study on one of the most important tectonic features beneath the Iranian Plateau, the remnant of a slab break-off, is addressed. At crustal scale, there are some features, i.e. surface uplift, indicating the slab break-off (Molinaro et al., 2006; Mousavi et al., 2018a). This hypothesis is well supported by the subduction-related magmatism, in particular the presence of adakitic magma in Zagros, which most likely traces subduction (Omrani et al., 2008). Agard et al. (2011) describes the connection between magmatism and slab break-off, suggesting that the present-day status of the subducting slab is important for a regional model. Firstly, the subducting slab is expected to be several hundred degrees colder than the ambient asthenosphere. Secondly, slabs are to some extent denser than the adiabatic mantle that allows them to sink in dense mantle materials. In the thermochemical modeling to calculate the density of lithosphere and asthenosphere, presence of a cold and probably fertile type composition beneath lithosphere influences the main setting of the thermal structure. The different phases of rifting and Neo-Tethys obduction, subduction and slab break-off influenced the (de)formation of overriding plate in crustal and lithospheric structure (Ghasemi and Talbot, 2006). However, the knowledge of the Iranian lithosphere is limited to seismological studies with varying resolutions and uncertainties

(Bijwaard et al., 1998; Villaseñor et al., 2001; Maggi and Priestley, 2005; Kaviani et al., 2007; Shad-Manaman and Shomali, 2010, Vergés et al., 2011; Mohammadi et al., 2013). Regarding the discrepancies between available regional and global tomography models, the deep structure beneath the Iranian Plateau is underestimated. These uncertainties in asthenosphere are migrated to the interpretation of lithospheric structure.

Last but not least, chapter 5 showed how the presence of a slab beneath lithosphere can be modelled by using geophysical observations. The basic geometry of the slab is based on a seismic tomography model. But, for initial temperature and geometry, I applied geodynamic modeling. Hereby, my geodynamic models are linked to plate motions (Mousavi et al., 2018b). Consequently, the slab deformation will be resulted. The geodynamic modeling results gave me an initial idea of how to set-up the geophysical mode, i.e. density, temperature and geometry of the slab. In the second step, geophysical modeling allowed to have a detailed lithospheric structure beneath the Makran subduction zone.

Contributions

Chapter 2 “Basement characterization and crustal structure beneath the Arabia–Eurasia collision (Iran): a combined gravity and magnetic study” is my own contribution and idea. I did all calculations and I created all figures. Jörg Ebbing assisted with writing the text. The manuscript has been published in 2018 in Tectonophysics by me and Jörg Ebbing.

Chapter 3 “3D crustal and lithospheric mantle structure of the Iranian Plateau from geophysical-petrological modeling” is my own contribution and idea. I did all calculations and I created all figures. Javier Fullea and Jörg Ebbing assisted with smoothing English of this chapter.

Chapter 4 “Integrated geophysical-petrological modeling of sub-lithospheric structure due to Neo-Tethys slab break-off” is my own contribution and idea. I implemented additional assumption to model in chapter 3. I did all calculations and I created all figures. Javier Fullea and Jörg Ebbing assisted with smoothing English of this chapter.

Chapter 5 “The structure of crust and upper mantle beneath the Makran subduction zone” is my own contribution and idea. I implemented the results from geodynamic modeling to geophysical modeling. I did all calculations and I created all figures and the text.

Chapter 2:
Basement characterization and crustal structure beneath the Arabia–Eurasia collision (Iran): a combined gravity and magnetic study

2.1 Introduction

The exact buildup of the crustal structure of the Iranian Plateau (Fig. 2.1) is still under discussion. A convergent tectonic regime has been proposed (Vernant et al., 2004), but due to complexity of crustal deformations under active shortening (Talebian and Jackson, 2004), the basement characteristics is less well known. Despite efforts to characterize the sedimentary basins with passive seismic profiles (e.g. Tavakoli-shirazi, 2012), there is still no basement model that also addresses distribution of igneous rocks. Recent studies on different Iranian areas by Namaki et al. (2011), Oskooi and Abedi (2015) and Abedi and Bahroudi (2016) interpreted the local properties of the magnetic crust beneath Iran. Teknik and Ghods (2017) established a map of the magnetic basement that shows a number of several well-known basins in Iran. However, large thicknesses of sedimentary cover (exceeding 15 km) and internal evaporitic events are some factors, which introduce uncertainties into their interpretation. For example, the study by Teknik and Ghods (2017) did not show the expected effects of magnetic anomaly highs in the Makran and Kopeh Dagh structural units on the basement map (Fig. 2.1). Furthermore, there are some disagreements between the map and the distribution of volcanic rocks outcrops (Pazirandeh, 1973). These problems motivated us to apply an integrated inverse and forward modeling approach as inversion make a projection of data characteristics into the basement map and forward scheme gives us more flexibility to examine any hypothetical susceptibility distribution or structural model. Bearing in mind, the basement structure we discuss here refers mainly to the magnetic basement which is refined by combined modeling of gravity data because: I) the basement structure is defined based on geophysical modeling mainly using magnetic data and II) the magnetic basement can represent the depth to sedimentary thickness to a large extent compared to uncertain definition by gravity data modeling. The latter should be constrained by seismic studies simultaneously.

We expect by mapping of the basement units to model the known sedimentary basins and to improve the interpretation of some poorly known sedimentary basins. Furthermore, our goal is to define intra crustal domains from the surface down to the bottom of the magnetic sources known as Curie temperature. For the original motivation see the chapter 1 of this thesis.

In this study, we apply inverse and forward modeling of magnetic and gravity data to compute the depth to the top of magnetization. We modify the first estimate of the topography of the base of sedimentary covers (referred to basement) obtained from inversion, using combined modeling of aeromagnetic and terrestrial gravity data over Iran. Our forward model is built using a trial and error method in which the susceptibilities and densities to different materials and depths and thicknesses to various layers are defined. We also use the information given by the aeromagnetic field processing, like the higher probability of existence of deep or shallow sources obtained from filtering of magnetic data, to interpret short to medium wavelengths in magnetic anomalies. We will show that using Curie depth instead of Moho depth can reduce the misfit of data in inversion. During the forward modeling, the geometry of the deep crustal structures is not modified except for the top of the basement. In the step, assuming a fixed geometry for the entire model, we examined the susceptibility structure of middle crust (range of 10-20 km) based on its regional effect on calculated magnetic anomalies. Distinguishing between magnetic intra-crustal

domains gives a complementary interpretation to crustal materials after density contrast figures the structural background. More information on crustal rheology and evolution can be extracted using this combined density and susceptibility structures. A better understanding of the magnetic domains is important to understand the buildup of the Iranian Plateau and to decipher the complex interactions during its tectonic evolution. As magnetic data is sensitive to susceptibility of rocks mainly igneous rocks which have different tectonic background i.e. rate of lithospheric cooling and subduction history. As, this information is not reflected in only density structure.

2.2 Tectonic and geologic setting

The Iranian-Tibetan Plateau convergence with the Eurasian and Arabian plates along the Alpine-Himalayan orogeny has resulted in various elements like topographic evolution of Zagros orogeny (Austermann and Iaffaldano, 2013) and deformation of the sedimentary basins (Talebian and Jackson, 2004). The orogeny is subject to continental folding and strike slip movements, for example, the fold and thrust belts in the Zagros Mountains as one of the most seismically active thrusts in the world (e.g. Berberian, 1995). Significantly, the Zagros Mountains, which overlie the collision zone between Arabian and Iranian plates, divides the region into different parts as reflected in seismicity and magmatism (Ghasemi and Talbot, 2006).

Seismicity in the Zagros generally correlates with surface faulting and the boundary between the sedimentary cover and basements rock (~ 10 to 20 km depth) and is not associated with active subduction, as might be expected (Talebian and Jackson, 2004). A compilation of stratigraphic information and structural regimes places important local constraints on modeling of the sedimentary cover. In the following paragraphs, we make a short literature review, firstly, on the structural units of the Iranian Plateau and, secondly, on the knowledge of the sedimentary basins in Iran which is used for validation of our modeling results.

The main Zagros thrust (MZT) is located at the boundary of the Zagros fold and thrust belt (ZFTB) and the Sanandaj–Sirjan zone (SSZ) (Fig. 2.1). The main Zagros Thrust is known as the main margin of the Arabian and Iranian plates along which shortening occurs (e.g. Berberian, 1995). The Sanandaj–Sirjan zone, adjacent to the Zagros fold and thrust belt, is located in the southernmost part of the Iranian Plateau, assuming the main Zagros thrust was the continental boundary before the closure of Neo-Tethys ocean in Permian (e.g. Ghasemi and Talbot, 2006). Ghasemi and Talbot, (2006) also addressed the Precambrian metamorphism in the Sanandaj–Sirjan zone (SSZ), which is related to lithospheric scale tectonics and geochronology. North of the SSZ, the Urumieh Dokhtar Magmatic Assemblage (UDMA) is separated from the Sanandaj–Sirjan zone metamorphic rocks to the south by a faulting system (Fig. 2.1). The magmatism of UDMA has been interpreted as being related to slab break-off (Ghassemi and Talbot, 2006). Surrounded by mountain chains (Zagros, Alborz and Kopeh Dagh), the Iranian Plateau, on average, is a flat area of Central Iran.

Northeastward plate movement of Arabia to Eurasia results in opposing deformation features in the sedimentary cover: SW-NE oriented decollement and NW-SE oriented thrust features (Jackson, 1981; Talebian and Jackson, 2004; Vergés et al., 2011). The sparse ophiolite outcrops in Urumieh Dokhtar Magmatic Assemblage link the intrusive basalt pillow to mid Cretaceous

ocean crust (Ghassemi and Talbot, 2006). They suggest that these likely appeared at the surface through obduction of the oceanic slab or from a compressive regime of overriding plates.

In the eastern part of the Zagros Mountains, the tectonic architecture of the central Iran unit is less well known compared to the Zagros Mountains. The existence of Precambrian to Quaternary rocks, volcanism and complicated responses to shortening highlight the complexity of the unit and different interpretations regarding the boundaries of this unit. Moreover, the extent of sedimentary basins (i.e. Dasht-e-Lut) in this zone remains under debate (Stöcklin, 1968; Takin, 1972; Nabavi, 1976; Aghanabati, 2004; Nissen et al., 2011; Ghorbani, 2013).

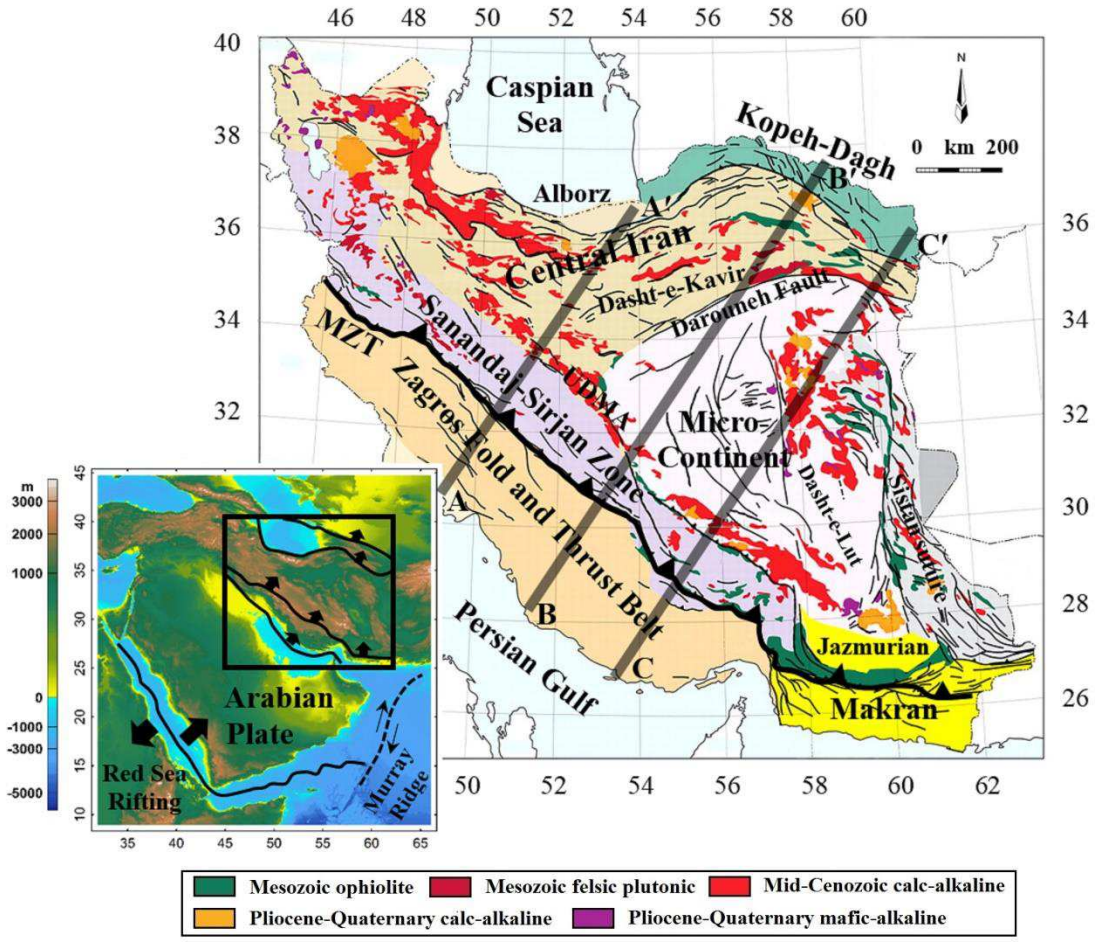

Fig. 2.1 Structural geology map of Iran containing all major faults (modified after National Geoscience Database of Iran,) and location of the three 2D profiles shown in Figs. 2.11, 2.12 and 2.13. MZT: Main Zagros Thrust and UDMA: Urumieh Dokhtar Magmatic Assemblage.

The Paleozoic sedimentary cover in the Persian Gulf is approximated to ~7 km, and increases toward Zagros fold and thrust belt where it reaches a maximum of 16 km (Hatzfeld et al., 2003; Molinaro et al., 2005; Morley et al., 2009). In the north, towards central Iran, stratigraphic studies indicate sedimentary sequences varying between Precambrian and late Cenozoic (McCall, 1997; Allen et al., 2003). The sedimentary basin in the Alborz Mts. reaches up to ~15

km thickness (Guest et al., 2006; Rezaeian et al., 2012). The Meso-Cenozoic sedimentary rocks in the Kopeh Dagh are related to the late Alpine orogeny, reflected in ~10 km sedimentary sequences in the Zagros foreland basin (Davoudzadeh and Schmidt, 1984; Brunet et al., 2003). The Kopeh Dagh lacks notable volcanic activity, although it is highly active in responding to shortening by faulting (Allen et al., 2003).

The Dasht-e-Kavir (great salt desert) basin, which is surrounded by the Alborz Mountains, Kopeh Dagh Mountains and the Dasht-e-Lut, are flat areas with almost no local topography for up to ~800 km (Fig. 2.1). The Dasht-e-Kavir basin is covered by 5-7 km thick sequence of tertiary gypsum, limestone and salt (Morley et al., 2009). In the southeast, the Jazmurian is other large extended basin (Fig. 2.1). The presence of magnetic interbedding in Makran is still debated, as is the thickness of the sedimentary sequences in the Makran accretionary prism (Shahabpour, 2010). To the south, in the Oman Sea, a Cenozoic sedimentary cover of up to 6 km thick is overlying oceanic crust (White and Louden, 1982).

2.3 Data sets

2.3.1 Gravity and magnetic data

Aeromagnetic data (Fig. 2.2a) are available from a compilation by the Geological Survey of Iran (GSI) and Aero-service Company (USA) between 1974 and 1977. The line spacing of the aeromagnetic campaign was ~7.5 km, mostly at the height of 500–1000 m above ground or similarly barometric elevation between 1000-3600 m (Yousefi and Friedberg, 1977). The data set does not cover the entire area seen by the limited coverage of the Zagros fold and thrust belt.

The observed magnetic data over the study area indicates that the major magnetic anomalies are along the strike of structural units (i.e. UDMA) (Fig. 2.1). From the map, it seems that boundaries of tectonic divisions correlate fairly well with magnetic anomaly strikes (Figs. 2.2a and 2.1).

The power spectrum of the magnetic anomaly is shown in Fig. 2.3. The cut-off wavelength for separating the regional and residual parts is selected (in a trial and error process and based on power spectrum plot) to be 70 km. Upward continuation to the height of 4 km also helps to smooth short wavelength features with high amplitudes. Before any further data processing, we applied a pole-reduction to aeromagnetic anomaly. Based on the IGRF in 1975, the year of acquisition, the average inclination, declination and total intensity are taken to be 50°, 4° and 45000 nT, respectively.

To compute the Bouguer anomaly over the Iran, we applied the terrestrial gravity database of the Bureau Gravimétrique International (BGI, France). The gravimetry survey over the whole country has been performed mostly by the Topographic Agency of Mapping Center (Iran) between 1960 and 1970, and partially by the University of Tehran and the BGI. In total, 8226 data point are available, which a data point density is ~1/20 km^2 for entire Iran.

a)

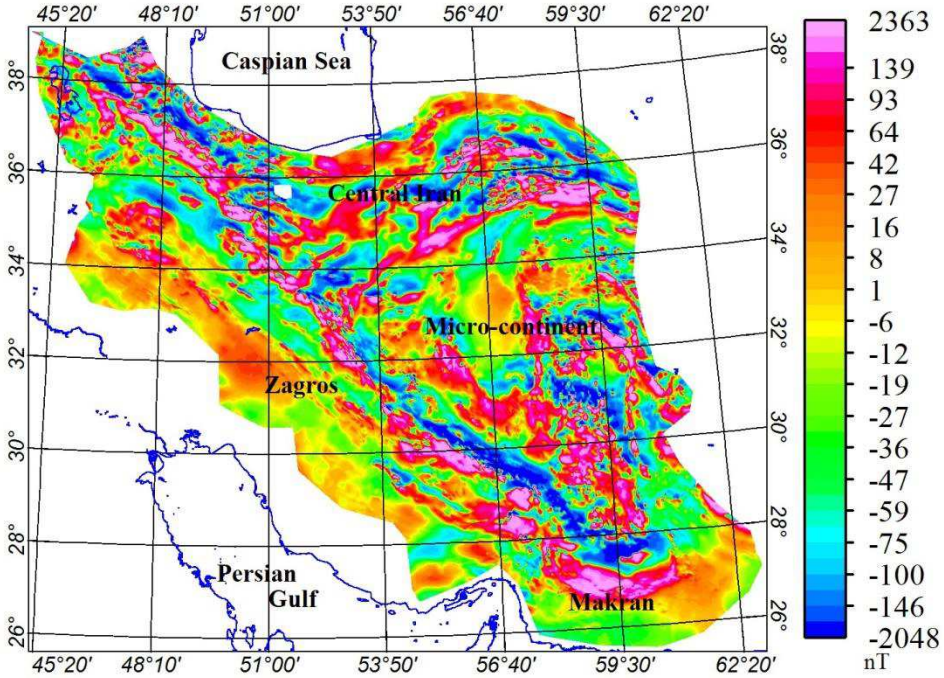

b)

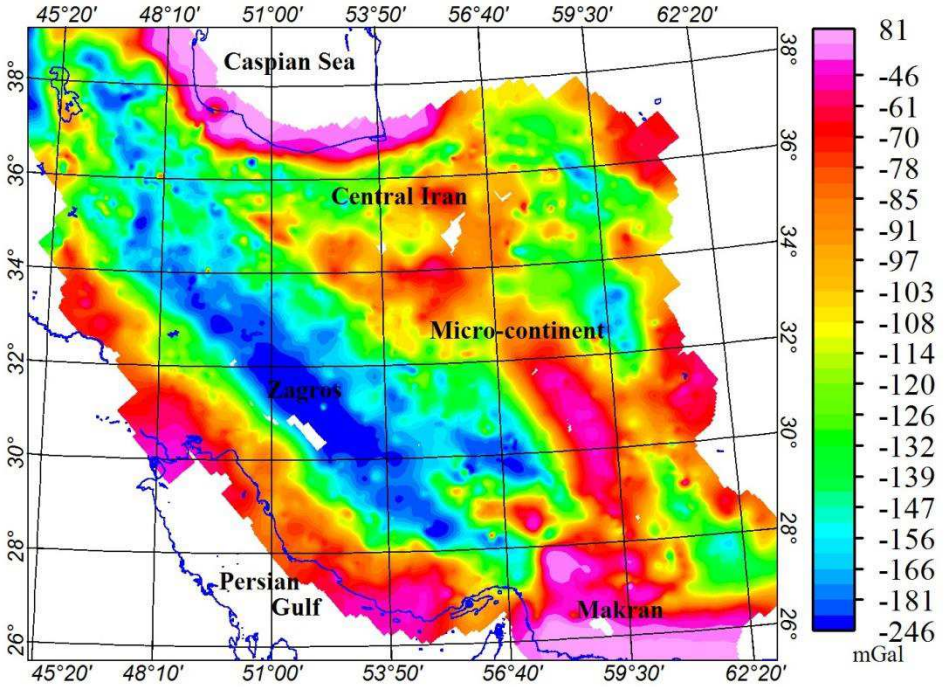

Fig. 2.2 a) Aeromagnetic anomaly map. Data were acquired at height of ~1 km with line spacing of ~7.5 km. No data is available for the entire ZTFB (Fig. 2.1). b) Bouguer anomaly map from compilation of terrestrial data points and after implementing Bouguer slab and topographic reductions.

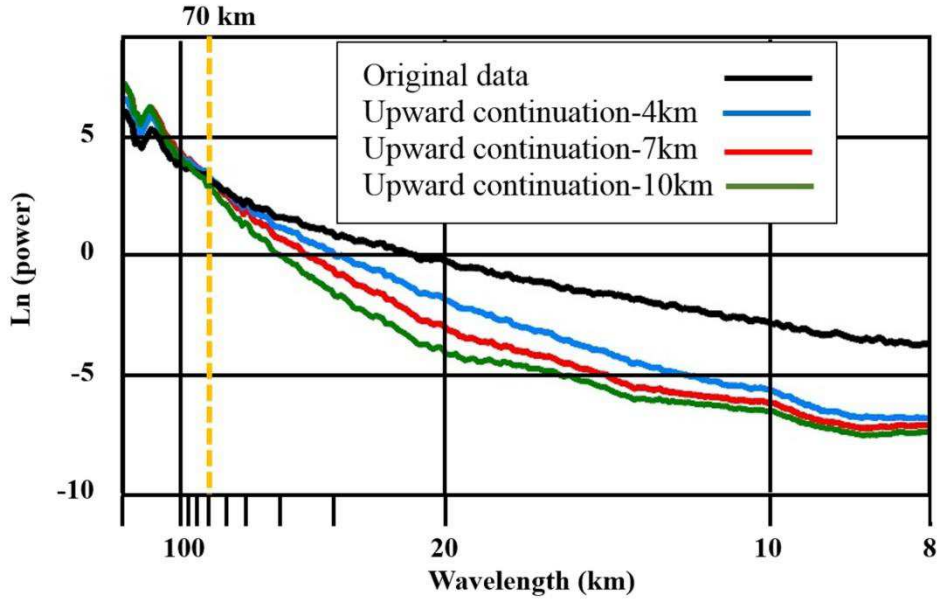

Fig. 2.3 The power spectrum of original aeromagnetic data with initial resolution after reduction to pole. The medium wavelength features between 10 and 70 km have different energy levels after different upward continuation at different altitudes (i.e. 4, 7 and 10 km). To note that the horizontal axis is a mixed log-linear scale.

The complete Bouguer anomaly was computed from the free air gravity data (Fig. 2.2b) using a reduction density of 2670 kg/m^3 and terrain correction was performed for high altitude areas. For terrain correction, we used the method by Holzrichter (2013) which is based on a mesh adoptive triangulating of topographic surfaces (polyhedral representation). The Bouguer anomaly shows minimum values ~−240 mGal[1] parallel to the Zagros Mountains (Fig. 2.1). The gravity field rises up to values between −120 and −70 mGal in central Iran and at the Dasht-e-Lut basin, suggesting crustal thinning (Shad-Manaman et al., 2011; Jiménez-Munt et al., 2012). A moderate decrease up to -100 mGal occurs in the Alborz range. The Bouguer anomaly in the Zagros fold and thrust belt (ZFTB, Fig. 2.1) is negative, as near the Persian Gulf and it decreases in Makran.

2.3.2 Physical parameters

Information for magnetic susceptibility of rocks is limited to some paleomagnetic studies (Aubourg and Robion, 2002) which is hardly comparable to the bulk susceptibility in the crust. However, we mainly refer to global estimates for bulk susceptibilities of crustal material (e.g. Clark and Emerson, 1991). In UDMA and its surrounding, magnetization is mostly related to the presence of igneous rocks, contrastingly, high amplitude magnetic anomalies are seen in locations with no evidence of igneous rock in the Makran and Kopeh Dagh area (Fig. 2.1). Other values are estimated from 2D and 3D susceptibility distribution using inversion of aeromagnetic data which is ~0.1 SI in Makran (e.g. Namaki et al., 2011; Abedi and Bahroudi, 2016) and up to ~0.5 SI in Zagros orogeny (Oskooi and Abedi, 2015).
Analysis of composite magnetic fabrics in the western Makran accretionary prism allows Aubourg and Robion (2002) to define the average susceptibility in its SW part. The samples are

[1] 1 mGal= 10^{-5} ms^{-2}

composed of continental rocks, greigite, magnetites from alteration of volcanic and colored mélange, where magnetic susceptibility ranges change from 0.0001 to 0.002 SI. Based on evaluation of ferromagnetic properties and thermal analysis of samples in SE Iran, the minerals change from greigite to magnetite at 330°C. This leads to a magnetic susceptibility variation of 50-100 µSI. In addition, Aubourg et al. (2010) studied 25 sites in the southwestern part of ZFTB (53°E, 29°N) and provided the mean bulk magnetic susceptibility of these samples. The compilation of magnetic information from mineralogy of cored rock represents a measure of bulk magnetic susceptibility between 10 - 670 µSI (Aubourg et al., 2010; Rochette et al., 1992).

Table 2.1. The model parameters including densities and susceptibilities of different rocks. Key crustal surfaces distinguish the major types of sedimentary successions, volcanic rocks, metamorphic rocks, upper, middle and lower crust (magnetic and non-magnetic). Upper mantle is divided into magnetic and non-magnetic, considering Curie depth variation, and lighter and denser domains due to the effect of thermal-compositional heterogeneities in upper mantle.

Row	Name of material	Susceptibility (µSI)	Density kg/m^3
1	Cenozoic rocks of central Iran	1	2550
2	Mesozoic rocks of ZFTB	1	2650
3	Paleozoic rocks of Iranian Plateau	10	2700
4	Igneous rocks	5000	2750
5	Metamorphic-mélange (SSZ)	3000	2830
6	Upper crust of micro-continent	2800	2830
7	Upper crust of central Iran	100	2850
8	Upper crust of ZFTB	1000	2850
9	Middle crust	100	2900
10	Magnetic lower crust	10	2950
11	Non-magnetic Lower crust	0	3050
12	Magnetic upper mantle (ZFTB)	10	3200
13	Non-magnetic upper mantle of ZFTB	0	3220
14	Upper mantle of central Iran and micro-continent	0	3150

The sedimentary units vary in density and have a negligible magnetization. The change to the bulk density in sedimentary rocks can be associated with different rock materials or compaction effects. For the scope of this study, the sedimentary thickness is considered equivalent to the depth to the top of magnetization. The sedimentary cover is composed of a sequence of sediments starting from Cambrian to present (e.g. Tavakoli-shirazi, 2012). Igneous and

metamorphic rocks are located below the sedimentary cover (or at the base of lighter sedimentary covers) with the exceptions of volcanic outcrops. The model parameters are summarized in Table 2.1 and more details about geometry of the model and potential field characteristics can be found in the text body.

2.3.3 Constraining data for inverse and forward modeling

For a starting model, we estimate the depth to Moho and the base of lithosphere (Lithosphere-Asthenosphere Boundary) by inversion of elevation and geoid anomaly data combined with thermal analysis. The applied method has been used previously in the Arabia-Eurasia collision zone (Jiménez-Munt et al., 2012) and is originally outlined in Fullea et al. (2007). The Curie point proxy (580°C isotherm) is extracted from the obtained thermal model of lithosphere using combined inversion of geoid and elevation data. The assumed Curie depth is very likely correlated with the general shape of lithosphere-asthenosphere boundary beneath the Iranian Plateau (Mousavi et al., 2016; Jiménez-Munt et al., 2012; their Fig. 2.4b).

a)

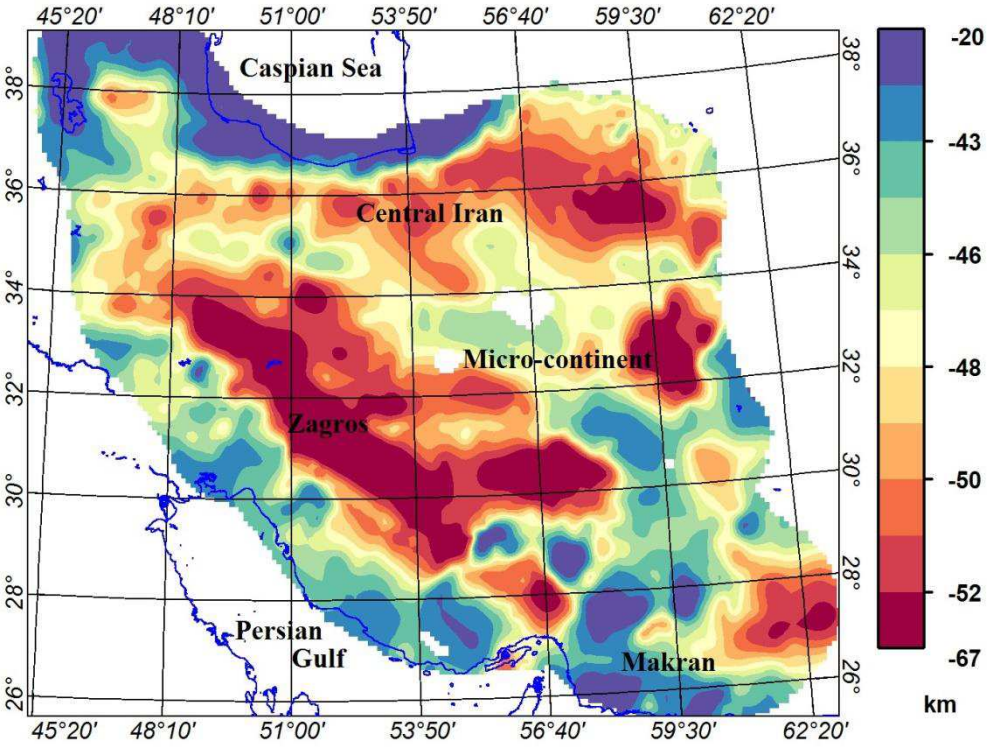

b)

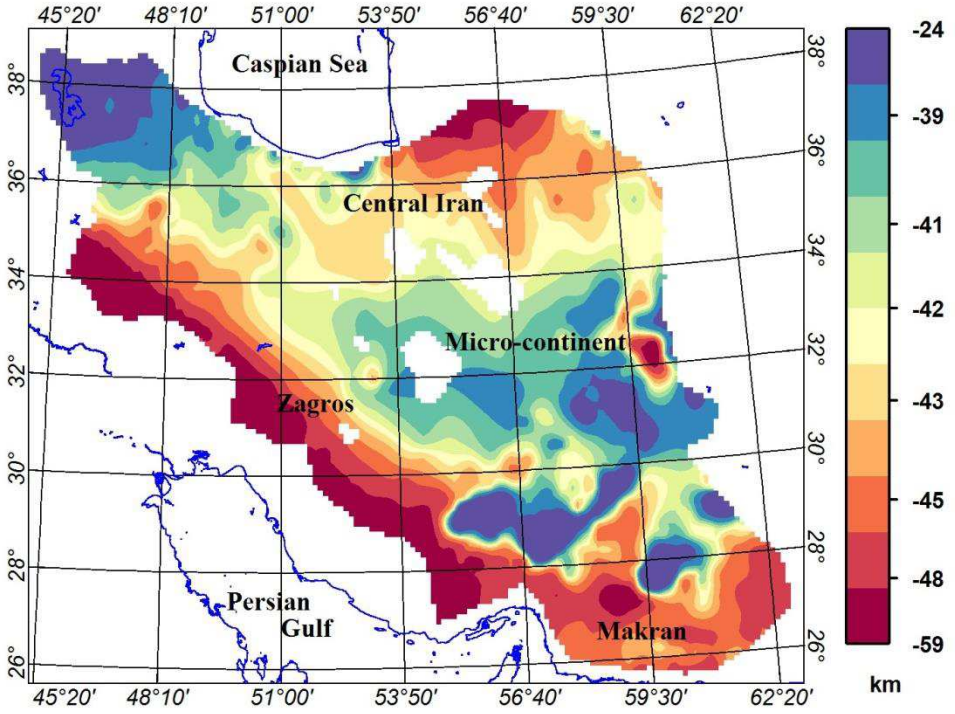

Fig. 2.4 a) Moho depth with depth varying 35-60 km (see chapter 3). b) Curie depth isotherm of 580 ºC (see chapter 3). The map of the Curie depth shows upwelling in Central and NW of Iran and deepening in the south-west of Zagros, Kopeh Dagh and Makran to ~ 75 km depth.

2.4 Field processing

Different wavelength features in magnetic anomaly data are assumed to reflect sources at different depths. Filtering of high and low wavelengths of the magnetic field is applied to distinguish the magnetic sources of varying depths. Afterwards, a tilt-derivative (TDR) filter is used to approximate the location of magnetic sources (i.e. volcanic intrusions, metamorphic rocks structures and widespread ophiolite belts).

2.4.1 Aeromagnetic data

The magnetic anomaly mainly reflects the basement topography and intra-basement sources (i.e. volcanic-plutonic rocks, metamorphic complexes and oceanic crust). Shallow local intrusive igneous rocks are characterized by high magnetic properties, large amplitude and short-wavelength anomalies (Figs. 2.1 and 2.2a).

Low-pass filtering of the magnetic anomaly is expected to enhance upper to mid-crustal level sources (Fig. 2.5a). However, the strong anomalies of volcanic and metamorphic rocks often mask deeper sources. Fig. 2.5b shows the short-wavelength part of the magnetic anomaly, which mainly reflects shallow structures. Using high- and low-pass filtering, we decide on the location of shallow and deep structures to reproduce the magnetic anomalies. The low-pass filtered data

show regional anomalies mainly located in Zagros fold and thrust belt (ZFTB), Kopeh Dagh and Iranian micro-continent (Figs. 2.1 and 2.5a). According to the definition of TDR, the tilt derivatives are mostly positive over a source and negative elsewhere (Fig. 2.5c)

In theory, the pseudo gravity map should enhance the main regional magnetic anomalies. For calculating pseudo gravity map we use the available toolbox MAGMAP (Geosoft, 2015). From spatial correlation of pseudo gravity and Bouguer anomalies (Figs. 2.5d and 2.2b), we define the source location for both aeromagnetic and gravity fields. The weak correlation of pseudo gravity and Bouguer anomalies indicates, in general, varying characteristics of density and susceptibility structures beneath Iran. Comparison of the pseudo gravity map with the Bouguer anomaly suggests deeper density anomaly sources for the gravity field except for features like the micro-continent and Jazmurian depression (Fig. 2.1).

a)

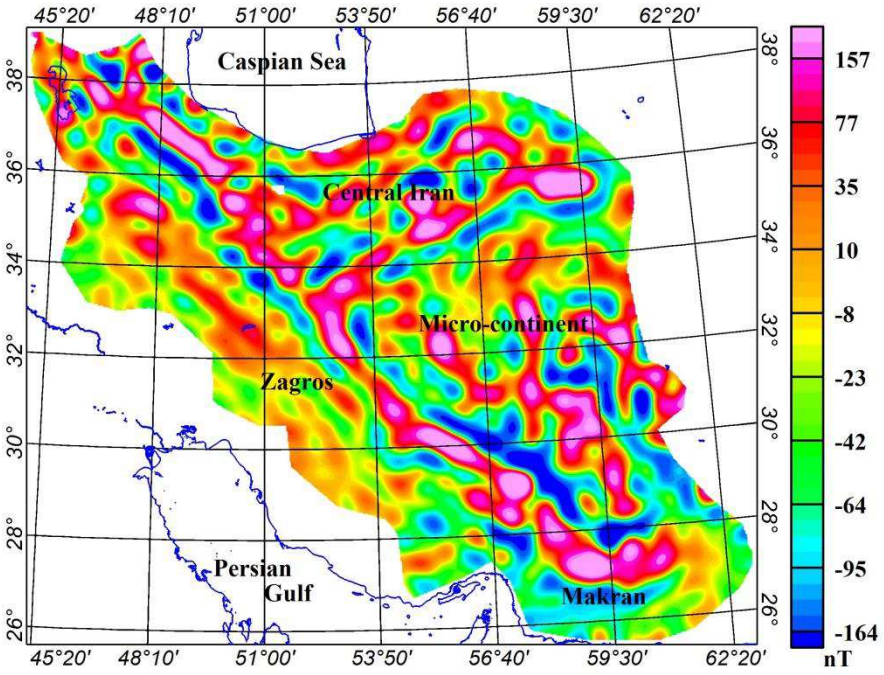
45°20'
48°10'
51°00'
53°50'
56°40'
59°30'
62°20'
38°
36°
34°
32°
30°
28°
26°
Caspian Sea
Central Iran
Micro-continent
Zagros
Persian
Gulf
Makran
157
77
35
10
-8
-23
-42
-64
-95
-164
nT

b)

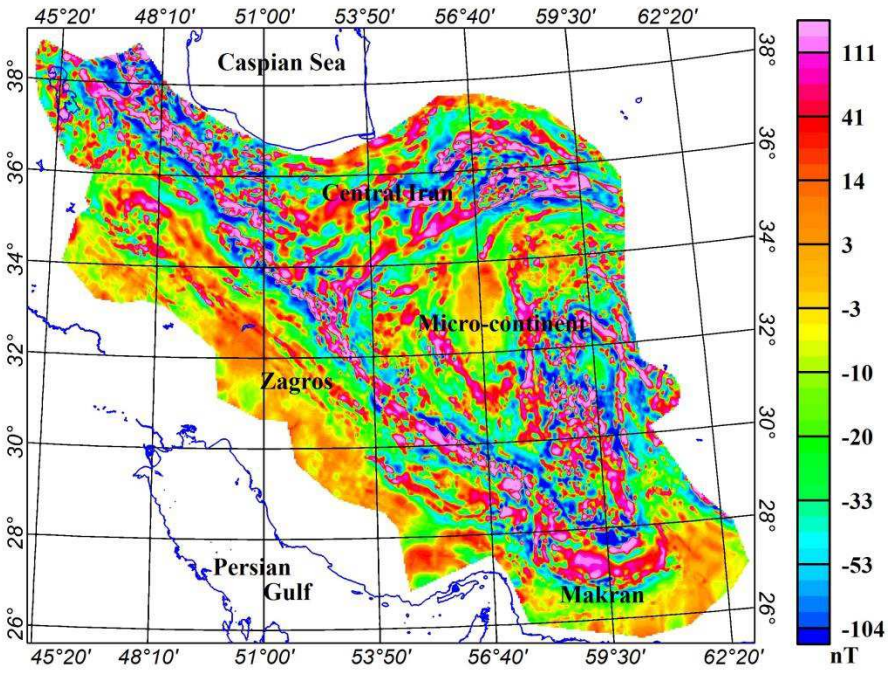
45°20'
48°10'
51°00'
53°50'
56°40'
59°30'
62°20'
38°
36°
34°
32°
30°
28°
26°
Caspian Sea
Central Iran
Micro-continent
Zagros
Persian
Gulf
Makran
111
41
14
3
-3
-10
-20
-33
-53
-104
nT

c)

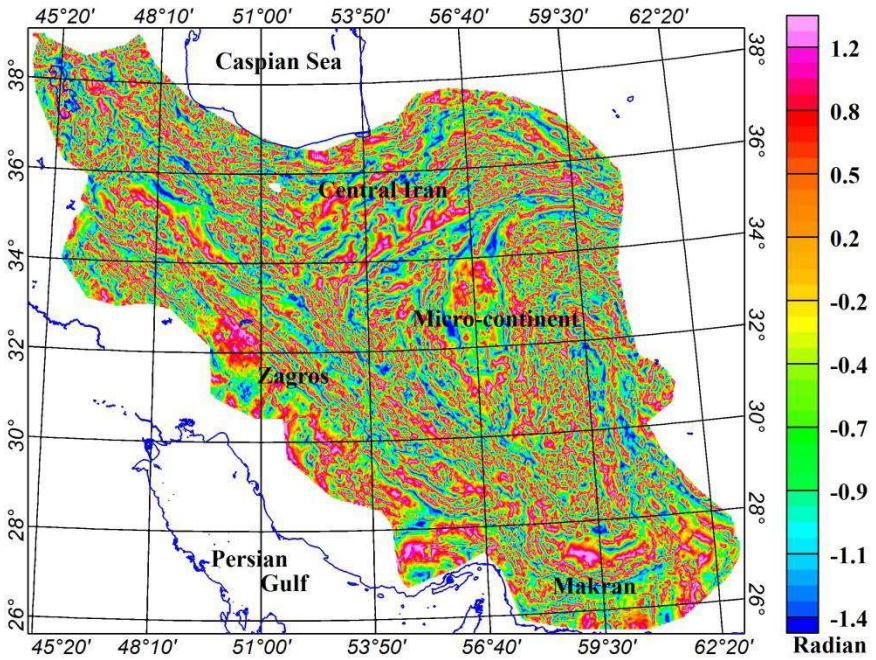
45°20′
48°10′
51°00′
53°50′
56°40′
59°30′
62°20′
38°
36°
34°
32°
30°
28°
26°
Caspian Sea
Central Iran
Micro-continent
Zagros
Persian
Gulf
Makran
1.2
0.8
0.5
0.2
-0.2
-0.4
-0.7
-0.9
-1.1
-1.4
Radian

d)

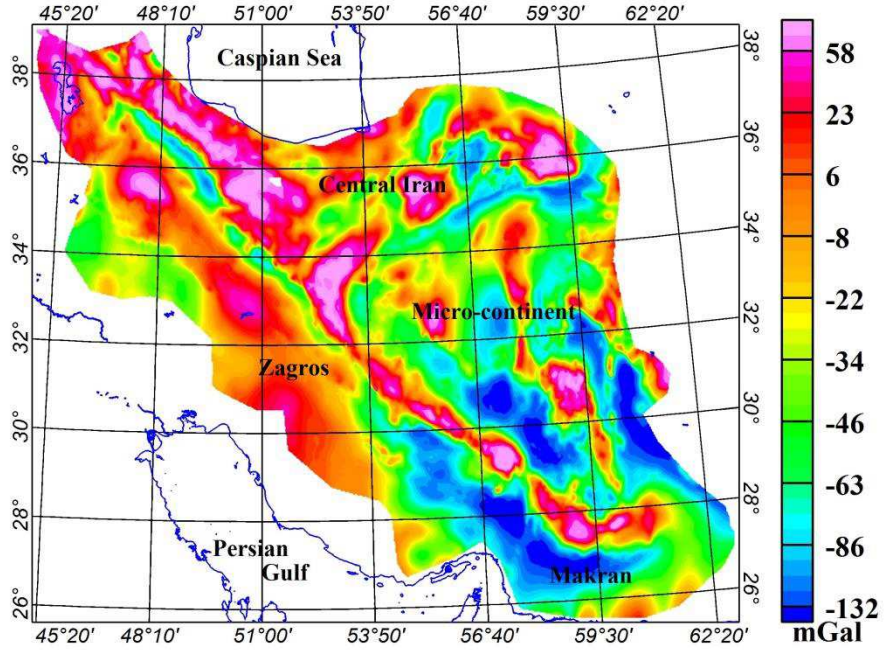
45°20′
48°10′
51°00′
53°50′
56°40′
59°30′
62°20′
38°
36°
34°
32°
30°
28°
26°
Caspian Sea
Central Iran
Micro-continent
Zagros
Persian
Gulf
Makran
58
23
6
-8
-22
-34
-46
-63
-86
-132
mGal

Fig. 2.5 The results of magnetic field analysis, a) low pass filtered magnetic anomaly using cut-off wavelength of 70 km for filtering, b) high pass (Butterworth) filtering using cut-off wavelength of 70 km, c) tilt-derivative map of aeromagnetic data, d) pseudo gravity anomaly resulted from aeromagnetic field. The patterns seen in low and high -pass filtered anomalies associate with long and short wavelength features, respectively. Tilt derivative map depicts the main magnetic lineaments which coincide to a large extent to the main faults over the area. Pseudo gravity map highlights the susceptibility sources. A weak correlation between Pseudo gravity and Bouguer anomalies indicates that magnetic anomaly has different sources from ones produces the gravity anomaly.

2.5 Methodology: Inverse and forward modeling

2.5.1 Structural and susceptibility inversion

The initial magnetic structure of the Iranian crust is modeled using GMSYS-3D (Popowski et al., 2006) by defining a few layers with various susceptibility contrasts. GMSYS-3D performs the calculation for the inversion routine in the wavenumber domain based on the Parker algorithm (Parker, 1972).

It is assumed that the model is composed of a series of vertical prisms with finite extension that have dimensions of 8×8 km (an estimate to flight line spacing of ~7.5 km of aeromagnetic survey) in our model. Initially, the inversion is carried out in term of definition of basement structure with the assumption of constant susceptibility for the whole crust.

2.5.2 Forward modeling

For the forward modeling, we use the IGMAS+ software (Interactive Gravity and Magnetic Application System, e.g. Götze and Lahmeyer, 1988; Schmidt and Götze, 1999; Götze, 2015; Alvers et al., 2014; Alvers et al., 2015). IGMAS+ approaches 3D modeling of geological structures with triangulated surfaces to approximate the complex shape. Each resulting polyhedron is described by a constant density and susceptibility and all polyhedrons of the same petrophysical properties describe a body. For defining the geometry of a body, we use parallel cross sections at a spacing of ~20 km (Fig. 2.10c).

The initial basement geometry is taken from inverse modeling and is modified using a trial and error process and a control of the results with the qualitative analysis predictions (section 4). The model parameters are density and susceptibility distributions (Table 2.1). Integrating gravity data with magnetic modeling allows the geometry of shallow structures to be better defined since susceptibility contrast of some layers beneath Iran are minor, unlike their density contrast (In the model setting, from top, sedimentary cover, igneous rocks, upper, middle and lower crust are our layered model sequences). Deep magnetization is supposed to be limited by 580°C Curie isotherm depth, which is the limit where rocks lose their ability to keep the ferromagnetic property.

2.6 Modeling results

2.6.1 3D inversion

Our initial model is composed of three layers including a non-magnetic layer representing sedimentary cover, magnetic crust down to Moho (varying between 30-65 km), and non-magnetic upper mantle beneath. The starting model of basement for structural inversion is a constant surface at depth of 1 km, which allows the outcrops to be easily revealed after inverse calculations. In the first and second models, the whole crust has a constant susceptibility (0.01 SI or 850 μcgs). Model 1 and 2 differs only using Moho (model 1) or Curie (model 2) depths as the bottom of the model. Fig. 2.6 shows that these models fail to fit the regional magnetic anomalies. The use of the Curie depth instead of the Moho depth with otherwise similar model geometry partially improves the fit of model to the data. Therefore, the use of the independently derived Curie depth (Fig. 2.4b) is an important prerequisite before addressing the depth to the magnetic basement.

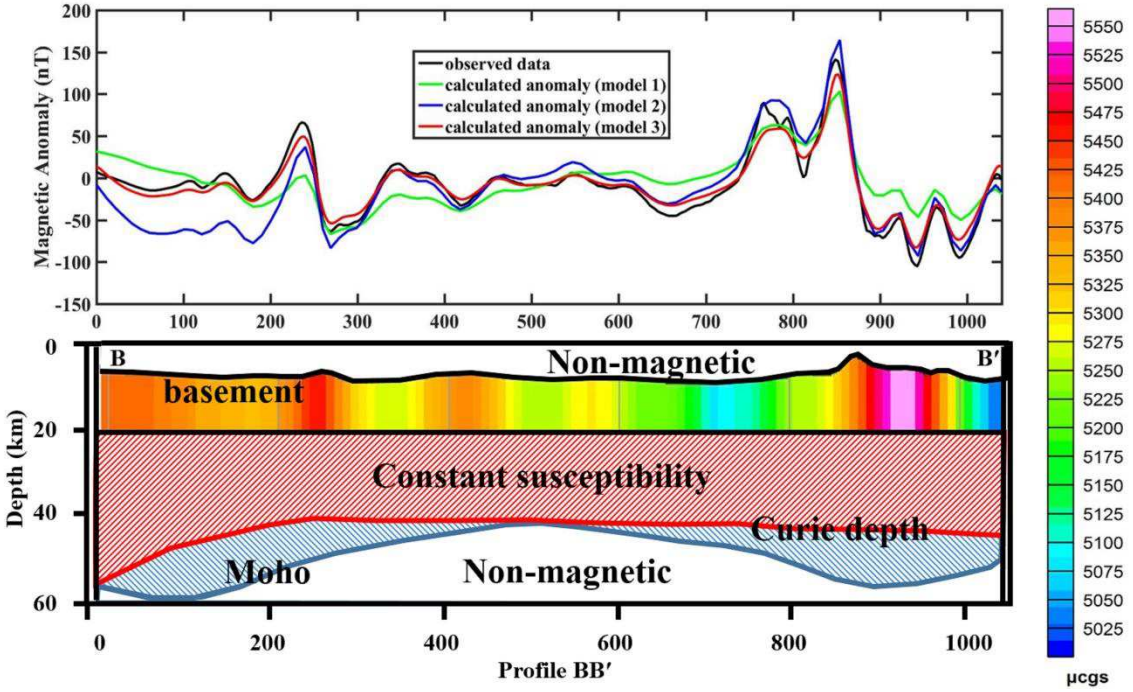

Fig. 2.6 Inversion calculations and cross section of inverted models along profile BB′ (see location in Fig. 2.1). Top panel) Calculated and observed magnetic anomalies for models 1 to 3 (see text for description of these models). Down panel) Model 1 is built using constant susceptibility for the crust and the bottom of the model corresponds with the Moho discontinuity. Model 2 is composed of the basement at top and Curie depth at the bottom, with constant susceptibility through the entire crust. Model 3 shows the results of susceptibility inversion to find the magnetization distribution in upper crust relied on within basement and horizon of 20 km. The deeper part of the crust again has a constant value of susceptibility, equal to that used for models 1 and 2. Relative errors (difference between calculated and observed values divided by calculated value) are as follows: model1 = 0.84, model2 = 0.58 and model3 = 0.28.

a)

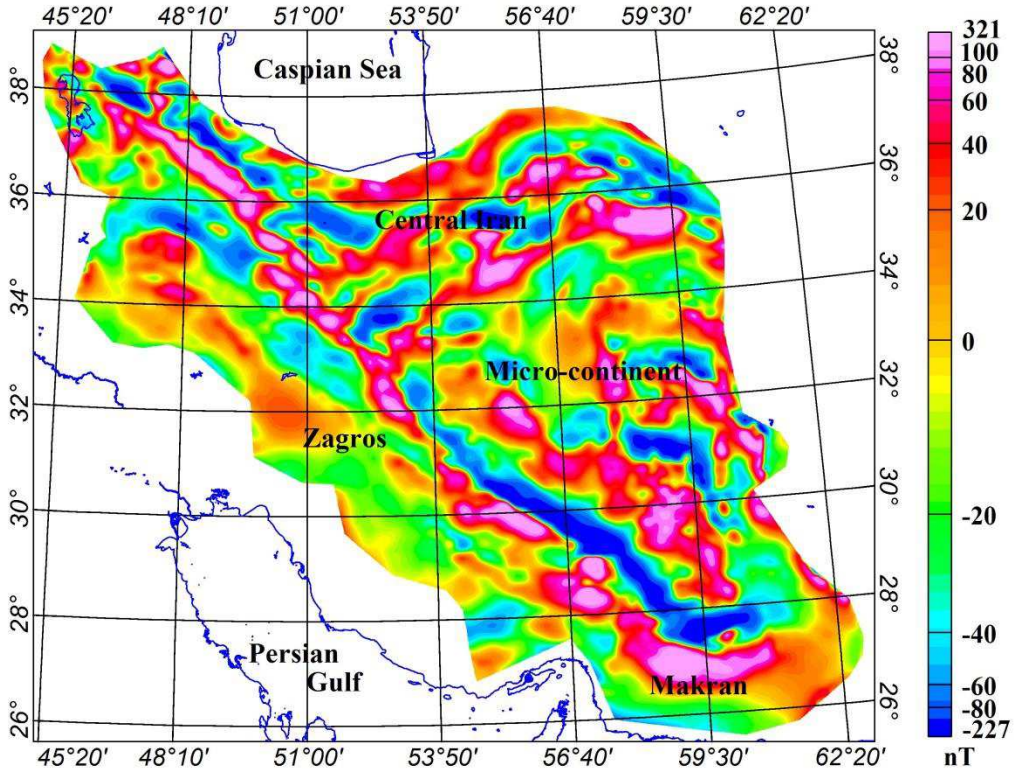
45°20'
48°10'
51°00'
53°50'
56°40'
59°30'
62°20'
38°
36°
34°
32°
30°
28°
26°
Caspian Sea
Central Iran
Micro-continent
Zagros
Persian
Gulf
Makran
321
100
80
60
40
20
0
-20
-40
-60
-80
-227
nT

b)

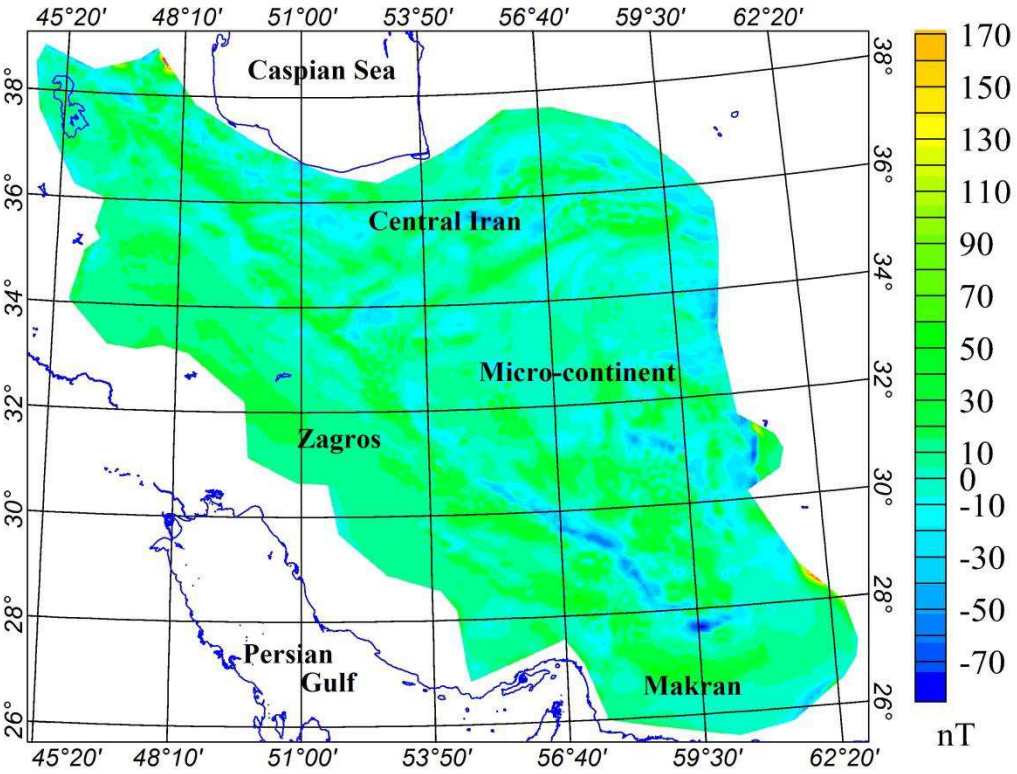
45°20'
48°10'
51°00'
53°50'
56°40'
59°30'
62°20'
38°
36°
34°
32°
30°
28°
26°
Caspian Sea
Central Iran
Micro-continent
Zagros
Persian
Gulf
Makran
170
150
130
110
90
70
50
30
10
0
-10
-30
-50
-70
nT

c)

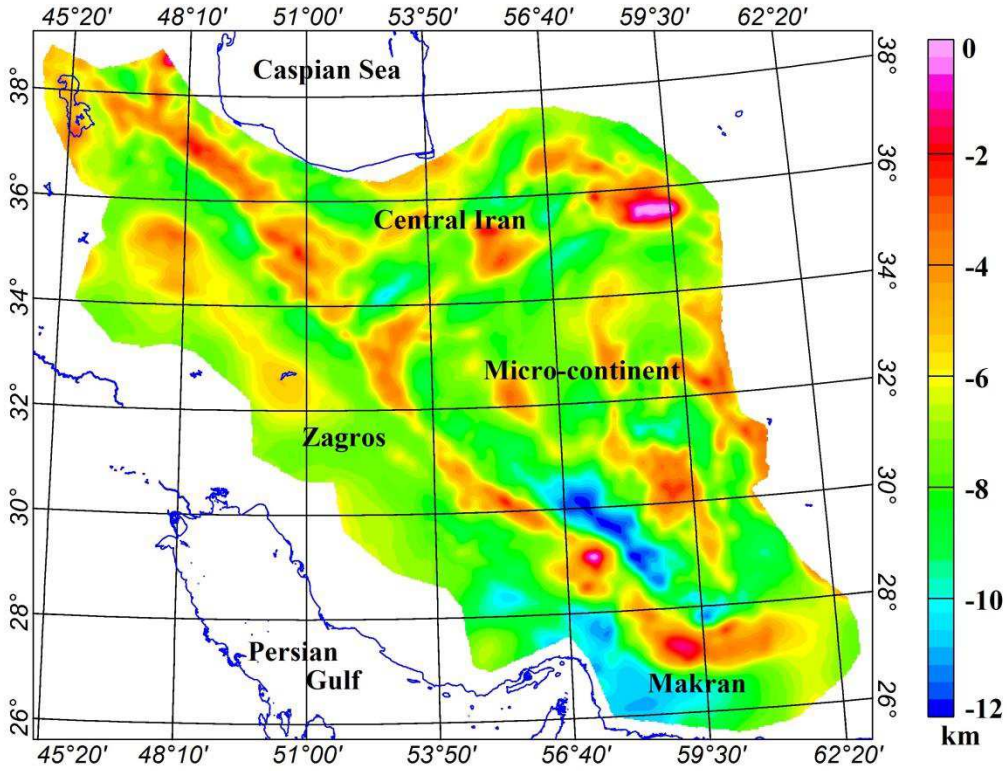
45°20'
48°10'
51°00'
53°50'
56°40'
59°30'
62°20'
38°
36°
34°
32°
30°
28°
26°
Caspian Sea
Central Iran
Micro-continent
Zagros
Persian
Gulf
Makran
0
-2
-4
-6
-8
-10
-12
km

d)

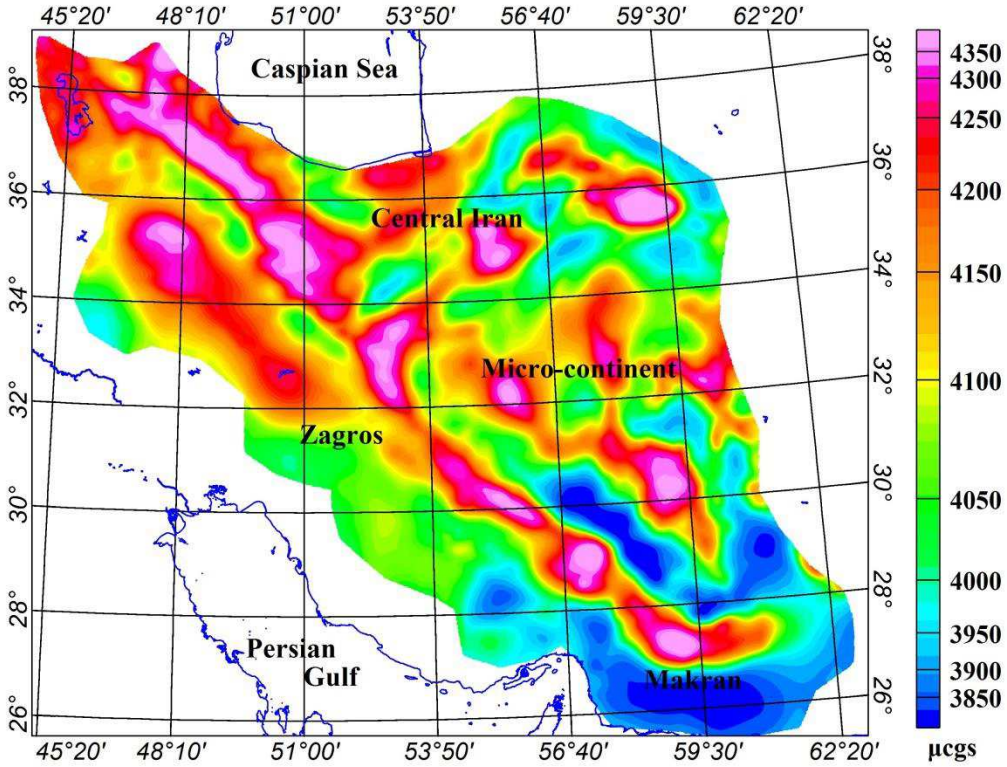
45°20'
48°10'
51°00'
53°50'
56°40'
59°30'
62°20'
38°
36°
34°
32°
30°
28°
26°
Caspian Sea
Central Iran
Micro-continent
Zagros
Persian
Gulf
Makran
4350
4300
4250
4200
4150
4100
4050
4000
3950
3900
3850
µcgs

Fig. 2.7 Inversion results from model 3. The basement geometry is identical in all models 1, 2 and 3 which allows us to check effects of susceptibility distribution entire crust on residual anomalies. a) Calculated data. b) Difference between calculated and observed data. c) Depth to basement. d) Susceptibility distribution in upper layer of the crust (in our model from basement to depth of 20 km).

Our inversion results have been selected following various tests with different susceptibility contrasts due to the weak knowledge of susceptibility in the region (Section 3.2). To define the susceptibility distribution in the entire crust, we first invert aeromagnetic data for the basement geometry when the base of magnetization corresponds with the Curie isotherm (Model 2). We split the crust into two different high- and low-magnetized bodies (Model 3, Fig. 2.6) and invert the magnetic data to resolve the susceptibility distribution in shallow high-magnetized part, which mainly produce magnetic anomalies.

In the third model, the uniform magnetic crust was replaced by high and low magnetic parts to set a higher susceptibility of ~0.04 SI for the uppermost ~20 km. The low-susceptibility magnetic body still has constant susceptibility between depth 20 km at the top and Curie depth at the bottom, which has a regional effect on the magnetic anomaly. In this model, the modeled features are more easily explained than for models 1 and 2. The basement rises up close to the surface at the magnetic anomaly high and deepens to ~12 km depth in magnetic lows. The susceptibility map also indicates the increase in susceptibility at the magnetic anomaly high, which is shown in Fig. 2.7d.

The topography of the basement often approximates the top surface of magnetic sources in the crust. For the structural inversion, we used an average estimate of the susceptibility for the starting susceptibility based on available data. However, the limited direct samples (Aubourg et al., 2002 and 2010) are located far away from significant magnetic anomaly highs and lows.

2.6.2 Forward modeling results

In the following, we represent our results on basement structure and intra-crustal magnetic domains by the best fitting magnetic and gravity modeling.

2.6.2.1 Depth to the basement

Now the basement is taken as a proxy for the base of sedimentary cover of a negligible magnetization. By implementing combined modeling of gravity and magnetic data, the uppermost surface of magnetic rocks is more reliable due to the significant density contrast between the sedimentary rocks and the underlying layers. Magnetization is confined between basement and Curie isotherm depth (Figs. 2.11, 2.12 and 2.13). Our model use constraints based on available information on sedimentary succession thickness and the bottom of magnetization at Curie depth (Fig. 2.4b).

The sedimentary cover represents the different rock types located in Zagros fold and thrust belt (ZFTB) and central Iran. We assume that Cenozoic sedimentary rocks in central Iran and parts of

the micro-continent have a -100 kg/m^3 density contrast compared to sedimentary covers in the Zagros deposited in Mesozoic time (Tunini et al., 2015; Mousavi et al., 2017). A +150 kg/m^3 density contrast distinguishes the Paleozoic sedimentary rocks from Mesozoic type in the Zagros fold and thrust belt (Table 2.1).

Fig. 2.8 shows the basement map for Iran. A large variation in the geometry of the basement is observed in the central Iran domain, which is dominated by major structural highs. The Dasht-e-Lut basin is seen in the magnetic basement where it deepens to ~14 km. Depth to basement reaches almost zero beneath the UDMA and the southern part of Kopeh Dagh. In central Iran and along the northern boundary of the micro-continent (so called "Darouneh Fault", see Fig. 2.1 for location), the depth of magnetic basement is 0 km based on following the magnetic anomalies high. The depth of basement is generally shallow (up to 6 km) in east of central Iran. However, there are some apparent basins depicted by lows on the basement map which are new candidates for previously unknown micro basins (Fig. 2.8).

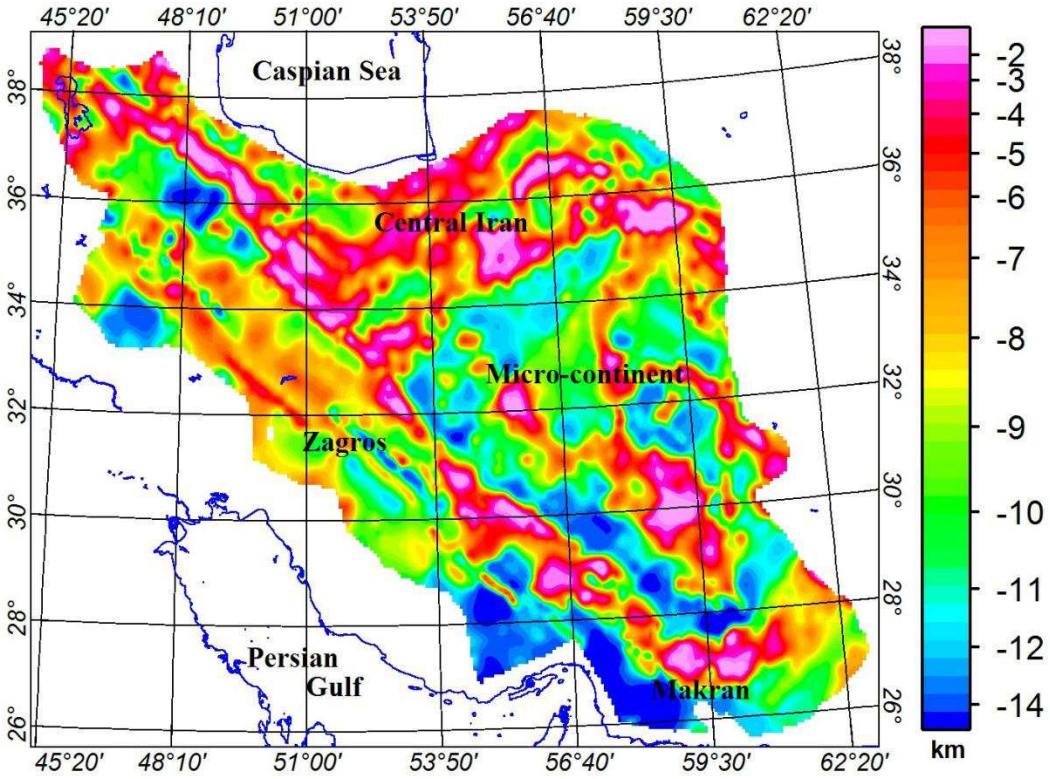

Fig. 2.8 The final 3D model set up of magnetic basement which shows that depth values vary between 0 and 15 km.

The basement map shows sedimentary cover ~10 km thick, in Kopeh Dagh, a thickness which is in agreement with stratigraphic reports. Additionally, the thickness of sedimentary cover in ZFTB is well correlated with what we expect from stratigraphy. Other studies report ~10 km thick Cenozoic sedimentary sequence in Alborz. However, the extension of basins is not completely known. North of the micro-continent boundary, there is a widely extended basin with

a depth of ~12 km which is likely representative of Dasht-e-Kavir basin (the Great Salt Desert) (Fig. 2.8). There are also some depressions evident in the SW part of UDMA, NW and south of Iran which are candidates for unknown basins.

Due to the typically lower magnetization of metamorphic rocks compared to igneous rocks, a major reflector can be traced by density contrast in SSZ where petrophysical properties are changed to reproduce a low in gravity anomalies. The depth of the magnetic basement is very shallow in the Sistan sedimentary basin, which coincides with volcanic activities. In Jazmurian basin, the basement is shallow, resulting in the largest magnetic anomaly in the observed aeromagnetic data (Fig. 2.2a). The increase in depth of basement in the western Makran corresponds with a lack of magnetization. In general, we think this magnetic basement map correlate strongly with known sedimentary basins and their thicknesses. Tectonostratigraphic reports, seismic studies and oil exploration in southern part of Zagros Mountains show varying thicknesses of sedimentary covers between 7 and 28 km (average of ~15 km) (Tavakoli-shirazi, 2012).

2.6.2.2 Upper crustal domains

In gravity and magnetic modeling, the upper crust can be distinguished from the lower crust based on density and susceptibility variation signifying the varying density and change in magnetization with depth in crust. In our modeling, a susceptibility variation was applied to the upper crust to divide upper crustal domains (only magnetically not gravitationally). Based on the low-pass filtering of the magnetic anomaly data (Fig. 2.5a), the micro-continent dominates with the widely extended and low amplitude anomalies which lacks shallow interpretation. However, the interaction between shallow and deep magnetic sources make it difficult to enhance the deep sources. From a tectonic point of view, we can deduce that the micro-continent unit is influenced by magmatic upwelling or magma decompression in lithospheric delamination. In central Iran and its NW domain, the high-amplitude magnetic anomalies are considered to be more likely related to shallow volcanic rocks with moderate susceptibility, rather a thick upper crust with high magnetization. Based on weak volcanic eruptions in ZFTB (Fig. 2.1), it is highly probable that features within the upper crust are responsible for the smoothed out magnetic anomalies observed in this part.

Our upper crustal domains divide the area into three units: central Iran (low magnetic zone); ZFTB and Makran (medium magnetic zone); and the micro-continent (high magnetic zone) through variation in the susceptibilities. The micro-continent domain is bounded within the curve shape magnetic lineaments (coincides with faulting) to the north, UDMA in west and Makran ophiolite in the south (Figs. 2.9 and 2.1). The upper crust between the NW of Iran and the Kopeh Dagh structural unit in the NE seem to have low magnetization. Fig. 2.9 shows the magnetic boundary within the upper crust, dividing ZFTB-Makran belt and the rest of the area where the igneous rocks of UDMA terminates from the ZFTB Meso-Cenozoic sedimentary rocks. In UDMA, the NW–SE oriented magnetic anomalies correlate with the magnetic anomalies strike (Figs. 2.2a and 2.4c) and might relate to subduction magmatism (Ghasemi and Talbot, 2006); although, the origin of magmatism is still under debate. We note that this study can put important constraint on the susceptibility estimates of the upper crust beneath the Iranian Plateau.

The magnetic anomaly in Jazmurian basin (Fig. 2.1) remains of unknown origin, although different possibilities enable us to interpret its high magnetization impact. Further to the north, volcanic activity indicates active magmatism. The ophiolite belt to the south line of Jazmurian shows the existence of an ancient oceanic crust. The high magnetic anomaly in Jazmurian seems unlikely to be related to either colored mélange or Mesozoic ophiolite (Pazirandeh, 1973; Aubourg and Robion, 2002) which are spatially extended in a manner that is incomparable to the anomaly extension. The shallow depth of the oceanic crust results in a similar magnetic anomaly as observed in aeromagnetic data (e.g. Abedi and Bahroudi, 2016). Additionally, fitting a model to the observed positive Bouguer anomaly (Fig. 2.2b) requires the presence of a dense material such as that of oceanic crust. This area is picked out by magnetic lineaments and is highlighted as having the same gravity and magnetic source in the pseudo gravity map (Fig. 2.5d). This interpretation of the magnetic signature is in disagreement with the model of Abedi and Bahroudi (2016), who interpreted this magnetic anomaly as relating to a diving slab structure with a high susceptibility, down to depth of ~100 km. However, some uncertainty remains as the aeromagnetic data cannot be resolved to such depth. From our modeling results, an oceanic affinity of the crust in Makran (~10 km thick, beneath a thin sedimentary sequence with a susceptibility of 0.028 SI, similar to the micro-continent material), or magmatic intrusions down to basement is more probable.

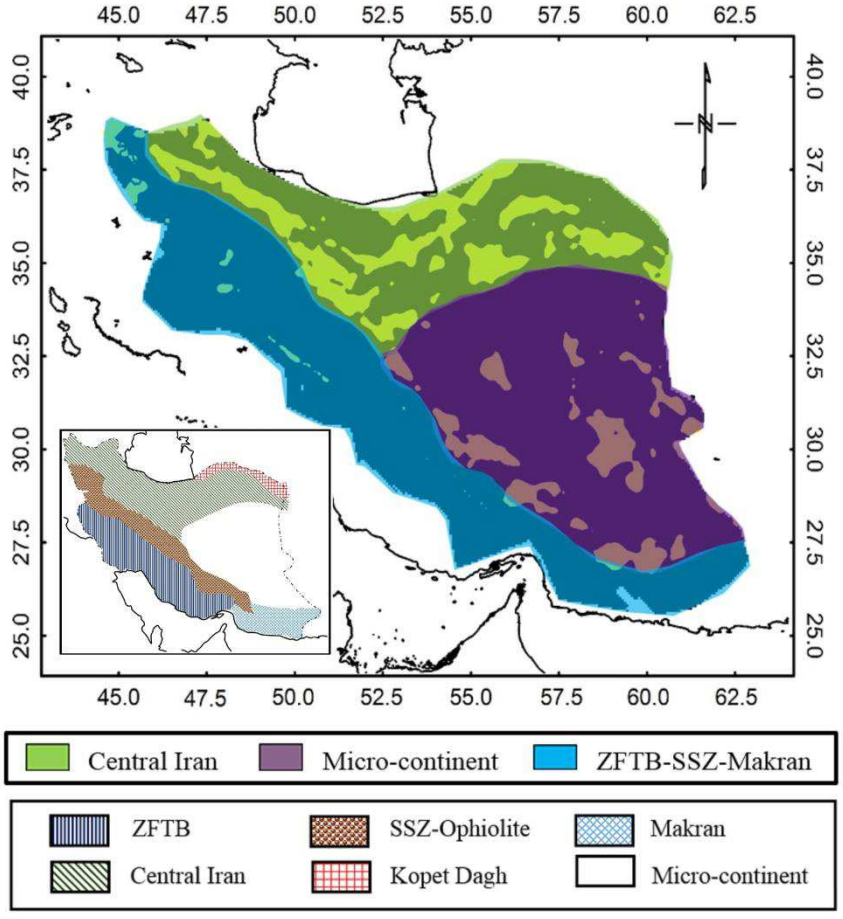

Fig. 2.9. Map of the susceptibility domains proposed for the upper crust beneath the Iranian Plateau from basement (Fig. 2.8) down to a depth of 20 km. The contours (light spots) in the background are simplified areas of minimums in basement in our model. Susceptibility in the upper crust of central Iran (i.e. Kopeh Dagh and Alborz), ZFTB (SSZ and Makran) and micro-continent are chosen 0.001, 0.01 and 0.028 SI respectively. For the purpose of comparison, we put the simplified structural map of Iran as subfigure. The shading areas in structural geology map is described in the lower legend.

Fig. 2.9 demonstrates a correlation between structural features and the boundary of the magnetic crustal domains to the north of the micro-continent (Fig. 2.1). In contrast, magnetic anomaly strike to the north of the micro-continent correspond with the main fault which could be a critical ambiguity if magnetic anomaly represent a shallow susceptibility source or deep basin faults. The micro-continent area is quite distinctive from its surrounding in the pseudo-gravity map (Fig. 2.5d). This complex architecture corresponds with the scenario of a plate rotation in tectonic activities, based on paleomagnetic and kinematic studies (e.g. Aubourg and Robion, 2002; Gaina et al., 2015). In the western part of the micro-continent, the magnetic anomaly is the combined effect of high-magnetic susceptibilities of igneous rocks and the upper crustal domain boundary (Figs. 2.8, 2.11, 2.12, and 2.13).

2.6.2.3 Calculated and residual anomalies

The final calculated and residual gravity and magnetic fields are shown in Figs. 2.10a and 2.10b. The gravity residual is within ± 20 mGal which indicates the model can reasonably fit long wavelength features. Moreover, the best fitting model depends on the refinement of intra-crustal layers associated with density structures, otherwise our model fails to properly address all of the local structures.

a)

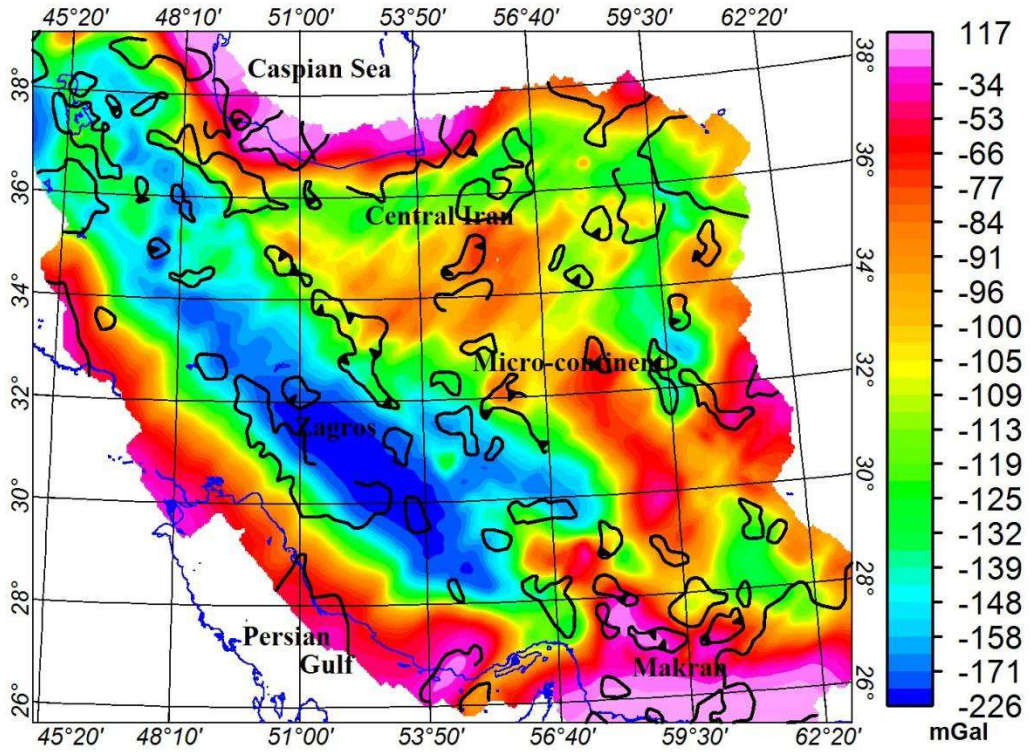
45°20′
48°10′
51°00′
53°50′
56°40′
59°30′
62°20′
38°
36°
34°
32°
30°
28°
26°
Caspian Sea
Central Iran
Micro-continent
Zagros
Persian
Gulf
Makran
117
-34
-53
-66
-77
-84
-91
-96
-100
-105
-109
-113
-119
-125
-132
-139
-148
-158
-171
-226
mGal

b)

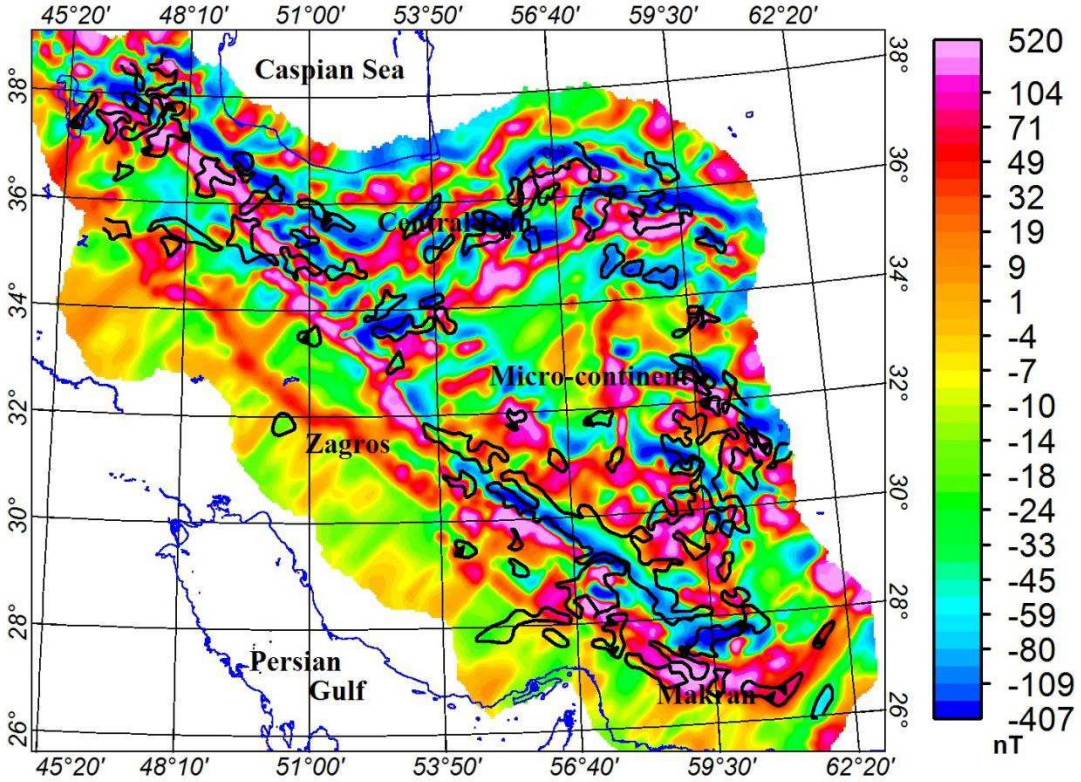
45°20′
48°10′
51°00′
53°50′
56°40′
59°30′
62°20′
38°
36°
34°
32°
30°
28°
26°
Caspian Sea
Central Iran
Micro-continent
Zagros
Persian
Gulf
Makran
520
104
71
49
32
19
9
1
-4
-7
-10
-14
-18
-24
-33
-45
-59
-80
-109
-407
nT

c)

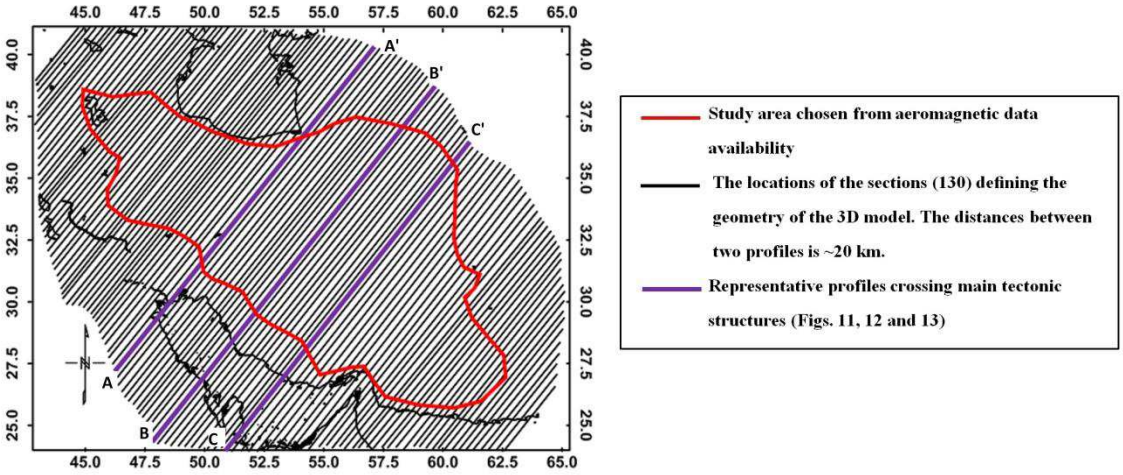

Fig. 2.10 a) Map in the background is calculated gravity data and contour lines (±20 mgal) are residual gravity anomalies. b) Forward magnetic modeling results including calculated anomaly overlaid by contour lines indicating regions with ±50 nT uncertainties (~10 % of measured the magnetic anomaly amplitude). c) Arrangement of profiles used for 3D model setting up. All profiles have extension of 3 times larger than the size of region. Model is also extended perpendicular in NW-SE direction up to three times of the study area. Purple lines are the location of extracted cross sections (see Figs. 2.1, 2.11, 2.12 and 2.13)

In some small extended regions, the difference between calculated and observed gravity data is relatively large (Fig. 2.10a). The possible explanation for this misfit is the simplified sedimentary cover. By using magnetic data to define the crustal structure, the uncertainties associated with density distribution are decreased since most of structures are assumed to be geometrically the same for both susceptibility and density cells (polyhedrons). Although, it does not mean that we necessarily use the same susceptibilities for those two modeling units with identical density values.

Calculated magnetic data suggests the model can explain most of the largest magnetic anomalies in Iran, for example UDMA that extends discontinuously ~3000 km where volcanic rocks crop out. Nevertheless, more efforts need to be put into modeling complex magnetic sources (i.e. basement faults and interbedding layers) by applying comprehensive datasets and integrated geophysical modeling. Despite a clear boundary between igneous (UDMA) and metamorphic (SSZ) rocks in the structural map of Iran (Fig. 2.1), uncertainty is involved in distinguishing these rocks due to lack of a precise indicator in petrophysical properties of these rocks and true information of their depths, thicknesses and locations. To decrease the ambiguities of present in our model, the available map for outcrops and structures of volcanic rocks in Iran provided by Pazirandeh (1973) has been used.

2.7 Discussion

In the following, we further describe the crustal units and their links to the tectonic setting of the area. The aim of this study is to define the basement characterization beneath the Iranian Plateau. The undulation of basement can be a proxy of sedimentary thickness. While most of minerals and hydrocarbon reservoirs are located in the sedimentary cover, basement receives more

attention from economic geologist and petroleum engineers. Current models of the basement beneath the Iranian Plateau are still locally extended and have some uncertainties (Namaki et al., 2011; Oskooi and Abedi, 2015; Abedi and Bahroudi, 2016; Teknik and Ghods, 2017). Also, the proxy of Curie temperature has not widely used as a constraint to characterize the deep part of the magnetized crust. While, Curie depth can be useful in order to constrain the deep part of the model.

2.7.1 NW part of Zagros toward Alborz range

Fig. 2.11 shows the crustal transect NW of Zagros and in the western part of central Iran, along the high magnetic and low gravity anomalies. On this profile, central Iran represents a high-magnetic region dominated by shallowing of igneous rocks in our model. We can correlate the zero depth of basement in the Alborz area with the presence of volcanic activities. The depth to basement in central Iran and Alborz Mts. decreases rapidly and a rapid variation in basement geometry is observed locally on this profile. The presumed higher densities of volcanic rocks compared to the surrounding sedimentary rocks is compensated by variation of the deeper crustal layers, so as to fit the model to the gravity data anomaly.

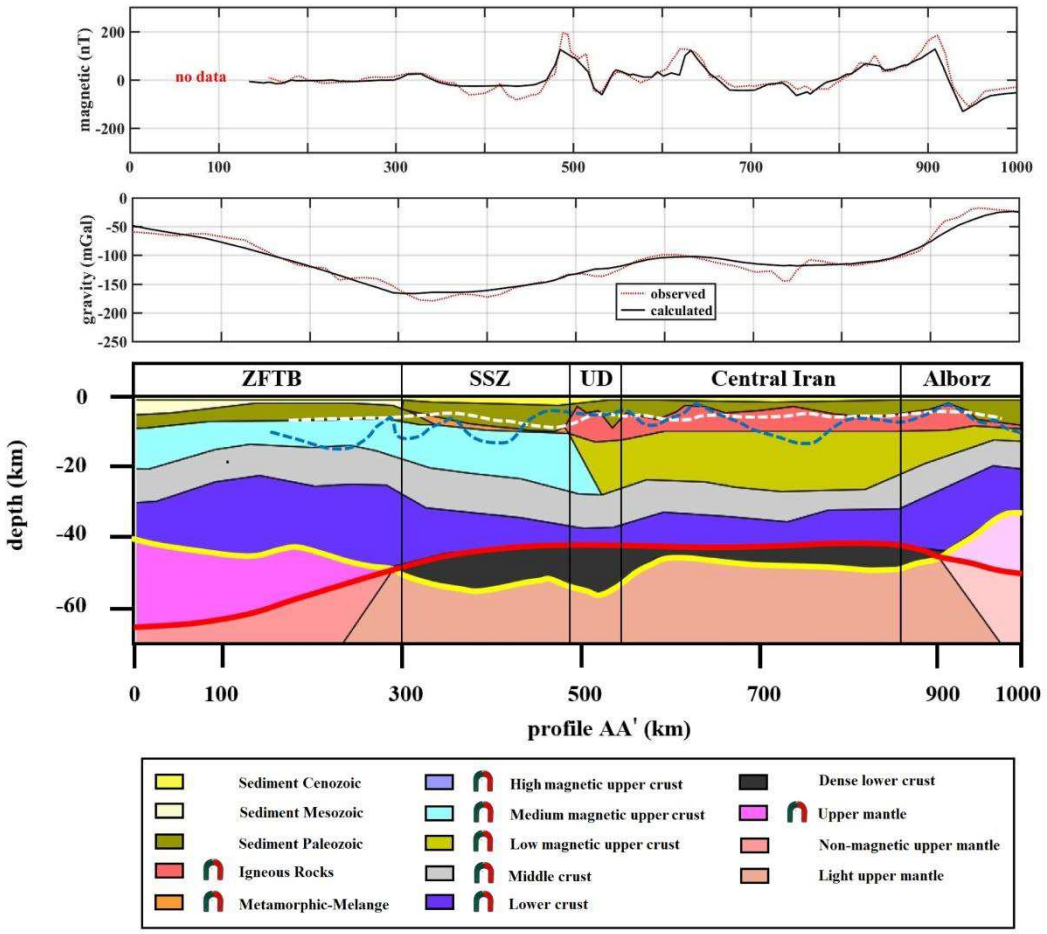

Fig. 2.11 Susceptibility and density distribution along Profile AA′ started at NW of Zagros crossing central Iran domain until Alborz range (see Fig. 2.1 for location). The legend shows model parameters in crust which are distinguished by different colors (Table 2.1, upper crust colors are the same as in Fig. 2.9). In the model cross section, the white dashed line is estimate of basement from inversion of aeromagnetic data (section 6.1) and dashed blue line is the magnetic basement from fractal analysis of aeromagnetic data in Iran by Teknik and Ghods (2017). A minor change in density and susceptibility of upper mantle has been inserted to apply density heterogeneities above and below the Curie depth. Red and yellow lines highlight Curie and Moho depths orderly.

The sedimentary cover of ZFTB and the Iranian Plateau are distinguished based on different history of underlying tectonic plates (i.e. Arabian plate and Iranian micro-continent block). The deformation in the upper crust is supported by seismological and geodynamical prospecting of the Iranian Plateau. Low density sedimentary material is thickened in the gravity anomaly lows where surface or basement faulting is evident. The basin thickness, which is mostly modeled here by the dense Paleozoic sedimentary rocks, varies to follow the topography of the basement. This variation of the sedimentary thickness results in shaping several micro basins in this transect beneath central Iran. The thickness of the sedimentary cover west of UDMA reaches a maximum of ~15 km, which is related to the presence of the Paleozoic sedimentary cover in the Zagros. The metamorphic rocks in western part of UDMA are modeled as being thin due to the weak magnetic anomaly observed in this part (Fig. 2.11).

At the western end of the profile, the Mesozoic sedimentary basin coincides spatially with one of the known sedimentary basins in ZFTB. This basin is located in Zagros hinterland sedimentary provinces, and is known as a significant prospect for petroleum explorations. The igneous rocks terminate on the west side of UDMA, where SSZ starts. The negative Bouguer anomaly located at SSZ requires thicker sedimentary cover (low dense material) to decrease density rather than high-density metamorphic rocks. We model MZT fault as corresponding with the margin of ZFTB. A thrust structure beneath UDMA is associated with different stages of rifting and subduction (Ghasemi and Talbot, 2006). Those structures help us to model the Bouguer gravity low in SSZ and UDMA. MZT is seismically inactive and if one follows dominated seismicity in the area, most of shaking epicenters are shallower than 20 km (Talebian and Jackson, 2004). From forward modeling and following the main magmatism regime in the area, the central Iran upper crust is distinguished from SSZ and ZFTB to figure out the less magnetic properties in deep crust of central Iran (Figs. 2.9 and 2.11).

2.7.2 Zagros orogeny to Kopeh Dagh, crossing central Iran

The transect displayed in Fig. 2.12 shows the 2D structure of major crustal units below the Iranian Plateau. These units are mainly associated with the Arabian-Iranian collision zone in the Zagros Mountains and the corresponding decollement. The micro-continent is a mainly flat area which has an apparently less complex orogenic history than Zagros and the Kopeh Dagh Mountains. Kopeh Dagh is at the extreme east of the profile, and is differentiated from central Iran by differing evolution of the orogeny and tectonic background. The absence of magnetic data in this area limits further analysis on the shallow susceptibility structure. The current model

of Kopeh Dagh is mainly based on gravity data analysis and stratigraphic studies, for deep and shallow parts respectively (Allen et al., 2003).

Forward modeling and the available map of volcanic rock outcrops (Pazirandeh, 1973) indicates that UDMA has minimal thickness on this profile. Deepening basement in UDMA corresponds with results from inversions and fractal spectral analysis (Teknik and Ghods, 2017). Like other cross sections perpendicular to the strike of Zagros, SSZ is associated with metamorphic rocks, which extend between MZT and UDMA. The Dasht-e-Kavir sedimentary basin located on the western side of the central Iranian igneous province, has an average thickness of 10 km (Figs. 2.8 and 2.12). The lack of a high amplitude magnetic anomaly might indicate the absence of significant magnetic intrusive rocks. This being said, it is important to consider that the presence of salt decrease the magnetic susceptibility (Teknik and Ghods, 2017). Moreover, the area lacks any significant volcanic activity. In our 3D model, the Dasht-e-Kavir basin is elongated into the plane of the representative cross section. For this reason, the basin seems to be extended relatively wide. The sedimentary and stratigraphic sequences are simplified to one representative material, which is a simplified estimation of all folding and lithological layering, due to limited constraints. This means that the magnetic basement in our model is more disturbed than in reality.

Toward the east of this profile, the top of the igneous rocks outcrops at the surface, a characteristics which corresponds with observed volcanic outcrops. The age of volcanism in this area is estimated to be late Cenozoic, and felsic plutonic outcrops are dated as Mesozoic (Aghanabati, 2004). Based on the limited extent of Mesozoic ophiolite at the southern boundary of Kopeh Dagh, we are not sure whether there is any relation between magnetic highs and the presence of those rocks in NE Iran. Our model shows the thickness of the sedimentary cover in Central Iran decreases in the presence of strong magnetic anomalies. The reason for this characteristic is unknown.

The upper crust of the micro-continent unit differs from that of central Iran due to its higher magnetic susceptibility (Table 2.1 and Fig. 2.9). An explanation for the strongly magnetic upper crust in the micro-continent is not easy to deduce, although it has a regional trend in final calculated anomalies. Pseudo-gravity transformation and low-pass filtering (Figs. 2.5d and 2.5a) helps us in this regard although the susceptibility contrast is determined based on trial and error using forward modeling. The susceptibility and density contrast distinguishes the non-magnetic and dense lower crust beneath Iranian crust from the magnetic lower crust. Integrated petrological geophysical modeling indicates greater density of the deep crustal portion below Iran was informed recently (Tunini et al., 2015). Such a dense layer might also coincide with the non-magnetic part of the lower crust layer (Fig. 2.12). Our results indicate crustal thickening below Zagros and Kopeh Dagh. In general, we observe the depth to the Curie isotherm is quite shallow on the eastern part of the profile, reaching to 25-30 km in Kopeh Dagh, and then increasing eventually towards the western side of the profile.

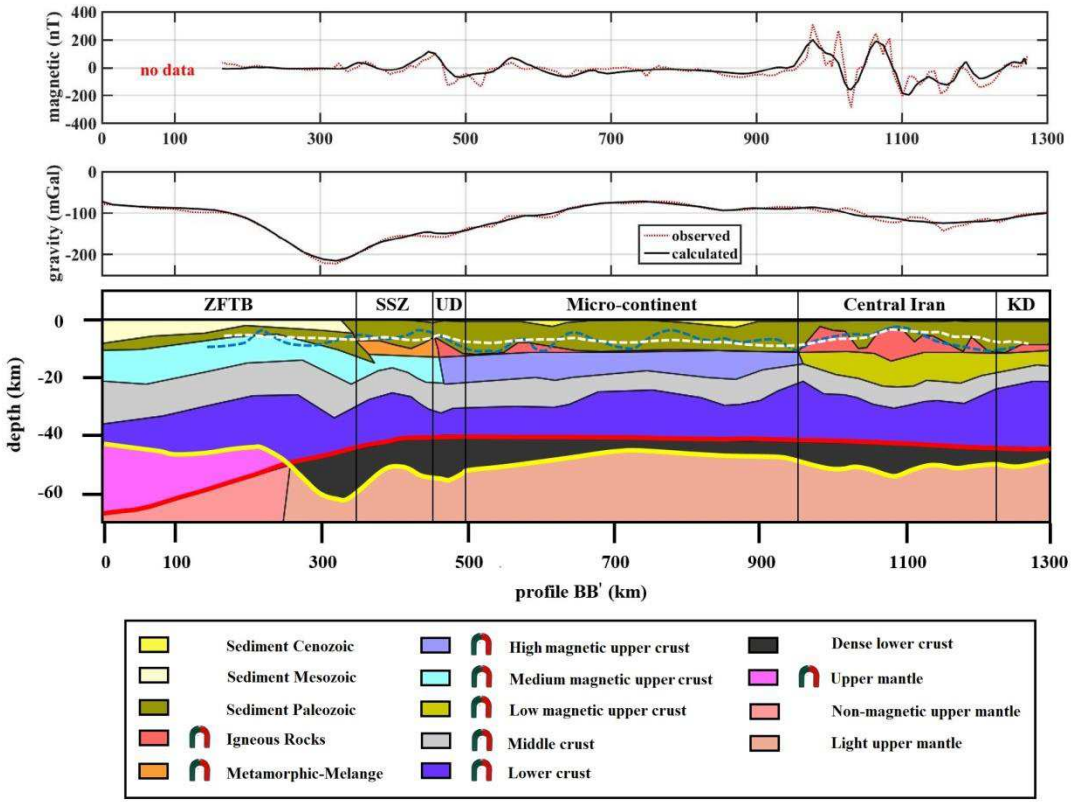

Fig. 2.12 Gravity and magnetic model for the region extending from the Zagros orogeny (ZFTB) to the Kopeh Dagh unit (KD). Color scale for cross section illustrates differentiated density and susceptibility parameters (Table 2.1). Two upper panels show the magnetic and gravity calculated and observed fields. Description to predefined basement, Moho and Curie geometries is similar as described in caption Fig. 2.11.

2.7.3 Magmatism in the Iranian micro-continent

The profile shown in Fig. 2.13 crosses similar structural units as profile BB′, although there is comparatively (Fig. 2.12) more extension over the Iranian micro-continent. This cross section demonstrates the complex structure relatively in the east of the micro-continent where late Tertiary volcanic rocks outcrop widely. On the western side of the profile, at ZFTB, sequences of Mesozoic and Paleozoic sedimentary rocks below ZFTB overlie on Paleozoic sediments. This region is characterized by low to medium densities, highly magnetic upper crust and averagely thin continental crust. In the foreland area of ZFTB, the base of the crust deepens.

The weak coverage of the aeromagnetic data over ZFTB results in imprecise modeling of sedimentary thickness, as combined gravity and magnetic modeling of shallow structures cannot be done. Therefore, the structure in this part is derived from modeling of gravity data alone. SW of Zagros, the absence of volcanic activities might indicate a low chance of finding interbedded intrusive magnetic rocks within the sedimentary rocks. At the eastern boundary of SSZ, modeling the faulting structures helps to characterize the density change (between SSZ and ZFTB). On this profile (Fig. 2.13), the sedimentary rocks cover reaches a maximum depth of ~15 km.

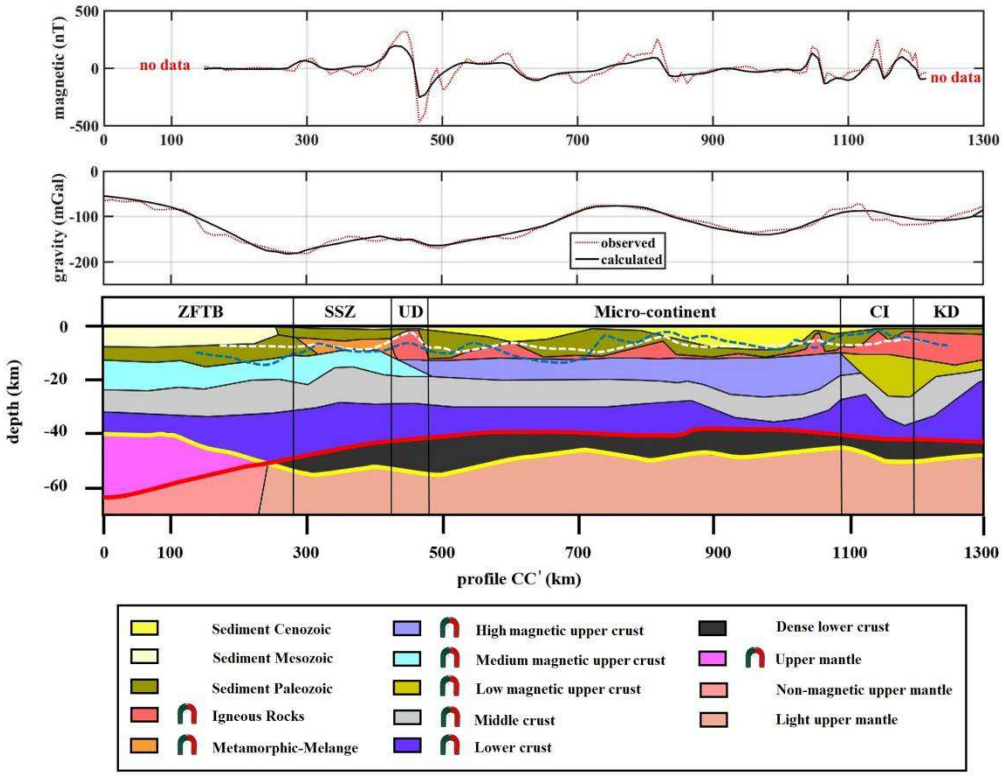

Fig. 2.13. Gravity and magnetic model for the region extending from the Zagros orogeny (ZFTB) to the Kopeh Dagh unit (KD). Upper panels are illustrating the goodness of measured data fit and lower panels are representing model parameters, important deep crust boundaries and alternative basement which have been abovementioned.

The depth to the magnetic basement near Kopeh Dagh Mountains corresponds with the expected ~10 km thickness of the sedimentary column (Brunet et al., 2003). The density contrast on the east of the profile (Fig. 2.13) is modeled from thrusting structure to improve the misfit of Bouguer anomaly. One can resolve this problem by modeling a different density for this region of volcanic rocks, as constrained by local lithological data. Gravity data modeling illustrates a thick and low density basin in the east part of the profile. However, the sedimentary sequence of this area is still relatively unknown, and further studies are needed to confirm if this interpretation of potential field data is correct.

The shallowing of the Curie depth on the east of the profile (Fig. 2.13) suggests that the high susceptibility value for micro-continent is appropriate, because the calculation of Curie depth was completely independent from magnetic data. Conversely, the calculated magnetic anomaly requires a regional trend to fit the observed data in our model. A few locating known faults in the micro-continent, the major faults are modeled, leading to a better fit of the local minimum of the Bouguer anomaly. In general, massive volcanic outcrops in the micro-continent are well addressed by our model (Fig. 2.13).

2.7.4 Validity of results

Any model is only as good as the parameterization and validity of assumptions. We first demonstrated that the Moho depth is not a good proxy for the bottom of the magnetic sources. An alternative, the use of a Curie depth derived from a lithospheric modeling, resulted in an improved fit and in general, confirmed the advantage of combing multiple geophysical data modeling. Curie depth is an isotherm which is taken as a proxy on the bottom of magnetization. We cannot name Curie depth as an indicator of change in petrology to make further interpretations. In the lack of many constraints (only few seismic lines) on deep crustal structure, however, we examined this idea whether assuming Curie isotherm for the bottom of magnetization can develop the fit to magnetic data. Our results show the bottom of magnetization can be represented strongly by the Curie depth instead of Moho depth. Having in mind, this proxy is only valid for fitting magnetic data. This exception reminds that the density and susceptibility structures do not necessarily coincide.

Despite these limitations, however, definition of intra-crustal magnetic provinces and the bottom of magnetization is counted one step towards a better understanding of petrology of the crust. We can distinguish our constraining information like previous basement structure and seismic studies or even our initial basement inferred from inversion from geophysical data modeling results. Intra-crustal magnetization domains are example of unconstrained output. Ideally, the lithospheric magnetization should be studied jointly, not sequential, with other geophysical data. However, as there is no direct physical relationship between magnetization and density/velocity, such model would require most likely some form inverse approaches which is beyond the scope of the present study. However, the sequential modeling example has shown which parts of the magnetic field are most sensitive to which crustal elements. Such analysis is also useful for other geological settings, but not necessarily has to result in the same conclusions, as the magnetization in crust is the result of a complex interplay of varying effects.

2.8 Conclusion

In this study, we have generated a new map of magnetic basement beneath the Iranian Plateau using available aeromagnetic and terrestrial gravity data. The field processing of magnetic field anomalies led to a first-order interpretation of the susceptibility distribution, which was used later in forward modeling. The 3D susceptibility distribution from inverse modeling explains the regional magnetic anomalies. Validating the susceptibility distribution of the upper crust requires sampling. To address these limitations, we refined the geometry (based on inversion of magnetic data) and the physical properties of the model through combined forward modeling of gravity and magnetic data. The modeled geometry of basement correlates well with geological surficial evidence. In order to avoid an invalid model, we used the same physical properties for volcanic rocks across the entire area and also used the Curie depth obtained from magnetic-independent analysis.

The basement map reveals several previously mapped basins of Iran, e.g. Dasht-e-Kavir and Dasht-e-Lut basins and the final model explains most of the basin structures and igneous rock outcrops. Based on our modeling results, the upper crust in Central Iran is much less magnetized

than that beneath the ZFTB and the Iranian micro-continent. The best fitting model of basement in this study is capable of fitting aeromagnetic data as the best indicator of shallow magnetization. In addition, the regional setting of our model is based on a thermally defined Curie depth map for the base of magnetization that reduces the uncertainties in determination of basement map. A natural extension of our study is to integrate the crustal architecture within a full lithospheric model in order to understand the evolution of the Iranian Plateau.

Chapter 3:

3D crustal and lithospheric mantle structure of the Iranian Plateau from geophysical-petrological modeling

3.1 Introduction

Geophysical modeling of the lithospheric structure leads to a better understanding of the tectonic background, e.g. subduction, shaping the Earth. In the last years, the use of thermochemical parameters to describe the geophysical properties of upper mantle is becoming more popular (Afonso et al., 2008; Fullea et al., 2010; Gradmann et al., 2013; Fullea et al., 2014, Tunini et al., 2015). In this way, geophysical models can account, in a consistent manner, for lateral and vertical variation in the upper mantle composition (i.e., as evidenced from mantle xenoliths) that affect for instance the density and seismic velocities fields, among others.

The structure of the present-day lithosphere beneath the Iranian Plateau (Fig. 3.1) has been modeled in a number of earlier geophysical studies, mostly in 2D. The lack of 3D model motivated us to provide a 3D lithospheric model (thermochemical structure) of the Iranian Plateau and surrounding areas by identifying heterogeneities in the upper mantle compositional and thermal fields. For this purpose, I consider a 3D geophysical-petrological approach where rock properties (e.g., density) are computed self-consistently within a thermodynamic framework (e.g., Fullea et al., 2009). Our thermochemical model is constrained by potential field data (Bouguer, free-air, and geoid anomalies and gravity gradient satellite data), highly sensitive to lateral and vertical density variations.

3.2 Tectonic setting

The opening of Red Sea, separating the Arabian Plate from the African Plate, results in a northeastward convergence of Arabia and Eurasia Plates. This long-lived convergence imprints the Iranian Plateau with a complex geological setting as reflected by strong lateral variations in age and composition (e.g., Golonka, 2007; Hatzfeld and Molnar, 2010). Recently reported GPS data shows convergence rates of ~8, ~5, ~3, and ~6 mm/yr in the Zagros Mountains, the Alborz Mountains, Central Iran, and the Caspian Sea, respectively (Guest et al., 2007; Vernant et al., 2004). In the following, I review the geological characteristics of the major tectonic terrains in the context of the Arabia-Iran-Eurasia northeastward convergence. The convergence of the Turan platform (SW part of Eurasia Plate) and the Iranian Plateau leads to the Kopet-Dagh orogeny created after the Cenozoic (Thomas et al., 1999). After the late Alpine orogeny, a ~10 thick Meso-Cenozoic sedimentary cover was formed in Kopet-Dagh terrain (Davoudzadeh and Schmidt, 1984; Brunet et al., 2003).

West of the Turan platform and the Kopet-Dagh Mountains, the origin of Caspian Sea with its dual oceanic-continental affinity is still a matter of discussion (Berberian, 1983; Brunet et al., 2003; Knapp et al., 2004; Egan et al., 2009; Green et al., 2009). Motavalli-Anbaran et al. (2011) suggest the oceanic affinity of the crust based on a seismic reflection study, which reported a fast

and thick crust. The Central Iranian block is a relatively flat area surrounded by Kopet-Dagh and the Alborz Mountains in the north, the Zagros Mountains in the west, and Sistan suture zone in the east (Fig. 3.1). Toward the north, the Alborz Mountain chain shows topography values of up to ~5 km (Fig. 3.1). Several authors have studied the sedimentary cover of the Alborz (e.g. Alavi, 1994; Ballato et al., 2011), indicating an average thickness of 2 km for Cenozoic, Mesozoic, and mostly Paleozoic sediments.

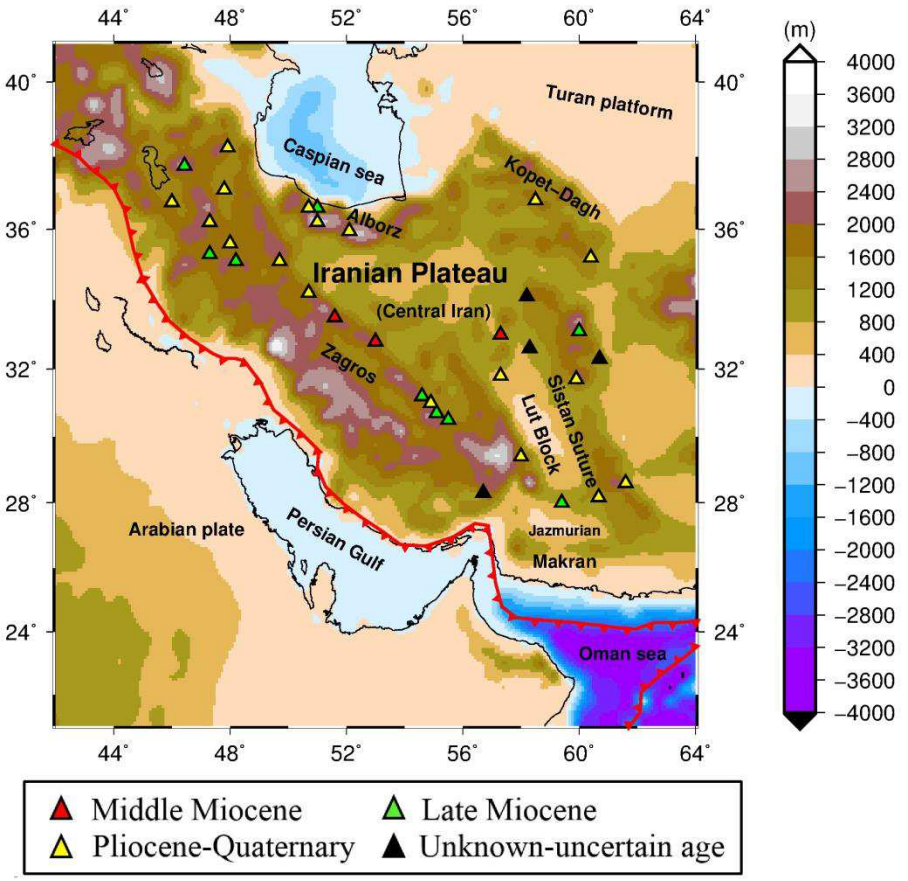

Figure 3.1. Topography map of the study region with the main structural units (after Berberian and King, 1981).

To the west, the Zagros Mountains are located northwest-southeast from the northwest of Iran (eastern Turkey) to the Makran subduction zone (Fig. 3.1). The Zagros Mountains have been collided simultaneous to the long-lasting subduction of the Neo-Tethys Ocean since Permian (e.g., Vergés et al., 2011; Mouthereau et al., 2012; McQuarrie and van Hinsbergen, 2013). The Zagros folded area is separated by major faults and is covered by a sequence of sediments of different ages including those of Paleozoic to Cenozoic age (e.g. Sepehr and Cosgrove, 2004; Sherkati et al., 2006; Casciello et al., 2009; Emami et al., 2010). To southeast of Zagros, a sharp change in crustal thickness in a N-S direction seems to be an evidence of the back-arc formation in Jazmurian basin (McCall and Kidd, 1982; Glennie et al., 1990; Burg et al., 2008) suggesting a subduction-related origin of the area.

3.3 Earlier geophysical studies

In the following, I review the previous studies done to explore the lithospheric structure underlying Iran and surroundings. Firstly, I summarize available estimates for Moho and LAB depths. The information described will be used to set the initial model for forward modeling approach. Second, all relevant information regarding the mantle composition are applied to define the first-order estimates on the compositional heterogeneities in lithospheric mantle beneath Iran. The validity of this proposed compositional domain will be tested in modeling steps due to straightforward relation between chemical composition and density values (Fullea et al., 2009).

3.3.1 Previous Moho and LAB for Iran

Moho depth of Iran has been previously studied by seismic receiver function studies (Gök et al., 2008; Gritto et al., 2008; Nasrabadi et al., 2008), active seismic imaging (Paul et al., 2006 and 2010), and waveform inversion for S-velocity (Shad-Manaman et al., 2011) (Fig. 3.2). These studies suggest Moho depth from 35 to 45 km beneath the Arabian Plate up to 44 to 69 km beneath the Zagros Mountains (Fig. 3.2). The existence of a crustal root beneath the Alborz Mountains has been discussed in different studies suggesting Moho depth values ranging from 35 to 67 km (Dehghani and Makris, 1984; Nasrabadi et al., 2008; Paul et al., 2010; Guest et al., 2007; Motavalli-Anbaran et al., 2011). Despite some seismic studies in northern Iran (e.g., Radjaee et al., 2010), the crustal structure remains uncertain in that area. A thin crust of 20-35 km has been estimated for the Makran offshore using different seismic studies (Niazi et al., 1980; Dehghani and Makris, 1984; Kopp et al., 2000; Yamini-Fard and Hatzfeld, 2008; Smith et al., 2013; Taghizadeh-Farahmand et al., 2013; Entezar-Saadat et al., 2017).

The most remarkable feature about lithospheric structure beneath Iran is a sharp lateral change in both P- and S-wave velocities interpreted as a lithospheric thinning beneath Central Iran (Bijwaard et al., 1998; Maggi and Priestley, 2005; Hafkenscheid et al., 2006; Alinaghi et al., 2007; Kaviani et al., 2007; Shad-Manaman and Shomali, 2010; Agard et al., 2011; Mohammadi et al., 2013).

During the last decade, many efforts have been devoted to model the lithospheric structure of Iran, particularly based on a 'pure' thermal (Molinaro et al., 2005; Motavalli-Anbaran et al., 2011; Jiménez-Munt et al., 2012) and more recently thermochemical modeling (Tunini et al., 2015). In those studies the crustal thickness shows a minimum of 42-43 km beneath the Arabian Plate and Central Iran (Jiménez-Munt et al., 2012; Tunini et al., 2015) and a maximum thickness up to ~60 km in the Zagros and Alborz Mountains (Molinaro et al., 2005; Motavalli-Anbaran et al., 2011; Jiménez-Munt et al., 2012). Additional crustal thickness estimates are a 48 km Moho under the Kopet-Dagh Mountains (Shad-Manaman et al., 2011) and also thin crust under the southern Caspian Sea rising up to a 30 km depth (Motavalli-Anbaran et al., 2011). A pronounced lithospheric thinning below Zagros and thick lithospheric ~220 km below the Persian Gulf and Turan platform with ~40 km discrepancies for the LAB depth has been found in prevoius lithospheric-scale studies (Jiménez-Munt et al., 2012; Tunini et al., 2015). To southeast, Entezar-Saadat et al. (2017) suggested a thin LAB beneath Oman Sea, which increases to 260 km in the Makran subduction zone due to the sinking slab (Fig. 3.3).

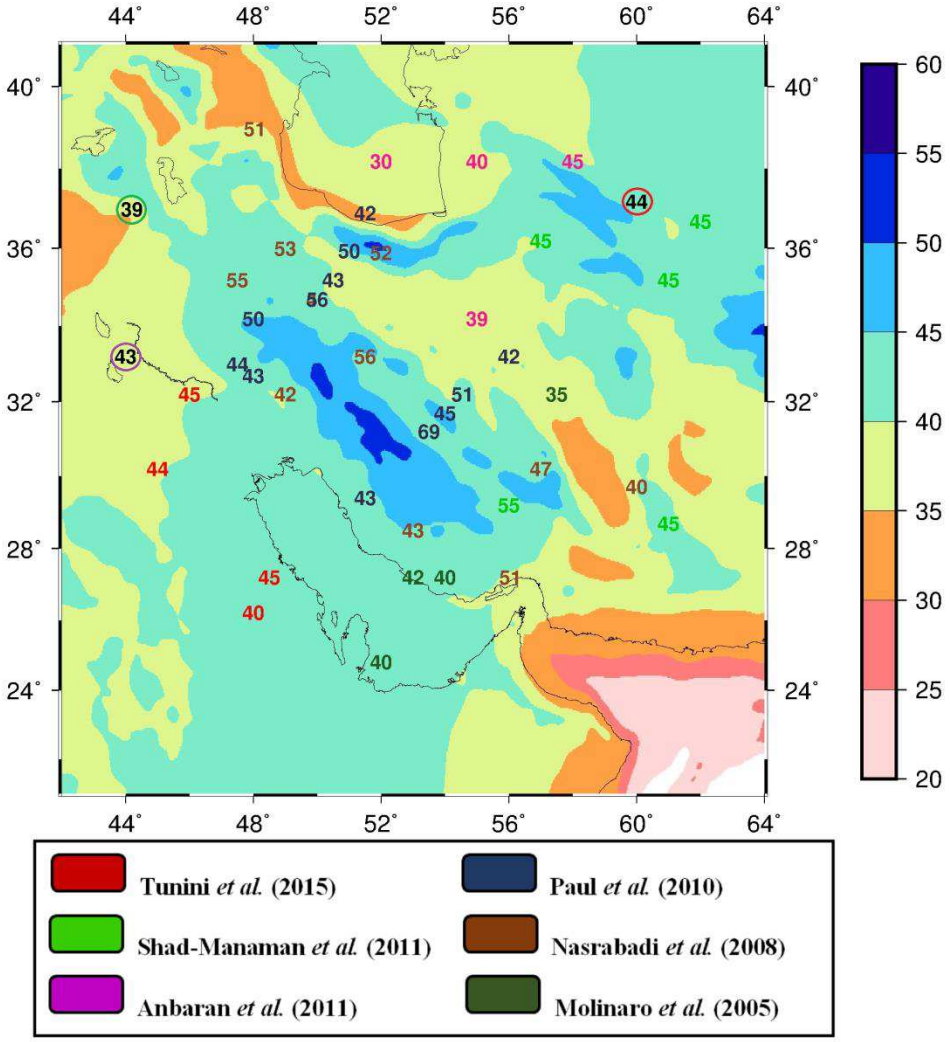

Figure 3.2. Moho depth map of the study area from inversion of geoid and elevation data (Fullea et al. 2007); numbers over the Moho map are crustal thickness values from previous studies. Each value has a color denoted in the legend except circled numbers in black. Black values inside colored circles are Moho estimates from Gök et al. (2008) (purple circle), Gritto et al. (2008) (green circle) and Nowrouzi et al. (2007) (red circle), respectively. The Moho in background is used in the initial model for forward modeling scheme and will be modified based on availability of other estimates from previous studies.

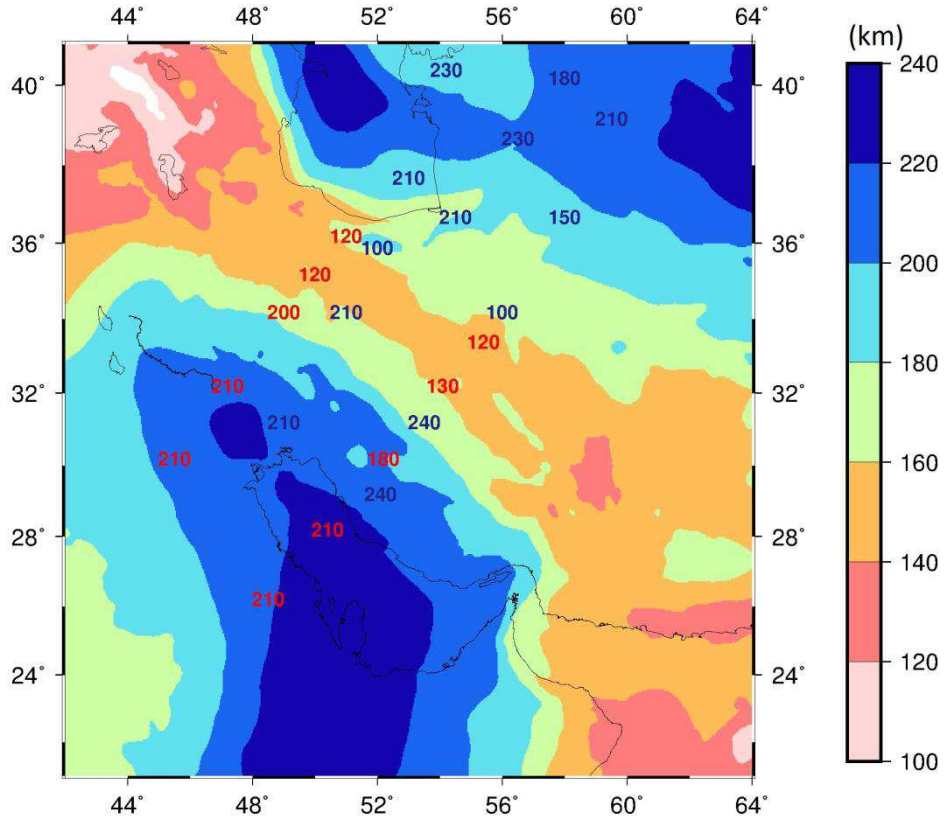

Figure 3.3. Depth to lithosphere-asthenosphere boundary (LAB) from inversion of geoid and elevation data (Fullea et al., 2007). Colored numbers indicate results from Motavalli-Anbaran et al. (2011) (in blue) and Tunini et al. (2015) (in red). In background, the LAB is used as the initial model in our 3D forward modeling scheme and will be modified based on previous studies and mainly for the purpose of fitting geophysical observables.

Mohammadi et al. (2013) imaged a relatively thick LAB with 130-150 km thickness beneath. Recently, Tunini et al. (2015) have tested the effect of mantle composition on density and seismic velocity beneath the Zagros collision zone. The main outcomes of the study by Tunini et al. (2015) in terms of lithospheric structure (along two transects across the Arabia–Eurasia collision zone) are: 1) The crustal thickness reaches ~63 km beneath the Zagros Mountains, progressively thinning to ~43 km under the Arabian Plate and Central Iran (Fig. 3.2), (2) The lithospheric thickness rises up to ~90 km beneath Central Iran and the Alborz Mountains, thickening to ~220 km below the Arabian Plate (Fig. 3.3), (3) Lithospheric mantle composition is represented by a Proterozoic Peridotite type beneath the Arabian Plate and progressively changes toward the Zagros Mountains to become a more depleted Harzburgitic composition.

3.3.2 Lithospheric mantle composition

Artemieva (2006) suggested s a Phanerozoic composition for the lithosphere beneath the Iranian Plateau (less than 50 Ma old). The continental lithosphere in Arabia seems to be of Neo-Proterozoic origin (~880 Ma) based on a wide variety of crustal and mantle xenoliths (Nasir, 1992; Abu-Aljarayesh et al., 1993; Grégoire et al., 2009; Nasir and Stern, 2012). To southeast,

the Oman Sea, with a bathymetry of near -4 km represent an oceanic lithosphere is a candidate for a young plate roughly ~50 Ma due to the relation between age and bathymetry (Doin and Fleitout, 1996).

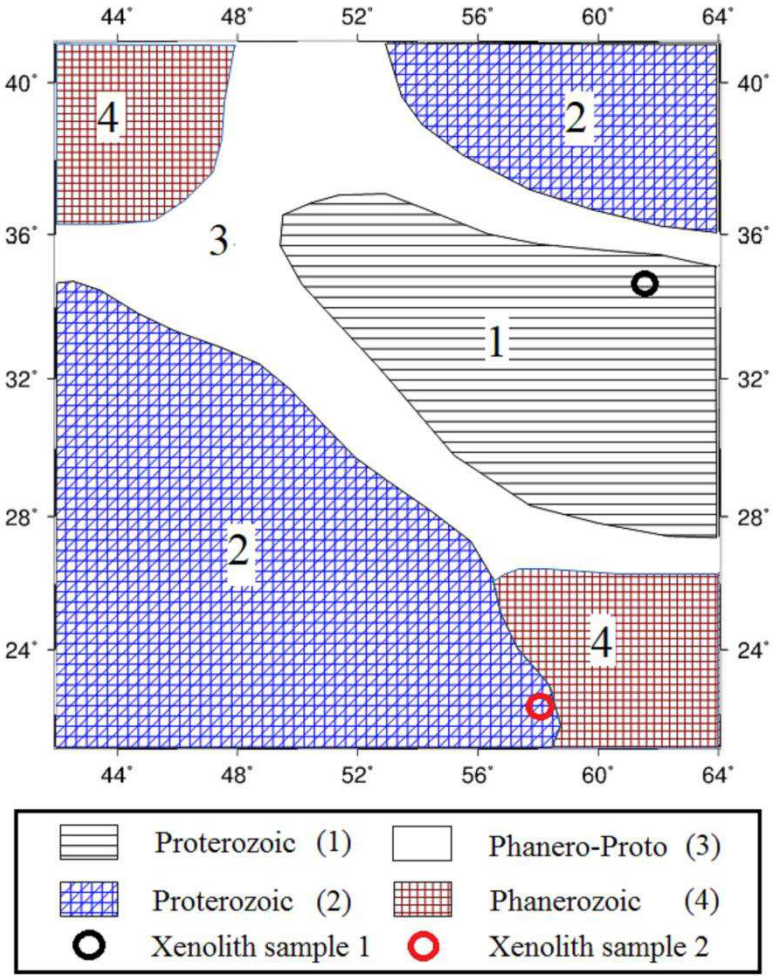

Figure 3.4. Lithospheric mantle composition domains based on tectonic hypothesis, petrological, and geophysical considerations. The numbers in figure correspond to the values in Table 3.1 (except Proterozoic (1), Ben-Xun Su, personal communication).

For setting our compositional model, I apply four different mantle compositional domains (Fig. 3.3. The lithospheric mantle in the northwest of Iran and in the Oman Sea is typical average Phanerozoic (mantle 4, Table 3.1). The mantle composition progressively changes from a Phanerozoic mantle at the southeast and northwest of Iran to more depleted mantle in collision zones of Zagros-Makran belt extended beneath the Alborz (south Caspian Sea) and counterparts under Kopet-Dagh unit (mantle 3, Table 3.1). In Central Iran I consider a Proterozoic type (mantle 1, Fig. 3.4) based on a xenolith suite in the northeast area (see Fig. 3.4 for location of xenolith sample 1). To define mantle 1 I averaged nine spinel lherzolite samples available as confidential data (Ben-Xun Su, personal communication). In the Arabian Plate, I apply a Proterozoic composition based on a xenolith suite reported by Nasir and Stern (2012) (mantle 2, Table 3.1). The same composition as for the Arabian mantle is applied to the Turan platform for

a similar affinity of lithosphere from tectonic background. Mantle 1 (Mg# 88.96) is the most fertile composition in the area while mantles 4, 2 and 3 (Table 3.1) are characterized by increased Magnesium numbers (Mg#=89.9, 89.93 and 90.453).

Table 3.1: Mantle compositions used in this study.

Oxides	Mantle Proterozoic (2)[1] Nasir and Stern, 2012	Mantle Phanero-Proto (3) Tunini et al., 2015	Mantle Phanerozoic (4) Griffin et al., 2009	PUM [2] McDonough and Sun, 1995
SiO_2	42.81	45	44.4	45
Al_2O_3	2.57	3	2.6	4.5
FeO	7.2	7.9	8.2	8.1
MgO	36.08	42	41.1	37.8
CaO	3.06	1.9	2.5	3.6
Na_2O	0.23	0.13	0.18	0.36
Mg #[3]	89.93	90.45	89.9	89.3

1. composed of mafic Granulite and spinel lherzolite
2. based on Peridotite, Komatiites and Basalts
3. Mg # = 100*MgO/(MgO+FeO)

* I must note that mantle 1 in central Iran micro-continent is a confidential data from Ben Su in china.

3.4 Geophysical data

I used multiple datasets to constrain our models: elevation, gravity, geoid anomaly and gravity gradients (Figs. 3.5 and 3.6). Free-air gravity is taken from the DTU10 dataset with a resolution of 1×1 min-arc (Andersen et al., 2010) (Fig. 3.5a). Bouguer anomaly is based on DTU10 free-air anomaly corrected for the Bouguer slab effect with a reduction density of 2670 kg m^{-3} (Fig. 3.5b).

Geoid undulations (Fig. 3.5c) for the under study area were derived from the global Earth model EGM2008 (Pavlis et al., 2008) with an original spatial resolution of ~10 km (up to order and degree 2190). To remove the effect of deep mantle sources, the geoid signal was filtered removing harmonic coefficients up to degree 9 (e.g., Bowin, 2000). Elevation data comes from the 1×1 min-arc resolution ETOPO1 global database (Amante and Eakins, 2009) (Fig. 3.1).

Gravity gradients are taken from the satellite mission GOCE (Bouman et al., 2016). Because of the low orbital height (~255 km) of the GOCE gravity data (Floberghagen et al., 2011), it has a high resolution (~80 km) in the transitional wavelength between earlier satellite and terrestrial gravity data (Ebbing et al., 2013). Satellite gradients at satellite level reflect local geology to only a small degree and are more sensitive to deep structures in the crust and lithosphere (Bouman et al., 2013). For the reason of that, measurement at height has less sensitivity to short wavelength features close the Earth surfaces despite the high accuracy of GOCE satellite data. Although, the downward continuation of measurements at satellite height enhances the signal and reflects better the short wavelength features (Bouman et al., 2013) the corresponding noise of

measurements is simultaneously amplified. Therefore, in this study I use gravity gradients at satellite height.

Satellite gravity gradient are given in Local North Oriented Frame (LNOF) where x, y and z components are pointing north (N), west (W) and upward (U) respectively (Bouman et al., 2013 and 2016). LitMod3D works in a Model Reference Framework (MRF) in which x, y and z are along east (E), north (N) and upward (U) direction. Therefore, xx, xy, xz, yy, yz, and zz components of observed gradients are shown by G_{NN}, G_{NW}, G_{NU}, G_{WW}, G_{WU} and G_{UU} in LNOF coordinates. These components are related to their one-by-one components in MRF, which are G_{EE}, G_{EN}, G_{EU}, G_{NN}, G_{NU} and G_{UU}.

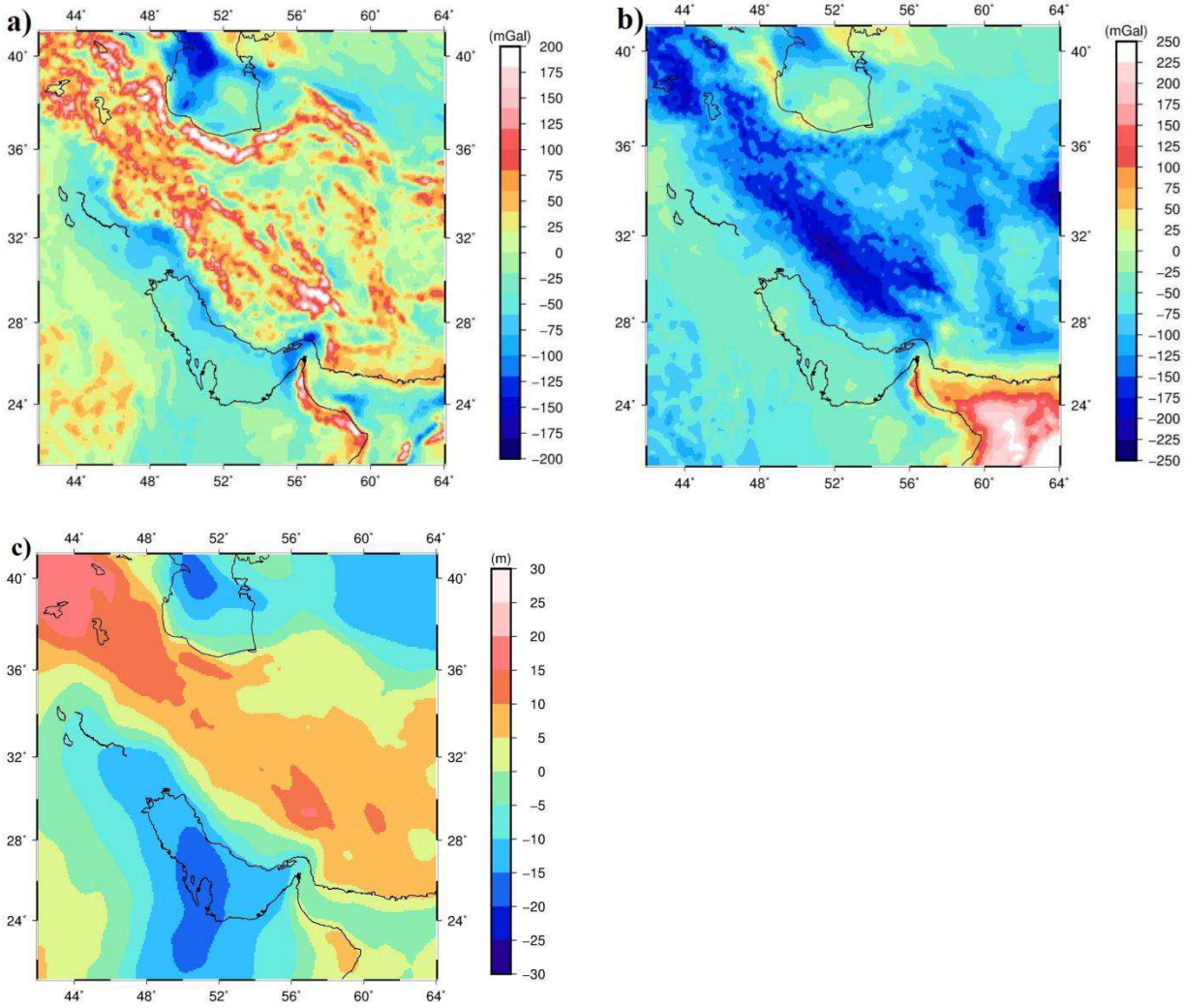

Figure 3.5. Geophysical data used in this study: a) Free-air anomaly, b) Bouguer anomaly, and c) Geoid anomaly. See text for further details.

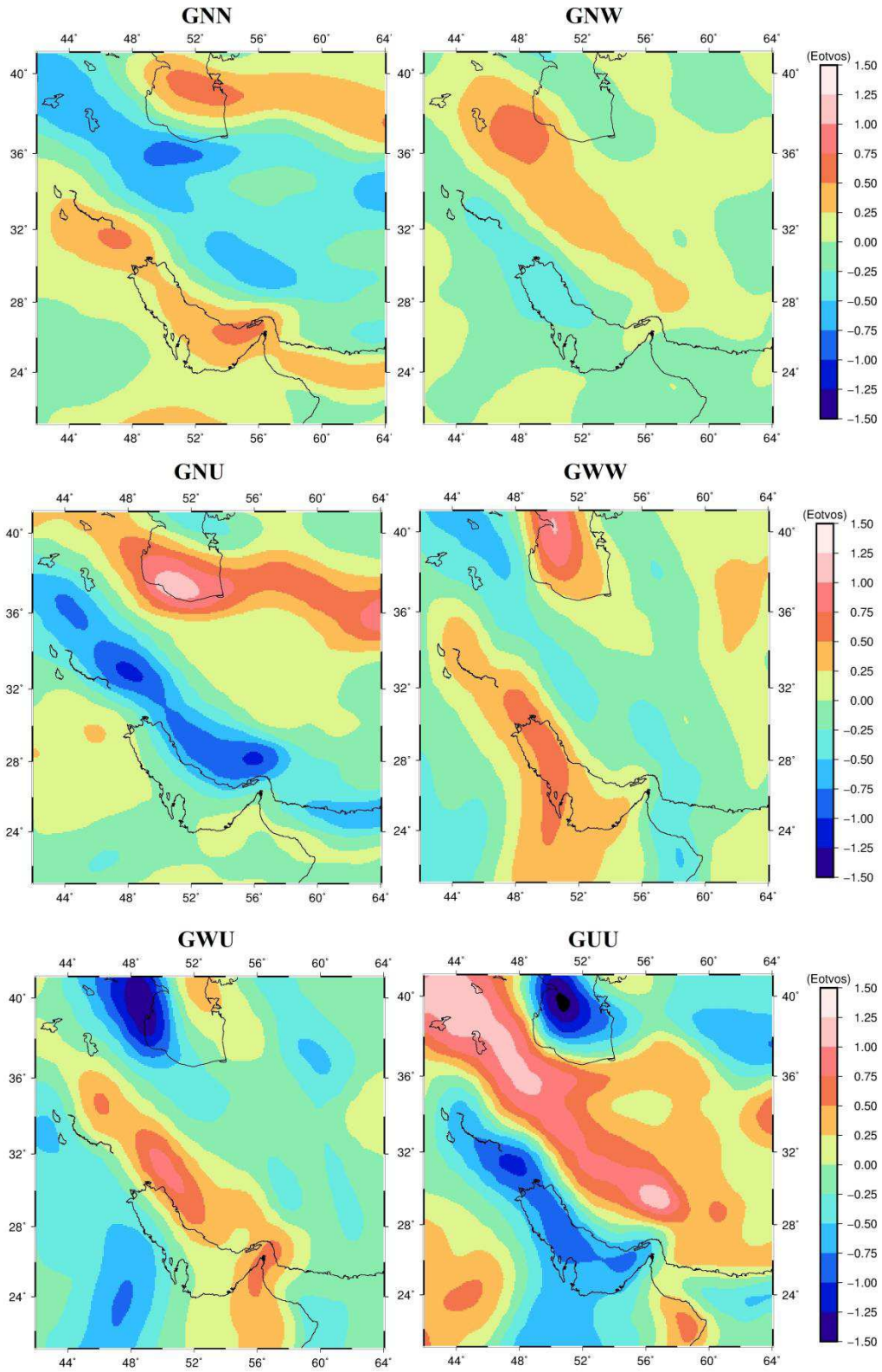

Figure 3.6. The full gravity gradient at 255 km above the ellipsoid; indices are north (N), west (W), and up (U) gradient components in the Local North Oriented Frame coordinate system.

3.5 Methodological background: Integrated geophysical-petrological modeling

To perform our integrated geophysical-petrological modeling within a self-consistent thermodynamic framework, I used the software (LitMod3D) described in detail in Fullea et al. (2009). Here, I present only a general overview of the main aspects of the method focusing on the fundamental prerequisites relevant to our study. Within the LitMod3D approach different equations describing the various physical (e.g., heat transport, or seismic wave propagation) and chemical processes (thermodynamic mineral phase equilibria) that link the thermochemical conditions within the Earth to geophysical-petrological observables are solved. An essential component of the integrated approach is to determine, within a thermodynamic framework, key physical parameters in the upper mantle (e.g., density and elastic moduli) as a function of pressure, temperature and bulk mineralogical composition.

I follow a trial and error procedure to estimate the 3D density, temperature, and composition distributions within the model matching various geophysical observables: elevation, geoid anomalies, gravity anomalies, and gravity gradients. Modeling several data sets simultaneously reduces significantly the uncertainties related to the modeling of these datasets separately or in pairs.

For thermal setting, the base of the lithosphere (LAB) separates the cold and relatively rigid layer (lithosphere) from the warmer and rheologically weaker asthenospheric mantle. The geotherms in the lithosphere are calculated by solving the 3D steady state heat conduction equation for a temperature-dependent thermal conductivity with appropriate boundary conditions are assumed; i.e., 0 ℃ at the surface, 1330 ℃ at LAB and no lateral heat flow across the vertical boundaries. Lateral heat flow may be associated with convection currents which are not included in current version of LitMod3D. In sub-lithospheric mantle, an adiabatic gradient is considered (e.g., Fullea et al., 2009). Below the rigid part of lithosphere, the heat transfer does not occur in a pure conduction form anymore (Turcotte and Schubert, 2002). However, it is high likely both conduction and convection mechanisms are responsible for heat transfer for several kilometres beneath lithosphere. Therefore, between the lithosphere and sub-lithospheric mantle I parameterize a "transition" region (a buffer or boundary layer) of variable thickness and characterized by super adiabatic gradient (i.e., heat transfer is controlled by both conduction and convection mechanisms, see Fullea et al. (2009) for details).

Stable mineral assemblages in the mantle can be determined using a Gibbs free energy minimization approach as described by Connolly (2005, 2009). The compositional space is defined within the major oxide system NCFMAS (Na_2O-CaO-FeO-MgO-Al_2O_3-SiO_2) that accounts for >98 wt% of the Earth's crust and mantle. Vertically, I define two chemically distinct mantle domains in our model: the lithospheric mantle, and the sub-lithospheric mantle. In the sub-lithospheric mantle I assume an average and fixed fertile primitive composition (i.e., PUM in Table 3.1). All the stable assemblages in this study are computed using a modified/augmented version of the Holland and Powell's (1998) thermodynamic database (Afonso and Zlotnik, 2011). The density in the mantle is derived from the density of each of the stable end-member minerals (e.g., Connolly and Kerrick, 2002; Afonso et al., 2008).

3.6 Modeling results

The initial model is set up by considering a first-order estimate of Moho and LAB depths (section 3.1) and unified mantle composition for the entire region. This model assists to examine whether using homogenous composition without modification on inversion-based structure (Moho and LAB) leads to fitting the geophysical observables. In addition, I decide on the best candidate among others for mantle composition background. Bearing in mind, using a unified mantle composition for a wide area with varying tectonic and structural features is very far to be a realistic approach. Summarized in section 3.2, I applied our proposed compositional domain (Fig. 3.4) to the initial mode. Later, for fitting geophysical observables, I modified the initial structure (Moho and LAB including intra-crustal layers).

3.6.1 Homogenous lithospheric mantle and inversion-based geometry

I start the modeling considering a two-layered model (crust and lithospheric mantle) derived from 1D combined inversion of elevation and geoid anomaly data (Figs. 3.2 and 3.3) in which lithospheric mantle density is temperature dependent (Fullea et al., 2007). This method has been used previously in the Arabia-Eurasia collision zone (Jiménez-Munt et al., 2012).

A number of numerical experiments were carried out to find whether uniform lithospheric mantle composition and geometry model derived from inversion without any modification would fit better the geophysical data.

Table 3.2: The test model is composed of crust, lithosphere and asthenosphere using Moho and LAB depths inferred from inversion (Figs. 3.2 and 3.3). The density in crust varies linearly with depth and the density in the lithosphere and asthenosphere is temperature and composition dependent. Through using four candidates for mantle composition beneath the Iranian Plateau (Table 3.1), the fit to observables has been formulated by showing statistics (mean and standard deviation) of the misfit (observed minus calculated values) in each test.

Composition No.		Elevation (m)	Geoid (m)	Bouguer (mGal)	FA (mGal)
2	mean	2007	0.002	1.61	1.15
	Std.	284	11.92	31	30.47
3	mean	1787	0.003	1.57	0.11
	Std.	274	10.79	30.2	29.65
1	mean	739	0.004	1.57	0.29
	Std.	195	9.81	24.21	24.38
4	mean	1091	0.004	1.69	0.23
	Std.	194	7.05	24.61	24.41

For the background composition of entire lithosphere beneath the Iranian Plateau, I chose a composition that minimizes the data misfit among different candidates (Fig. 3.7 and Table 3.1). The composition of Iran (mantle 1 in Table 3.1) resulting in a density distribution that, on average, matches the constraining geophysical observables used in this work, compared to other compositions. Different tests, using a sensible range of composition for the lithospheric mantle beneath the Iranian Plateau, indicate that the initial model without any geometrical/compositional modification fails to explain the constraining data (gravity field and isostatic elevation). In addition, I can conclude that the lack of lateral variation in composition and crustal structure over the area leads to a poor fit to geophysical observables (Fig. 3.7 and Table 3.2).

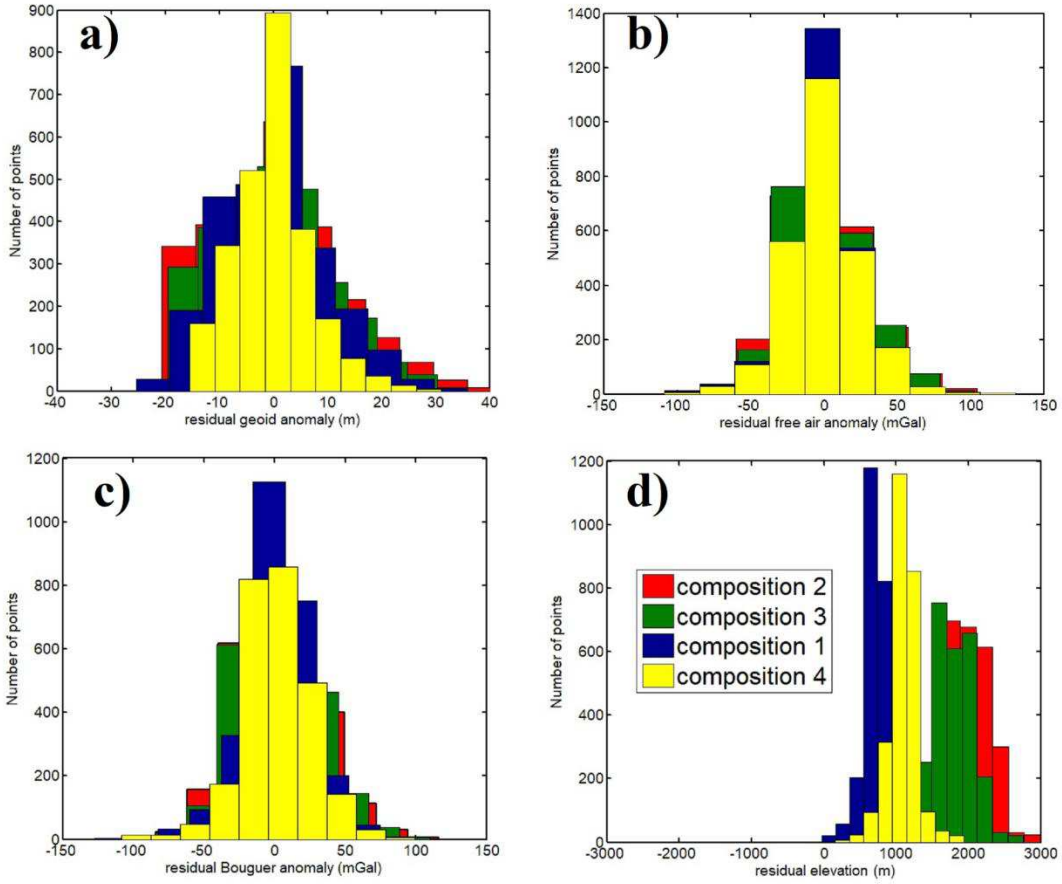

Figure 3.7. Histogram of the residual anomalies: a) free-air anomaly, b) Bouguer anomaly, c) geoid anomaly and d) elevation; each plot displays histograms of residual anomalies corresponding to different tests using different compositions for entire area listed in Table 3.1. Mantle composition 1 provides a relatively better fit to observables among others. The difference in elevation misfits is clearly distinguishable.

Mantle 1 (Table 3.1) characterizes mainly the mantle lithosphere beneath the NE of Iran (from xenolith sample, Su et al., 2014) but characterizes the background composition for entire area (Table 3.2 and Fig. 3.7). Comparing Figs. 3.2, 3.8b and 3.8d shows the correlation between free-air residual anomalies and the shallow Moho depth used in the initial model. Further, a thicker

crust is supportable by previous seismic studies, which I have already discussed in section 3.1 and summarized in Fig. 3.2.

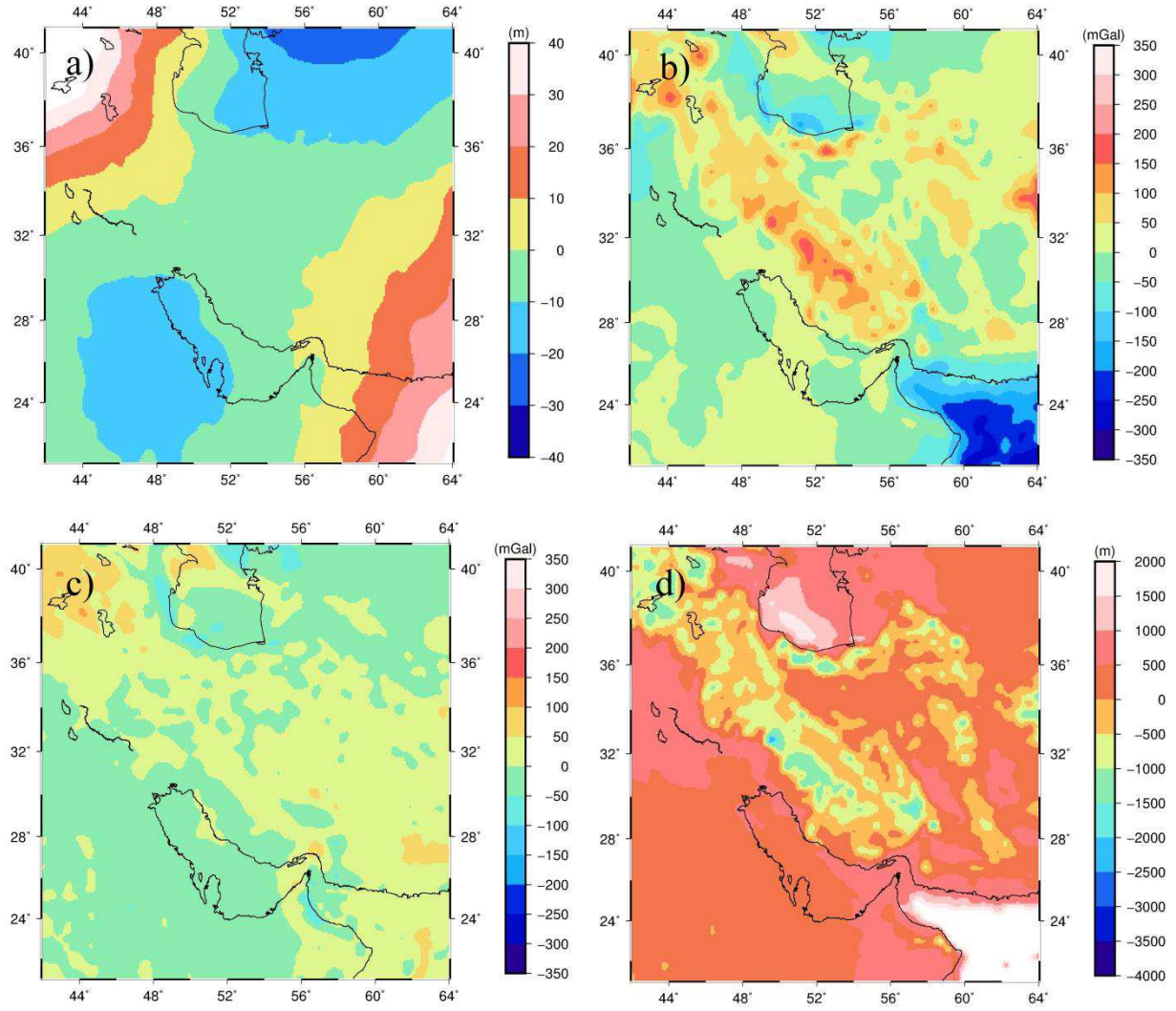

Figure 3.8. Residual geophysical anomalies (misfits between calculated and observed data) obtained from model using mantle 1 (Table 3.1) for uniform lithosphere. The misfits indicate an inappropriate density distribution using mantle 1 for entire area. The density distribution of the model reflects in geophysical observables. Importantly, the uncertainty from all observables and model structure (crust and lithosphere) are similar through different tests that allow estimating only the effects of compositional dependent density on potential field data.

The large magnitude elevation residual is present in the Oman Sea (Fig. 3.8d). This residual anomaly can be removed by either a thinner crust or a lithosphere thickening. This is because LitMod3D calculates the elevation based on assumptions of the isostasy (Afonso et al., 2008 and Fullea et al., 2009). Geophysical misfits shown in Fig. 3.8 illustrate that using mantle 1 in Oman Sea fails to predict geophysical data. It suggests either modifying geometry of the model or

changing the composition to less dense material while using initial Moho and LAB depths from inversion. From the geoid residual anomaly (Fig. 3.8a), the mantle 1 leads to a high density in both the northwest of the area and the Oman Sea where lithospheric thickness is not so high. This contradicts using such a highly fertile Phanerozoic mantle (mantle 1, Table 3.1) for these regions, which may be more suitable only for composition of central Iran domain where xenolith sample locates (Fig. 3.4).

Using a highly fertile composition, in the Turan platform (northeast of the area, Fig. 3.1) and the Arabian Plate (southeast of the area, Fig. 3.1) restricts the best fit to the observed geoid anomaly (Fig. 3.8a). In addition, the xenolith samples suggest a depleted Proterozoic type for the mantle composition beneath the Arabian Plate (e.g. Nasir and Stern, 2012). However, there is no mantle xenolith available close to the Turan platform. As the region (the Turan platform domain in the NE portion of mantle 2, Fig. 3.4) is not largely extended, I assume the effects of composition from this domain are limited. Theoretically, using the same composition of the Arabian Plate for the Turan platform avoids the density model undulating so largely.

3.6.2 Heterogeneous lithospheric mantle and crustal structure

As using homogeneous lithospheric mantle failed to explain simultaneously all constraining data, I applied a plausible 3D compositional heterogeneities of the lithospheric mantle beneath the Iranian Plateau (Table 3.1 and Fig. 3.4).

A reliable crustal structure compatible with previous studies (Fig. 3.2) needs to be defined and kept fixed in the mantle modeling process. The crustal model considered in this study consists of seven layers (characterized by different physical properties, see Table 3.3): 4 types of sediments, upper, middle and lower crust. For the sediments I consider different density values based on lithology (Table 3.3) distinguishing between (1) the Caspian Sea and Oman sea (very low density sediments), (2) Central Iran (Cenozoic, medium dense sediments), (3) and the Arabian Plate and the Turan platform (Mesozoic, dense sediments). The Paleozoic sediments are mainly underlying the Zagros-Makran belt and the Alborz-Kopet-Dagh (Paleozoic). Each layer has an average thickness of ~10 km (Fig. 3.9). It must be noted that granitic and metamorphic complexes are distributed in the margins of collision zones (Zagros, Makran, and Kopet-Dagh) and Central Iran; however, based on their density, similar to that of the Paleozoic sediments (Tunini et al., 2015; Mousavi et al., 2017; Mousavi and Ebbing, 2018), I model these bodies as part of the Paleozoic sediments (Table 3.3).

3.6.2.1 Lithospheric structure

The thinnest crust in our model is present in the Oman Sea (25-30 km) rising up to ~35 km in the south Caspian Sea (Fig. 3.9a). Our Moho reaches a maximum of ~65 km depth in the high Zagros and is moderately deep in the Alborz Mountains and the eastern part of Central Iran. In the other high topography areas, in particular, the northwest of Iran there is not significant crustal root in our model (Fig. 3.9a). A very thin crust (~30 km) is observed in Talesh Mountains west of the Caspian Sea.

Table 3.3. Physical properties of the materials used for modeling in the crust, lithospheric mantle, and asthenosphere; ρ (kg/m^3), K [W (km)$^{-1}$], and H (μWm^{-3}) and β (GPa) represent density, thermal conductivity, volumetric heat production and compressibility respectively.

No.	Material description	density	Thermal conductivity	Heat production rate	Compressibility
-	Water	1030	-	-	0.0
1	Sediment_Caspian and Oman Sea	2450	2.0	1	0.0
2	Sediment_Central Iran	2550	2.0	1	0.0
3	Sediment_Arabia_Turan	2650	2.2	1	0.0
4	Paleozoic sediments	2730	2.5	1	0.0
5	Upper crust	2850	2.8	1	0.0
6	Middle crust	2850	2.1	0.4	0.0
7	Lower crust	2910-3100	2.0	0.1	14×10^{-4}
8	Dense lower crust (Central Iran)*	3100-3250	2.0	0.1	28×10^{-4}
m1, m2 m3, m4	Lithospheric mantle	**	***	0.01	-
-	Sublithospheric mantle	**	-	-	-

* only in model assuming asthenospheric heterogeneities (Chapter 4). The presence of slab in asthenosphere requires the modification of LAB depth in order to compensate the mass excess reflected in calculated potential field data. However, thinning of lithosphere causes lack of mass in lithosphere body. Increasing density of crust compensate the inferred mass shortcoming after adding slab. ** Mantle densities are computed according to the corresponding temperature, pressure and bulk composition, see section 5 for more details. Density is calculated based on characteristics of the chosen composition in specific temperature-pressure condition. *** The temperature-dependent thermal conductivity is computed iteratively while solving the thermal problem. LitMod3D assumes that the thermal gradient in lithosphere are equivalent to the amount of heat production, literally means the model is in steady-state condition assuming no convection current in the model.

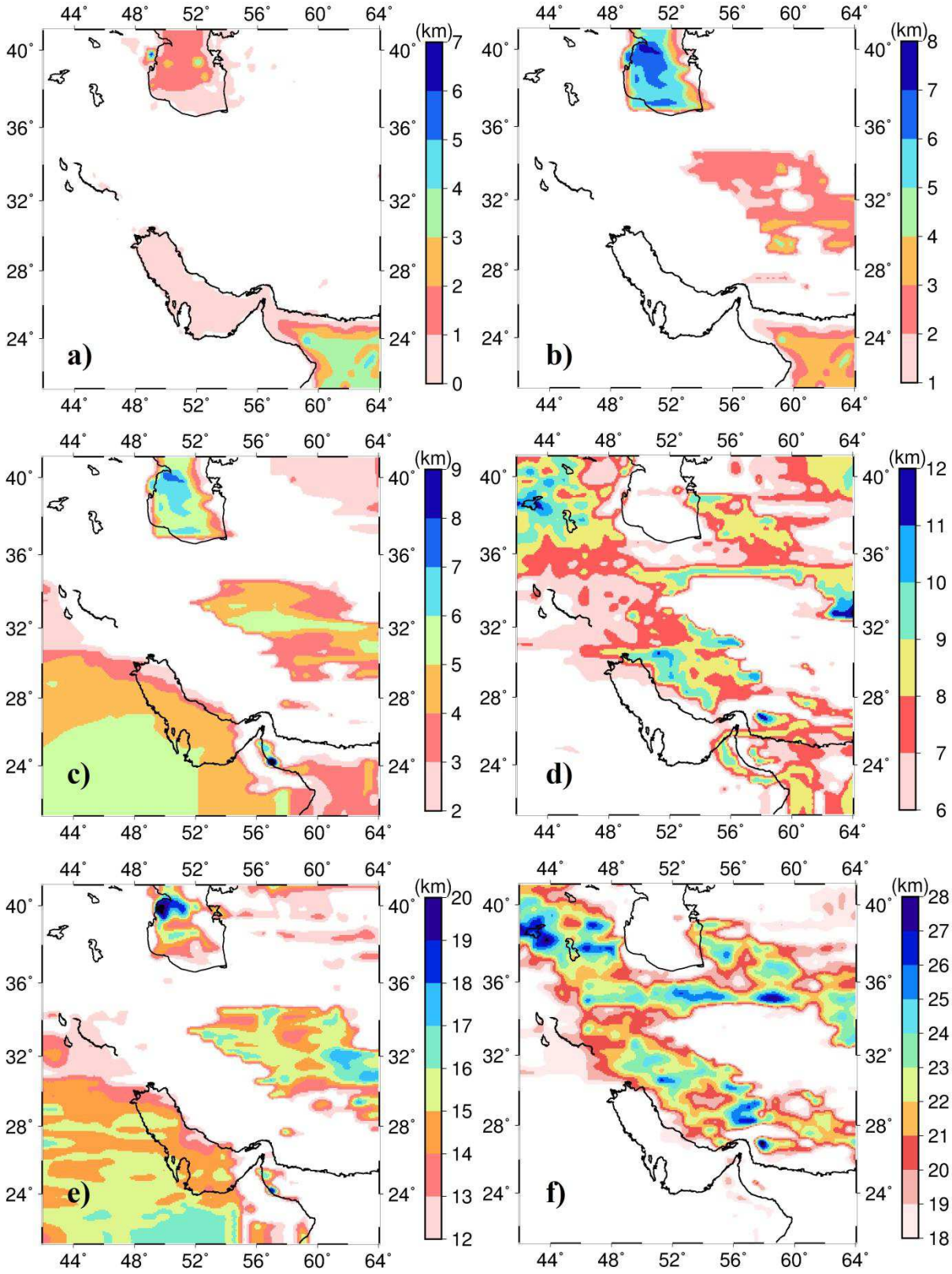
a)
b)
c)
d)
e)
f)
(km)
44° 48° 52° 56° 60° 64°
40° 36° 32° 28° 24°
0 1 2 3 4 5 6 7
1 2 3 4 5 6 7 8
2 3 4 5 6 7 8 9
6 7 8 9 10 11 12
12 13 14 15 16 17 18 19 20
18 19 20 21 22 23 24 25 26 27 28

Figure 3.9. Intra crustal interfaces separating: a) 1: very low and low dense sediments, b) 2: low and medium dense sediments, c) 3: medium and high dense sediments, d) 4: Paleozoic sediments and upper crust, e) 5: upper and middle crusts, and f) 6: middle and lower crusts. Numbers in (a) to (f) refer to Table 3.3.

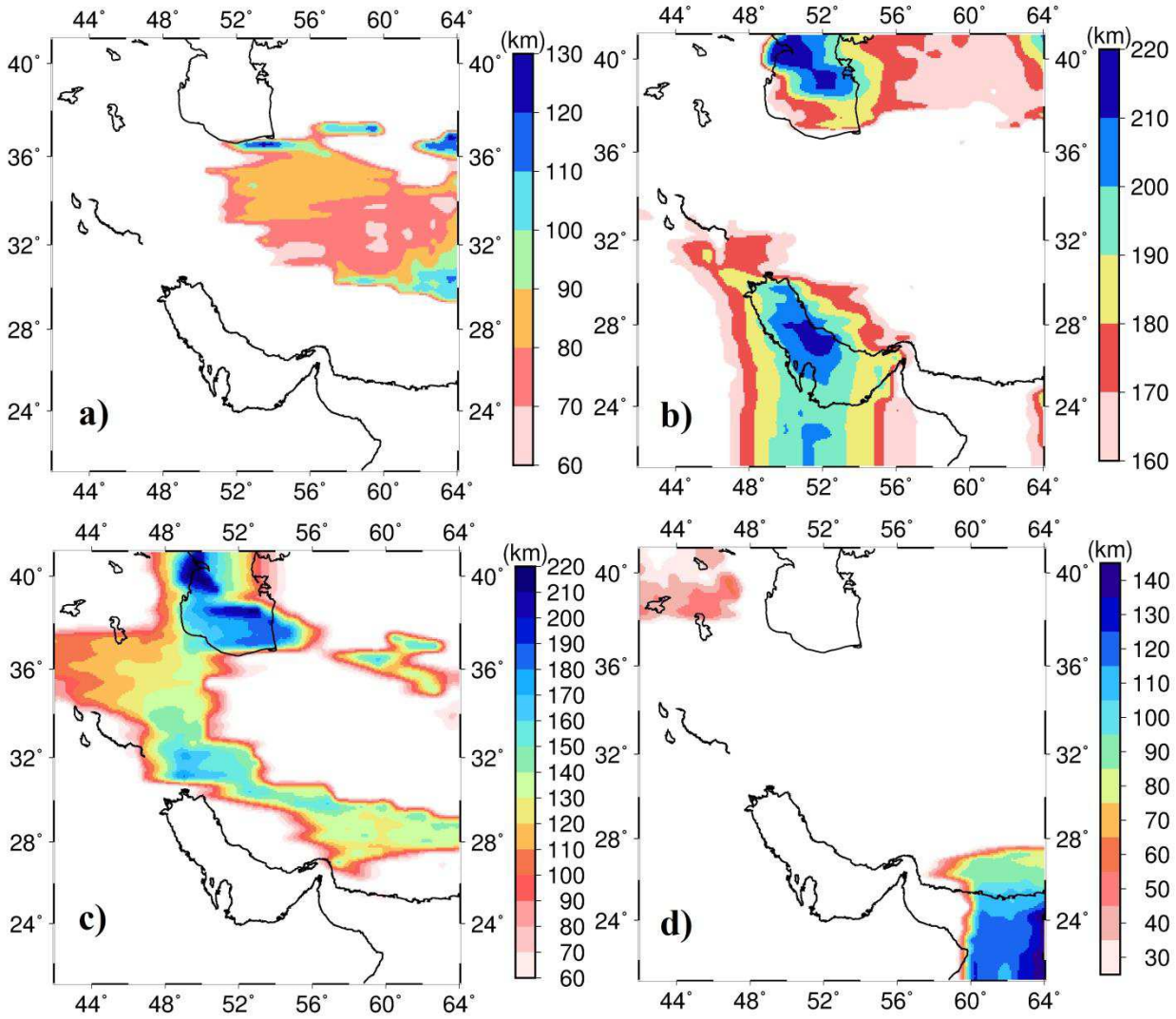

Figure 3.10. Lithospheric mantle interfaces (distinguishing lithospheric mantle domains in our model). a) Proterozoic upper mantle No. 1, b) Proterozoic upper mantle No. 2, c) Phanero-Protro upper mantle No. 3, and d) Phanerozoic upper mantle No. 4. Numbers refer to Table 3.1. The depth values are normalized by subtracting Moho depth from absolute lithosphere depths. The subtraction of Moho depth from LAB depth has been performed for the purpose of visualization while each compositional domain appears independently and colors denote the lithospheric thickness instead of absolute depth of LAB referenced to ground surface.

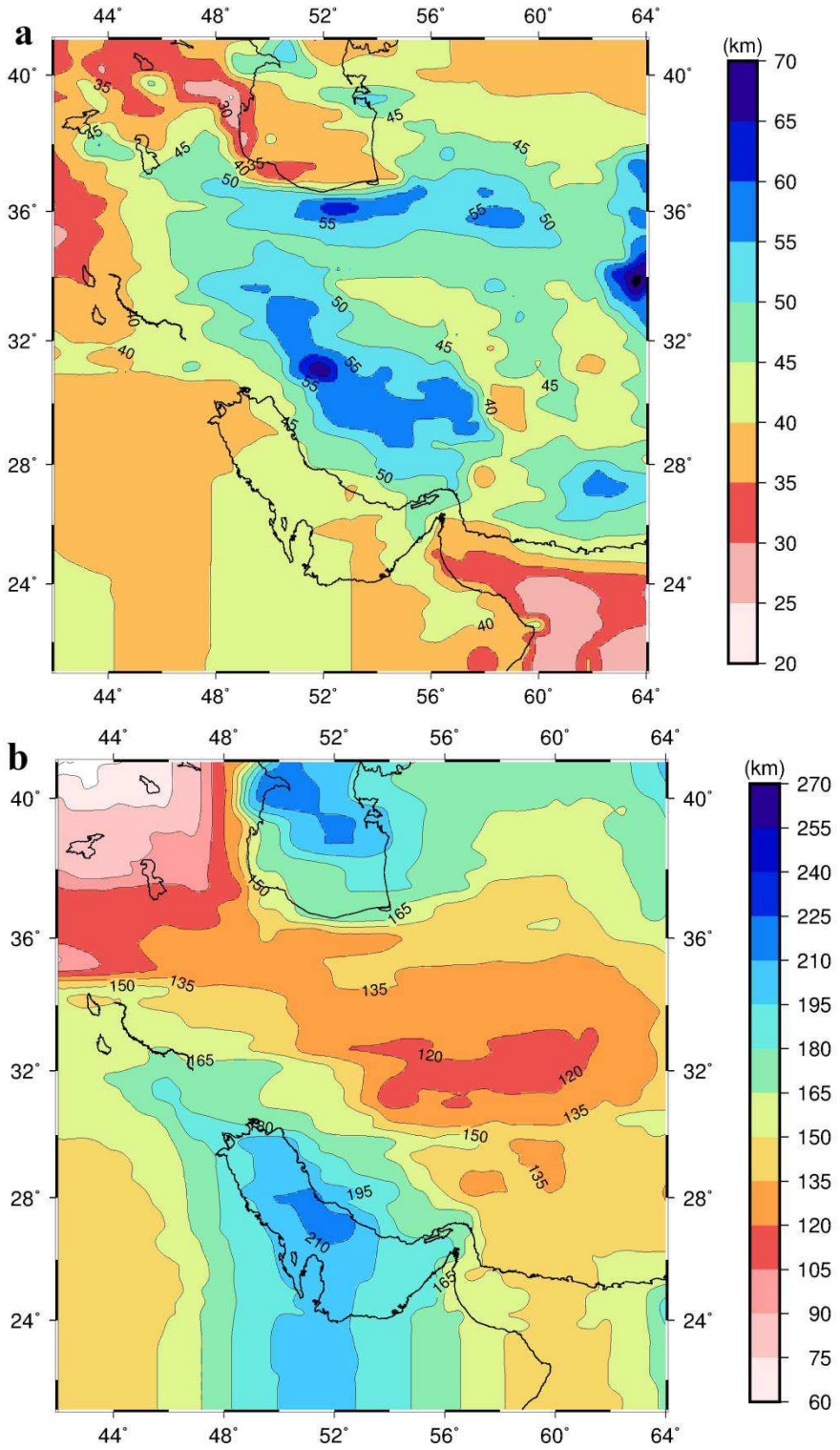

Figure 3.11. a) Final Moho depth and b) LAB depth obtained from integrated modeling of elevation, gravity potential fields, xenolith data and gravity gradients of the Iranian Plateau.

A thin lithosphere is modelled in the northwest of Iran (up to ~65 km) while the LAB depth falls down to ~160 km in the southern part of Central Iran, the Oman Sea, and the eastern part of Arabian Plate (Fig. 3.10b). Furthermore, the LAB in the Persian Gulf and the Caspian Sea is relatively deep ~210 km with the deepest parts reaching to ~220 km locally. The general trend of the LAB follows the initial model geometry (Figs. 3.3 and 3.11), with the largest changes being located in the Oman Sea that requires a thicker lithosphere to match our constraining data.

3.6.2.2 Geophysical residual anomalies

Residual anomalies (observed minus calculated values) indicate that our final heterogeneous model can fit data reasonably well (Figs. 3.12 and 3.13). However, there are some local free-air and isostatic elevation residual anomalies that can be explained by simplifications in the upper crustal density structure (i.e., sediments, metamorphic, and igneous/ophiolite complexes). In general, the residual Bouguer anomaly and gravity gradient maps show a good fit to observed data (Figs. 3.12 and 3.13).

Satellite gravity gradient components are sensitive not only to the amplitude and location of mass anomalies but also to its spatial orientation (i.e. mass "directionality"). The gravity gradient residuals are relatively small except for G_{EU} gravity gradient component (Fig. 3.13). G_{EU} residual misfit is comparatively large in southeast of the study area (the Makran subduction zone, Fig. 3.1). This larger misfit is likely related to S-N oriented density contrast imposed by a subducting slab.

The model including only lithospheric compositional heterogeneities beneath the Iranian Plateau (Fig. 3.11) can fit geophysical observables. I expect some discrepancies between this model and previous works due to additional constrains from lithospheric chemical composition applied in this study. Bearing in mind, using only geophysical modeling to define the thermochemical structure of the Earth's interior is in general highly uncertain (Afonso et al., 2013a, b). However, this model has a stronger support if it will be able to predict velocity anomalies suggested by seismic tomography models (e.g. SL2013sv, Schaeffer and Lebedev, 2013).

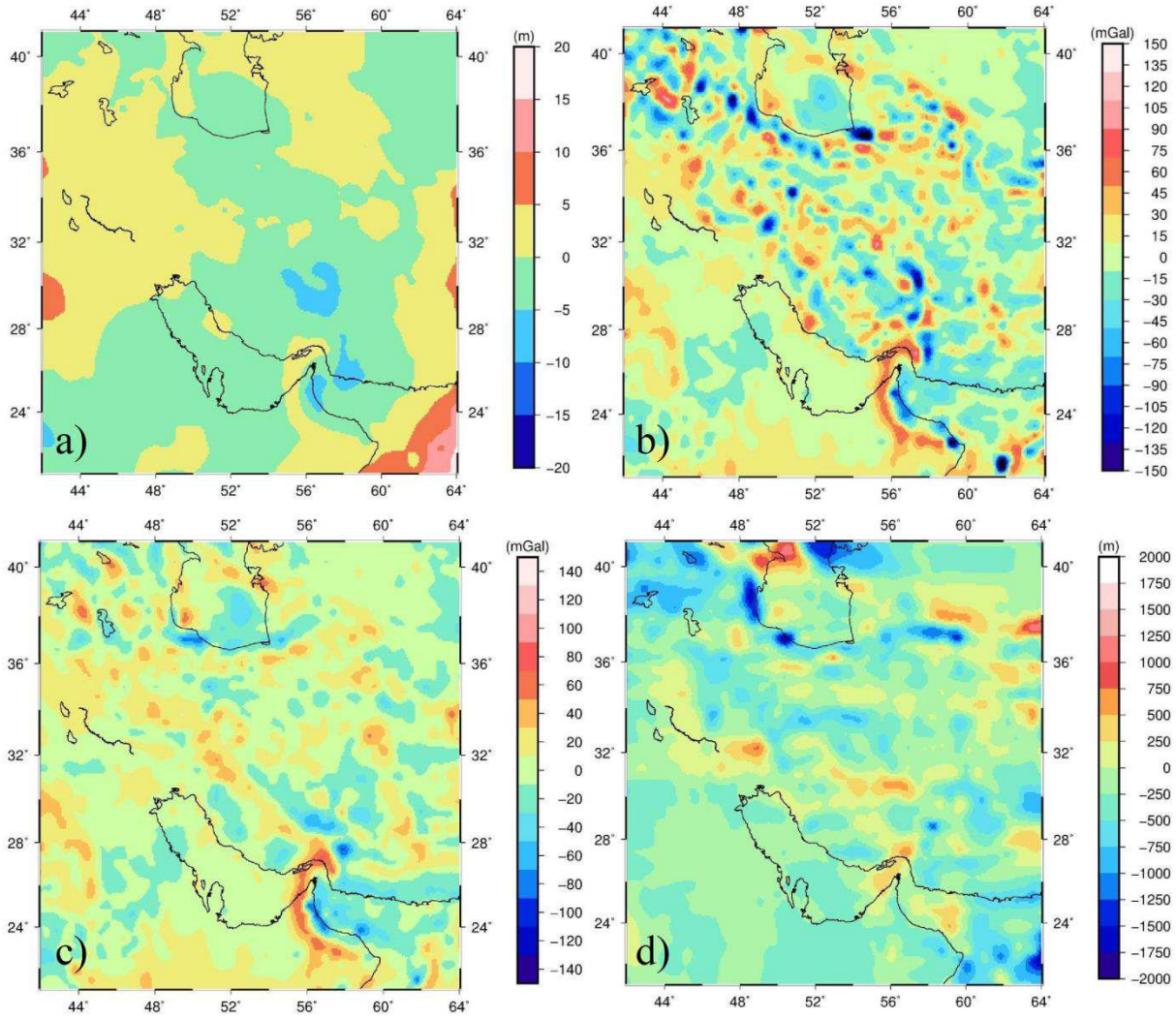

Figure 3.12. Residuals for the best fitting model including intra-crustal layers and lithospheric heterogeneities. a) Geoid anomaly, b) Free-air anomaly, c) Bouguer anomaly and d) elevation.

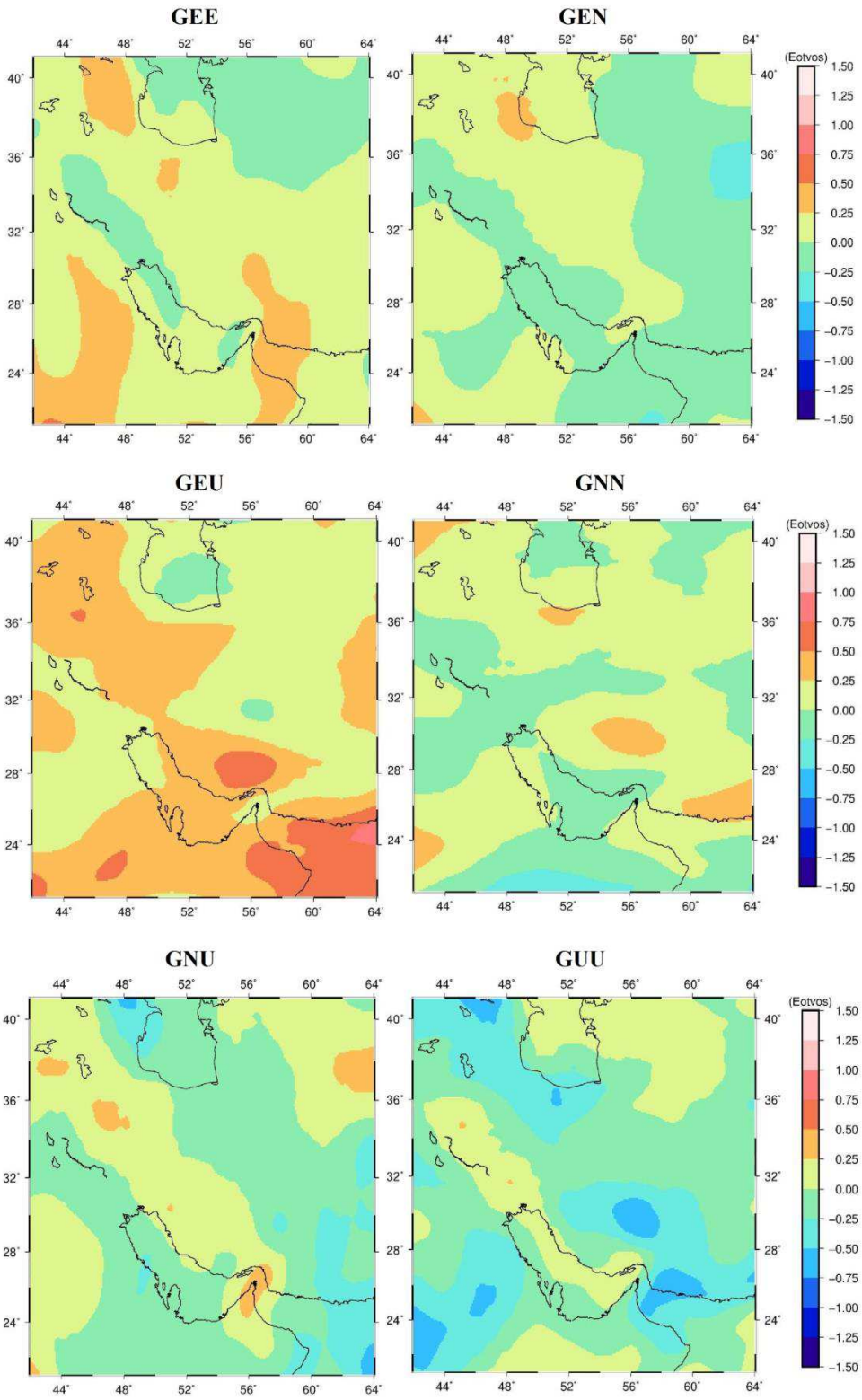

Figure 3.13. Residual maps of gravity gradient components for the best fitting heterogeneous lithospheric model. The calculated and observed gradients have been compared in Model Reference Frame.

3.7 Discussion

In the following, first, I illustrate the first model assuming lithospheric heterogeneities but owning homogenous asthenosphere. Four transects through the model have been selected to discuss the different characteristics of our heterogeneous lithosphere (Fig. 3.14). I expect some discrepancies between our first estimate of LAB (in the absence of slab) with previous estimates due to: i) the present 3D approach to model density structure that highlights the lateral effect which is rarely considered in previous studies (Molinaro et al., 2005; Motavalli-Anbaran et al., 2011; Tunini et al., 2015) and ii) lack of compositional effects in the previously pure thermal modeling of lithosphere beneath the Iranian Plateau.

3.7.1 Crustal layers and lithospheric compositional domains

The transect AA', which cuts three mantle compositional domains, is characterized by thick crust beneath the Alborz Mountains (≥55 km) and a relatively thin crust below the Caspian Sea (~40 km). The LAB rises up to ~135 km in a thick crust area under the Alborz Mountains. In Profile BB', the LAB is located at ~125 km depth below Central Iran deepening to ~180 km depth below the northern part of the Arabian Plate. A decrease in LAB depth is also seen towards the northeast after Kopet-Dagh in Turan platform. The most striking feature of the model along the three parallel profiles crossing Zagros Mountains is a significant thinning of the lithospheric mantle beneath Central Iran, shown in Figs. 3.14a, 3.14b and 3.14c.

The Proterozoic nucleus of the Iranian Plateau is surrounded by a Phanero-Proto type mantle (mantle 3, Table 3.1) overlain the Zagros, Alborz, and the Kopet-Dagh Mountains. The low CaO and high MgO content of mantle 3 marks a depleted Phanerozoic composition related to melt extraction in the framework of Neo-Tethys subduction (Agard et al., 2011; Ghasemi and Talbot, 2006). In contrast, CaO and MgO contents in the mantle xenolith sample 2 (Table 3.1) indicates this composition is more fertile than the average Phanerozoic type (e.g. Griffin et al., 2009). The transition from depleted Phanerozoic to a fertile Proterozoic composition and again fertile to depleted composition occurs in the northwest-southeast along profile DD´ (Fig. 3.14d). As can be seen, the highest densities in the lithospheric mantle are found in the Persian Gulf due to the combined effects of composition and a low temperature associated with lithospheric thickening (Fig. 3.14b).

Our LAB in all profiles follow the general trend of initial model from combined inversion, which is more smoothed, compared to those suggestions from the pure thermal geophysical modeling. Neither our inversion nor forward results supports the dramatic undulation of modelled LAB by Motavalli-Anbaran et al. (2011) (Figs. 3.14a and 3.14b). However, our LAB depth along Profile BB´ has satisfactory consistency with suggested LAB depth by Tunini et al. (2015). In order to avoid very crowded visualization of cross section, I compare our modelled Moho with seismically based one from Paul et al. (2006 and 2010). The result of this comparison illustrates the consistency of our crustal structure compared to the previous estimates except our Moho is, in general, smoother.

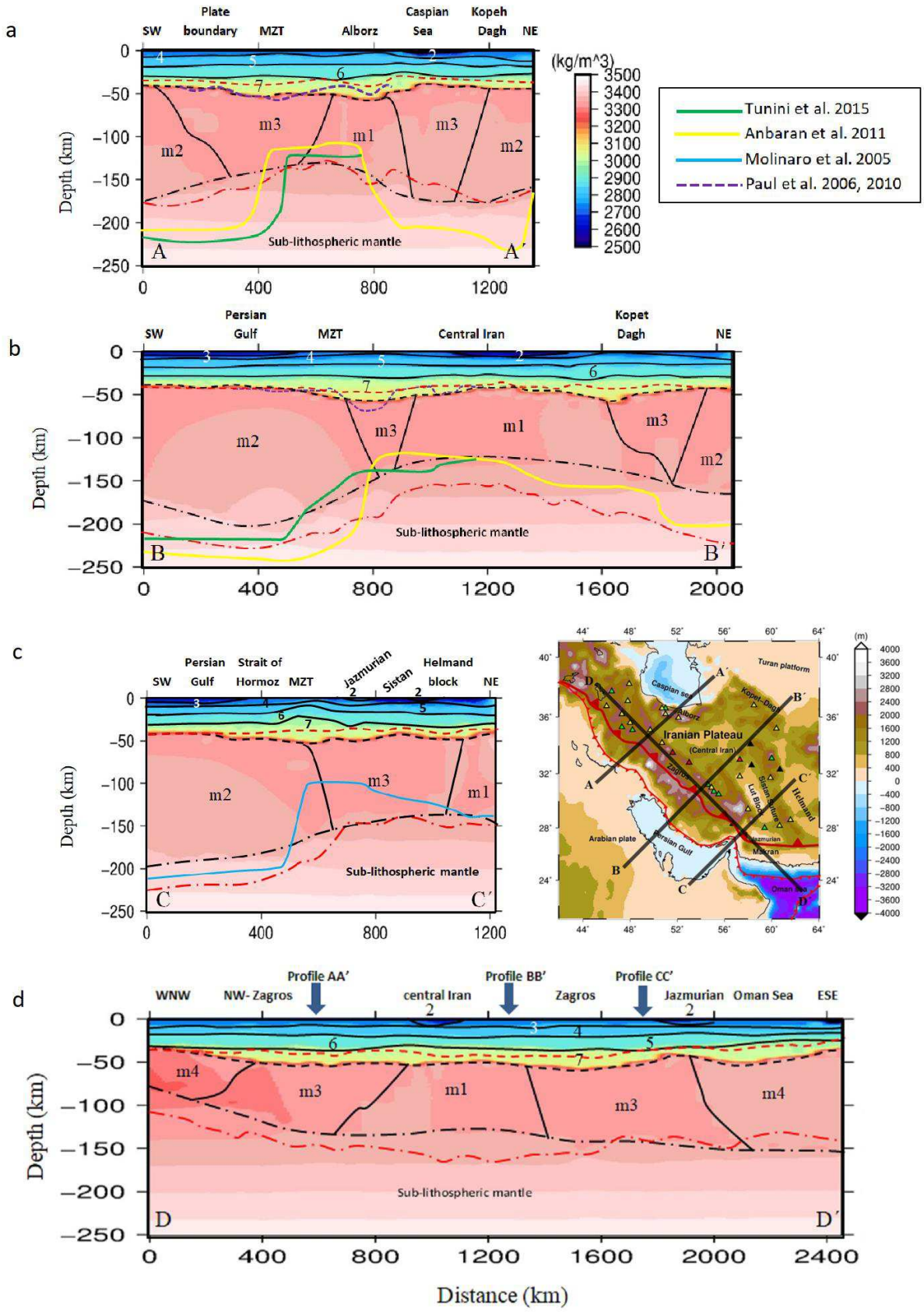
a
SW
Plate boundary
MZT
Alborz
Caspian Sea
Kopeh Dagh
NE
Depth (km)
m1
m2
m3
Sub-lithospheric mantle
A
A′
(kg/m^3)
Tunini et al. 2015
Anbaran et al. 2011
Molinaro et al. 2005
Paul et al. 2006, 2010
b
SW
Persian Gulf
MZT
Central Iran
Kopet Dagh
NE
Depth (km)
m1
m2
m3
Sub-lithospheric mantle
B
B′
c
SW
Persian Gulf
Strait of Hormoz
MZT
Jazmurian
Sistan
Helmand block
NE
Depth (km)
m1
m2
m3
Sub-lithospheric mantle
C
C′
Turan platform
Caspian sea
Kopet-Dagh
Alborz
Iranian Plateau
(Central Iran)
Zagros
Sistan Suture
Lut Block
Helmand
Arabian plate
Persian Gulf
Jazmurian
Makran
Oman Sea
A
A′
B
B′
C
C′
D
D′
(m)
d
Profile AA’
Profile BB’
Profile CC’
WNW
NW- Zagros
central Iran
Zagros
Jazmurian
Oman Sea
ESE
Depth (km)
m1
m3
m4
Sub-lithospheric mantle
D
D′
Distance (km)

Figure 3.14. Profiles across our heterogeneous lithospheric model. a) Profile AA', b) profile BB', c) profile CC', and d) profile DD'; dashed lines indicate the Moho depth and dotted-dashed lines are LAB depths. Red lines are initial model (from inversion) and black lines are results from this study (only lithospheric heterogeneities). Different crustal bodies and lithospheric mantle compositions are denoted by different numbers as described in Table 3.1 and Table 3.3, respectively.

3.8 Conclusion

Here, I introduced a forward step to better understanding of on three-dimensionality problem of lithospheric mantle structure below Iran. This study puts constraints on the mantle composition beneath Iran based on various geophysical observables. Our proposed 3D lithospheric composition distribution is supported mainly by in-situ xenolith samples and suggested mantle composition from previous 2D studies. Interestingly, our preferred model reproduces the main seismic features (both magnitude and location) suggested by tomography models.

Compositionally, the modeled lithospheric structure is characterized by the most depleted lithospheric mantle in the area underlying the Zagros-Makran belt in similar to the Alborz-Kopet-Dagh Mountains. Following tectonic scenario of the area and the best fitting geophysical model, the same composition was proposed for Turan platform, in southwest Eurasia. The Oman Sea and northwestern Iran mantles are candidates for more fertile composition than in the Zagros collision zone.

From a structural point of view, the main characteristics of our final lithospheric model are:

(1) a thick lithosphere beneath the Arabian Plate, north of the Persian Gulf, and beneath the northern part of the Caspian Sea;
(2) a comparatively thin LAB beneath Central Iran and progressive lithospheric thinning from Central Iran toward the northwest;
(3) a thick crust below the Zagros, Alborz, and eastern part of the Central Iran;
(4) a crustal thinning beneath the Oman Sea and the northwest of Iran.

In conclusion, the obtained Moho depth and LAB are in general agreement with previous lithosphere models, but slightly different in terms of depth to the LAB, and especially the sharpness and location of the lithospheric mantle thinning.

Chapter 4:

Integrated geophysical-petrological modeling of sub-lithospheric structure due to Neo-Tethys slab break-off

4.1 Introduction

In order to model sub-lithospheric thermal effects, I convert the high-velocity zone in velocity model to thermochemical anomaly in our model. In the next step, comparing calculated and measured geophysical data allows us to evaluate the fit to observables. I modify the previously found LAB structure in order to compensate the gravitational effect of slab. Here, I check the consistency of the obtained lithospheric thickness with respect to the proposed dynamic model of break-off imaged slab by tomography. LitMod3D predicts seismic velocities of the model due to user-defined thermal and compositional setting of the model. Predictions of Vs velocity by our model will be compared with available seismic tomography, SL2013sv (Schaeffer and Lebedev, 2013).

Fullea et al. (2014) discussed on the inferred bias to LAB depth ignoring sub-lithospheric structures (i.e. slab) because of the thermal effects in presence of the cold slab. Moreover, our model without sub-lithospheric assumptions fails to interpret the sub-lithospheric seismic anomalies (e.g. global shear wave velocity model SL2013sv (Schaeffer and Lebedev, 2013)). The most widely accepted hypothesis about the origin of the present-day sub-lithospheric high-velocity zone beneath the Arabia-Eurasia collision zone relates to remnant of Neo-Tethys slab break-off (van der Meer et al., 2017). In order to model sub-lithospheric thermal effects, I convert the high-velocity zone in SL2013sv tomography model to thermochemical anomaly in our model. In the next step, comparing calculated and measured geophysical data allows us to evaluate the fit to observables. Sequential modification of LAB is needed to compensate the gravitational effect of first, compositional heterogeneities in lithosphere and second the disturbing effects of slab as a disturbing anomaly on geophysical observables. Here, I check the consistency of the obtained lithospheric thickness with respect to the proposed dynamic model of break-off and images of slab by seismic tomography. In sense of collision-related subduction, numerical models are able to represent such an evolution of the time-varying status of Neo-Tethys slab beneath the Iranian Plateau (e.g. van Hunen and Allen, 2011).

4.2 Tetonic setting

Several studies investigated the past 45 million-year volcanic activities and magmatism in the Iranian Plateau mainly occurred in Eocene time (Pearce et al., 1986; Keskin et al., 1998; Agard et al., 2011; Neill et al., 2013; Allen et al., 2013; Kaislaniemi et al., 2014). The sequence of volcanic activities from Miocene to Quaternary shows the magma upwelling in the upper mantle. Geochemical studies of the magmatic rocks over Iran (Fig. 4.1) indicate low partial melt production (Ghasemi and Talbot, 2006; Monsef et al., 2010; Neill et al., 2013), which is characterized by the subduction related volcanism like that occurs in slab break-off. Other surface phenomena in the Iranian Plateau link the present-day surface phenomena like rapid surface uplift, changes in thermal gradients and exhumation of ultra-high-pressure rocks to slab break-off (Davies and von Blanckenburg, 1995; Molinaro et al., 2005).

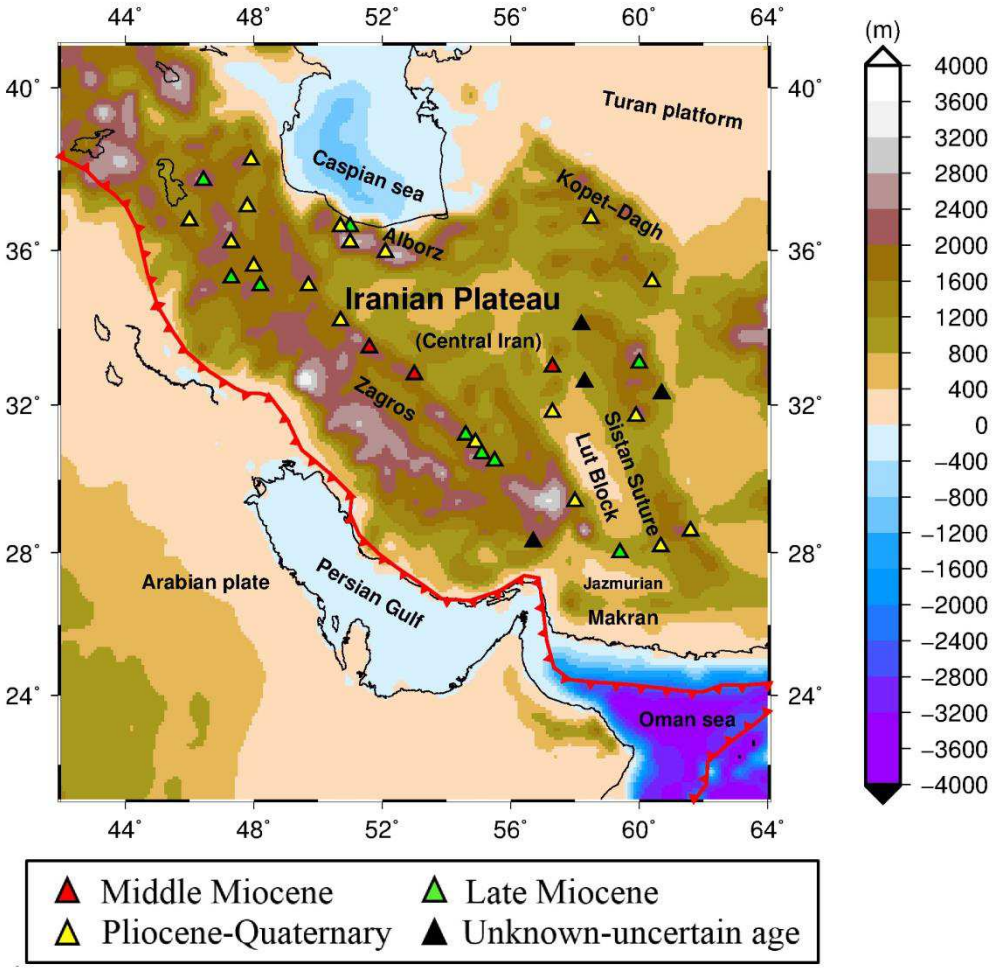

Figure 4.1. Topography map of the study region including age and location of volcanoes. The red line is the plate boundary front, taken from Bird (2003), illustrates the deformation frontal boundary of the Alpine-Himalaya collision zone. Topography has been taken from ETOPO1 global database (Amante and Eakins, 2009).

4.3 Modeling results

For modeling sub-lithospheric heterogeneities, I again use LitMod3D software (Chapter 3, section 3.3 for more description) in an innovative approach to assume the slab body within adiabatic mantle. Here, the homogeneous asthenosphere is modified by adding the thermochemical heterogeneities due to the imaged slab from seismic tomography. The crustal setting and lithospheric compositional heterogeneities are the same as the model described in chapter 3 with a change in crustal density to avoid modification of crustal geometry (The Moho depth Fig. 4.2 has been constrained by seismic studies summarized in Fig. 4.2). A change to physical properties of crust (in model with asthenospheric heterogeneities the density of the lower crust beneath central Iran is higher $\Delta\rho\approx150$ kg/m^3) is necessary to fit the geophysical observables.

The Central Iran (e.g. Lut block, Fig. 4.1) has been detached from Gondwana at early Triassic (e.g. McCall, 1997). In chapter 3, I showed the lithospheric mantle composition beneath Central Iran is fertile (Su et al., 2014) high likely due to the mafic intrusions. Mafic intrusions (which are not always incorporating with the volcanic eruptions) evidenced by wide spread plutonic rocks (Aghanabati, 2004). Such phenomenon incorporates with magmatic underplating in Central Iran. The mafic intrusions might follow crustal geotherm but could be still similar to source material regarding density/lithology. This is why I consider +150 kg/m^3 denser material at the bottom of crust in Central Iran (Fig. 4.2b).

a)

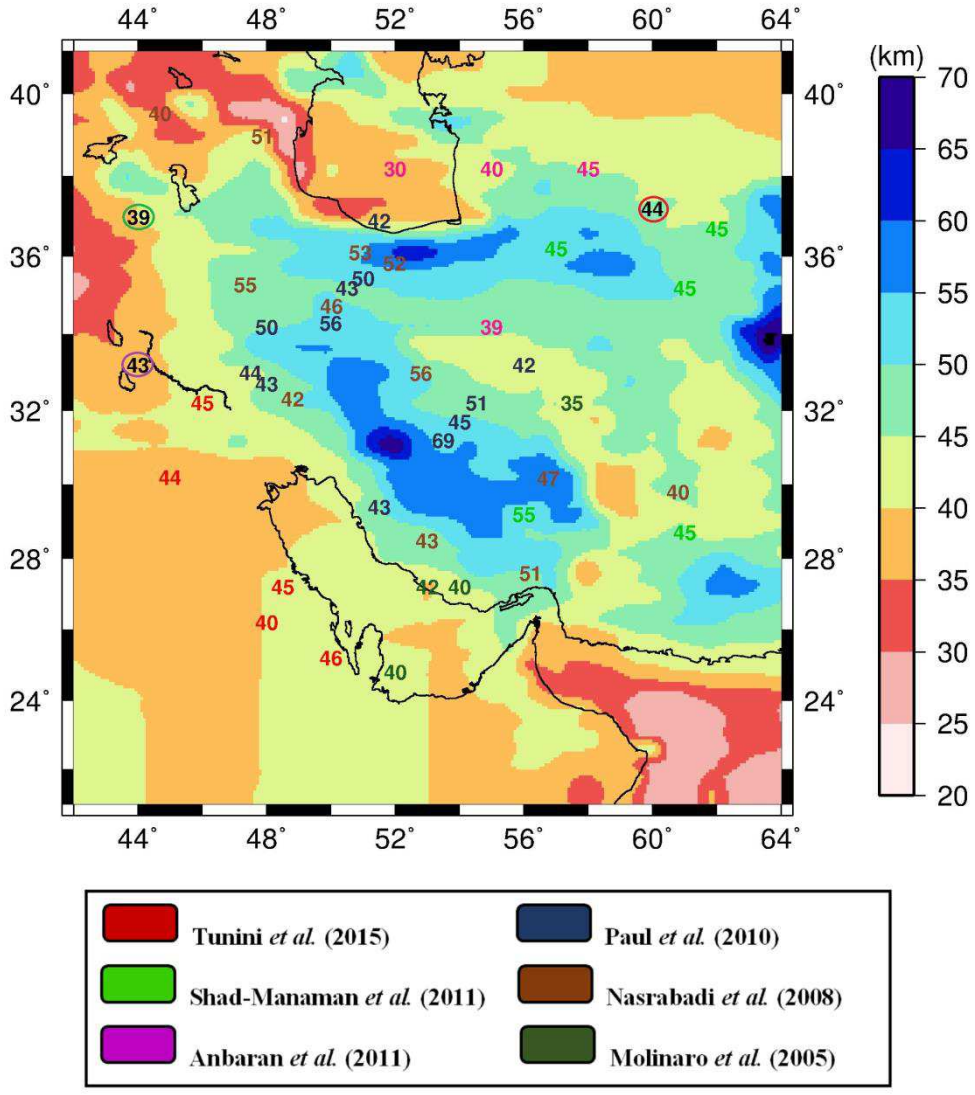

b)

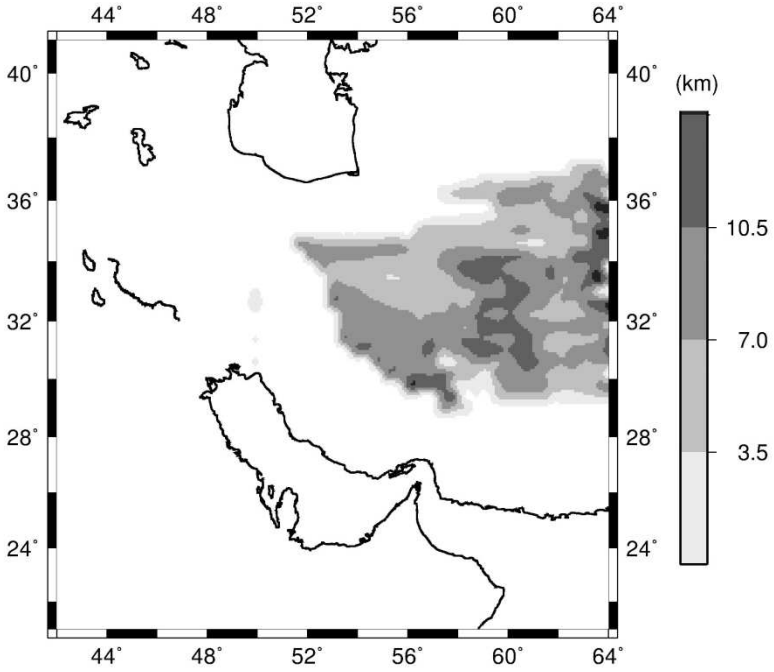

Figure 4.2 a) Modelled Moho depth map without sub-lithospheric heterogeneities from chapter 3. Numbers over the Moho map are crustal thickness values from previous studies. Each value has a colour denoted in the legend except circled numbers in black. Black values inside coloured circles are single Moho estimates from Gök et al. (2008) (purple circle), Gritto et al. (2008) (green circle) and Nowrouzi et al. (2007) (red circle), respectively. The Moho in background is used as the initial model for forward modeling (chapter 3) and will be modified based on availability of other estimates from previous studies. b) The thickness map of the relatively dense mafic intrusions (+150 kg/m^3) in Central Iran. The remaining crustal set-ups, including geometry and physical properties, are the same as the model described in chapter 3 (Fig. 3.9).

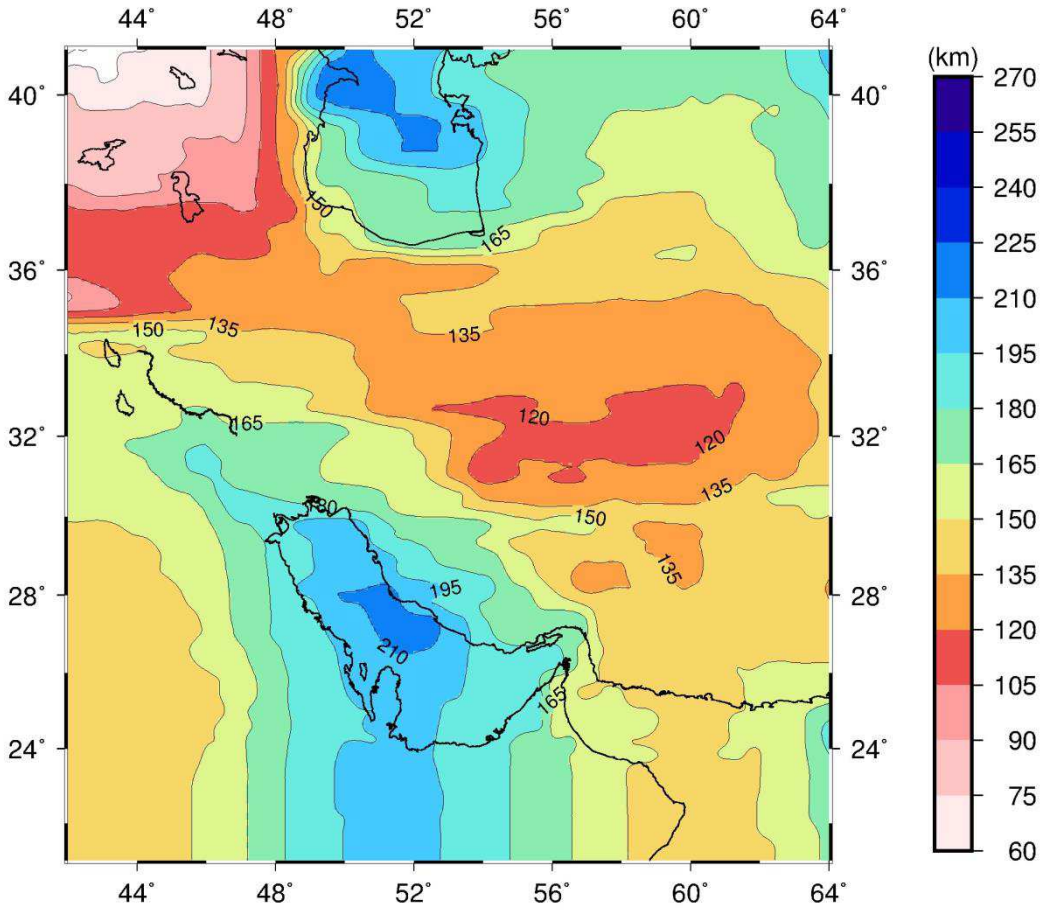

Figure 4.3. Modeled LAB depth without sub-lithospheric heterogeneities from chapter 3. Coloured numbers indicate results from Motavalli-Anbaran et al. (2011) (in blue) and Tunini et al. (2015) (in red). In background, the LAB is used as the initial model in our 3D forward modeling scheme and will be modified based on previous studies and mainly for the purpose of fitting geophysical observables.

4.3.1 Sub-lithospheric heterogeneities

Fig. 4.4 shows our modelled Vs anomalies compared to global shear wave tomography model SL2013sv (waveform inversion of the surface and shear wave forms; Schaeffer and Lebedev, 2013) at 80, 110, 150, 200, 260, 330 and 410 km depths. If I assume one-by-one correlation between seismic features and in-slab temperature, the model without asthenospheric heterogeneities is not able to predict thermal features (>200 km) expected from SL2013sv model (Fig. 4.4a). Based on SL2013sv model, a high velocity zone is located under central Iran extended between ~250 and ~400 km depths and migrating towards northeast. Fig. 4.4b shows the geometry of the proposed thermal contrast between slab and mantle representing the slab remnant beneath the Iranian Plateau which is not automatically generated by the homogenous asthenosphere in the previous model (Fig. 4.4c).

The composition of deep slab (> 200 km) is less constrained than the lithospheric part constrainable by xenolith samples. However, I chose a fertile composition for slab like Spinel Peridotite type (Griffin et al., 2009).

Table 4.1 Mantle compositions used in this study from chapter 3. The only difference is the slab composition added in this table.

Oxides	Mantle (2) Proterozoic[1]	Mantle (3) Phanero-Proto[2]	Mantle (4) Phanerozoic[3]	Slab[4]	PUM [5]
SiO_2	42.81	45	44.4	44	45
Al_2O_3	2.57	3	2.6	2.3	4.5
FeO	7.2	7.9	8.2	8.4	8.1
MgO	36.08	42	41.1	41.4	37.8
CaO	3.06	1.9	2.5	2.2	3.6
Na_2O	0.23	0.13	0.18	0.24	0.36
Mg #[6]	89.93	90.45	89.9	89.8	89.3

1. Peridotite composed of mafic Granulite and spinel lherzolite; Nasir and Stern, 2012
2. Tunini et al., 2015
3. Griffin et al., 2009
4. Spinel lherzolite, Griffin et al., 2009
5. based on Peridotite, Komatiites and Basalts; McDonough and Sun, 1995
6. Mg # = 100*MgO/(MgO+FeO)

The refined lithospheric thickness by adding the hanging part of the slab and the necessary thinning to compensate the effects of cold/dense slab is shown in Fig. 4.3. For imaging hanging parts of the slab, I increased the lithospheric thickness to avoid the extra shallowing of slab. This can lead to a strong gravitational effect of slab and extreme thinning of LAB depth (Fullea et al., 2014). As one of the most striking features in the modified LAB is the relatively thin lithosphere of central Iran ~100 km (previously estimated at ~120 km using a thermochemically homogenous asthenosphere). Also, the depth to LAB in northern part of the Caspian Sea rises up to ~204 km depth in the modified LAB (Fig. 4.3) (previously estimated at ~240 km without sub-lithospheric heterogeneities). Again, the lithosphere is thinned progressively toward the NW of Iran, where it reaches a thickness of ~75 km. Deepening of the LAB beneath eastern Makran assimilates the continuity of sinking slab. However, the modelled discontinuity between slab and lithosphere enables us to propose a potential break-off due to rheologically weak oceanic slab in Makran and supportable by vertical discontinuity of high absolute velocity in SL2013sv (Fig. 4.4a).

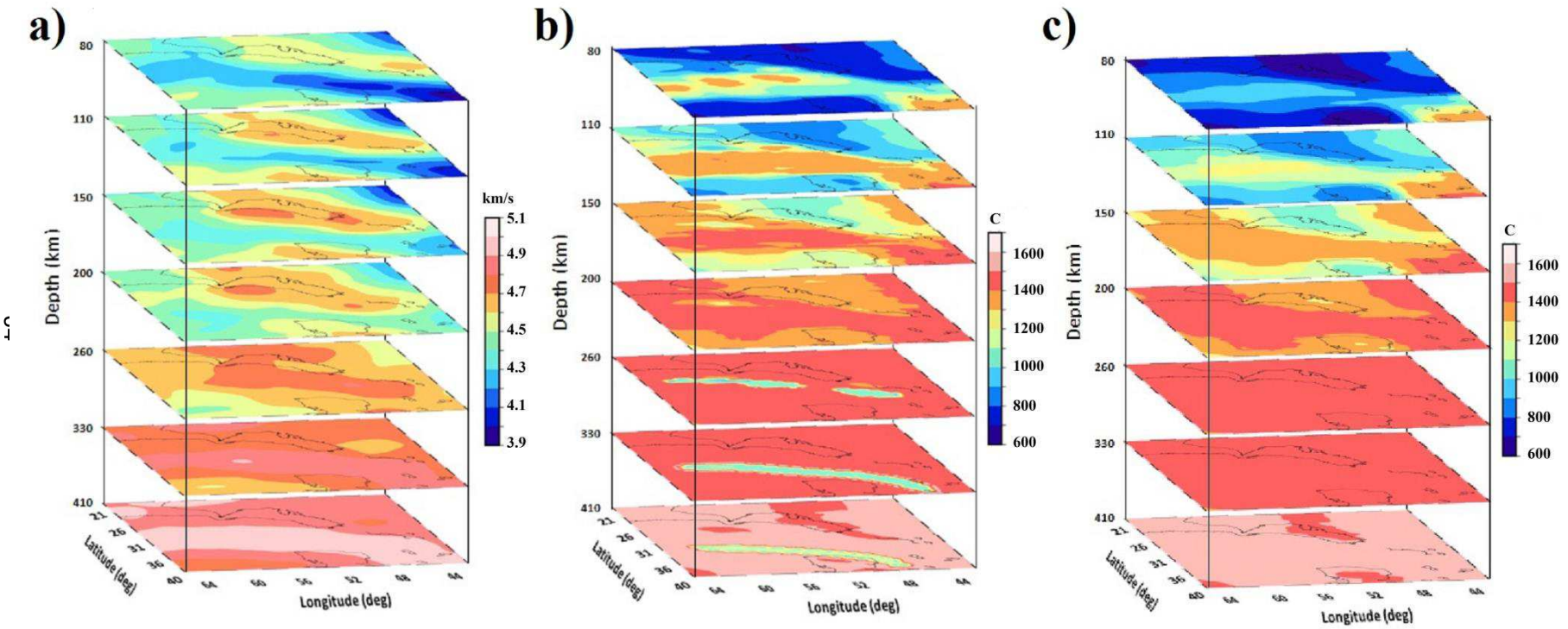
a)
b)
c)
Depth (km)
80
110
150
200
260
330
410
Latitude (deg)
21
25
31
35
40
Longitude (deg)
64
60
56
52
48
44
km/s
5.1
4.9
4.7
4.5
4.3
4.1
3.9
C
1600
1400
1200
1000
800
600

Figure 4.4. a) Horizons of Vs anomalies from SL2013sv tomography model (Schaeffer and Lebedev, 2013) at 80, 110, 150, 200, 260, 330, and ~410 km depths. The 3D thermal structure of the model b) in the presence of the slab, and c) without the slab. After adding a cold slab, the LAB will be modified by rising up and the warm sub-lithospheric material can be emplaced at shallower depth. The vertical axis of plots has no real scale for the purpose of better visualization however some horizons are more compact.

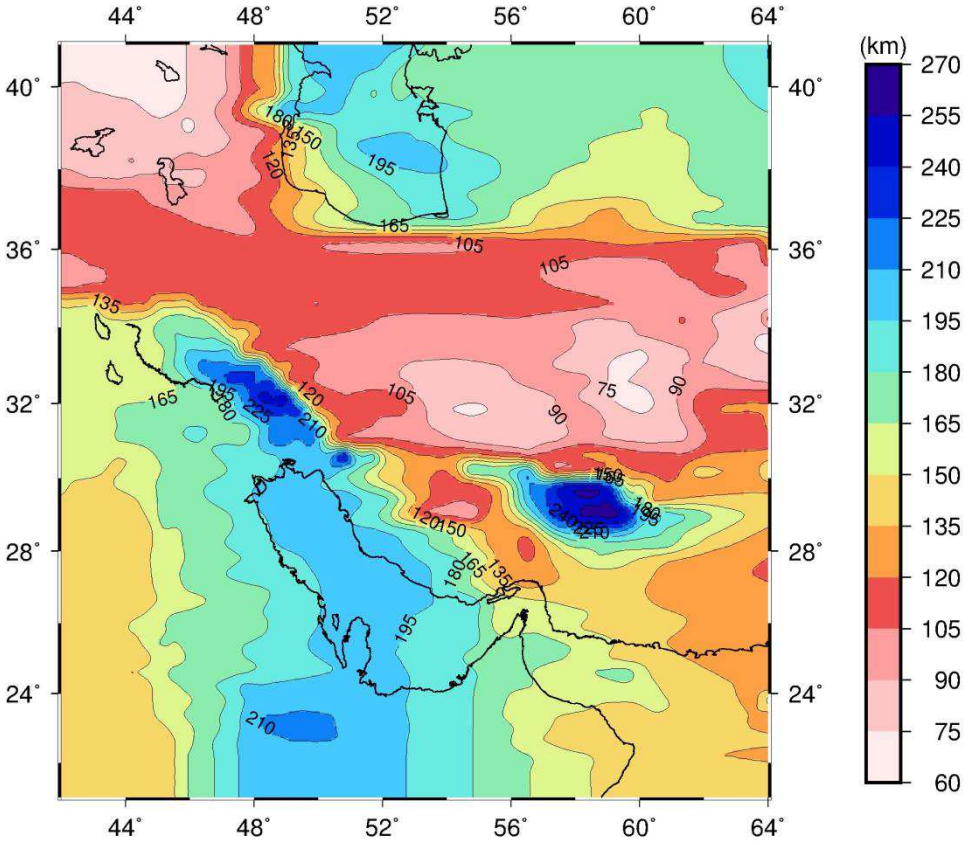

Figure 4.5. Modified lithospheric thickness for model with slab and added partial thickening due to hanging parts of the slab. Lack of hanging part in central Zagros assimilates break-off slab as suggested by Omrani et al. (2008).

Fullea et al. (2014) indicated that the perturbing effects of sub-lithospheric density anomalies (associated with the slab) have an impact in lithospheric-scale geophysical-petrological modeling. The effects of sub-lithospheric density anomalies reflect in gravity gradients (Fig. 3.6) and other geophysical data (Fig. 3.5). To compensate the density effect of the dense/cold slab, I decreased lithospheric thickness by ~20 km. Next, the best fit of seismic velocities requires the lithosphere over the Iranian Plateau to be less than ~120 km thick (Priestley et al., 2012). Tunini et al., (2015) modelled a thinner lithosphere up to ~90 km beneath Central Iran. Therefore, I decreased the lithospheric thickness by extra ~20 km that results in the ~90-120 km thick lithosphere beneath Central Iran. The extra lithospheric thinning is compensated by a density increase at the bottom of crust associated with the magmatic underplating (see section 4.3, Fig. 4.2b).

4.3.2 The effect of in-slab temperature on physical parameters

For choosing the appropriate in-slab thermal contrast with adiabatic mantle, I conducted several tests to check the sensitivity of in-slab temperature on modelled physical properties. For the composition of slab, I chose a depleted Phanerozoic mantle (Mg#=89.9, Table 4.1 chapter 4.3) which leads to a medium dense and enough fast shear wave velocity material in P-T condition (Afonso et al., 2008; Griffin et al., 2009). Afterwards, larger Vs velocities are achieved by decrease of in-slab temperature.

Fig. 4.6 shows the 1D visualization of density, Vp, and Vs from our test models with different in-slab temperature (ΔT=100 to 400 °C). Based on our modeling results, any decrease of in-slab temperature compared to the ambient asthenosphere always leads to a higher velocity compared to ambient warmer asthenosphere. Since the slab is compositionally more depleted (I assume slab composition is spinel lherzolite, Table 4.1) than ambient mantle, the density of slab is still less than asthenosphere using $\Delta T <$ 300 °C and increases only using higher in-slab thermal contrast (i.e. $\Delta T >$ 300 °C) between slab and asthenosphere.

My results show that the compositional derivative of density is much larger than the thermal derivative of density (unlike their counterpart seismic velocity derivatives) (Fig. 4.6). In similar, ~2 % reduction in Al_2O_3 (between slab and asthenosphere (PUM), Table 4.1) would trade off with a temperature decrease ΔT = 200-300 °C. In this thesis, I assumed Spinel Lherzolite Peridotite for the composition of slab (density excess of the slab relative to the ambient mantle will be approximately $\Delta\rho \approx 20$ kg/m^3 considering ΔT = 400 °C). Resulting density excess of the slab relative to the ambient mantle (that is slightly less than the expected value of $\Delta\rho \approx 40$ kg/m^3 for the density contrast between the slab and the ambient mantle (Afonso et al., 2007)) is in agreement with lack of deep earthquakes (> 30 km) in Zagros high likely associated with a suspended slab. To note, the Zagros collision zone has been formed by tectonic forces from Arabia-Eurasia convergence (e.g. Talebian and Jackson, 2004). Therefore, supporting plate could drive a relatively dense ocean floor to subduct.

Upon the invariable pressure over alternative tests, density change in shallow part of slab heavily depends on the temperature where composition effect does not allow an abrupt increase in density of cold slab.

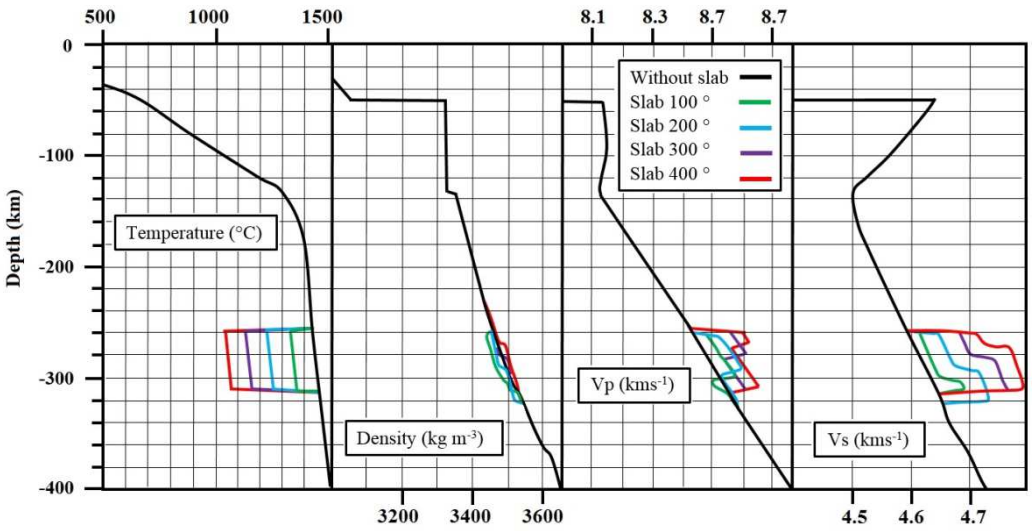

Figure 4.6. The vertical profiles of temperature, density, Vp, and Vs velocities in tests with various slab temperatures. Different colours stand for different temperature contrasts and resulting effects on other parameters (density, Vp and Vs). The vertical profile passes cold slab in depths ranging 260 and 310 km. A small value of for thermal contrast between slab and ambient mantle leads to negative density contrast which contradicts the scenario of subduction by mass excess. Deceasing slab temperature lets the density exceeds the density of ambient asthenosphere.

4.3.3 The in-slab temperature and changes to calculated geophysical data

Here, I statistically compare residual anomalies (observed minus calculated values) of potential field data (free-air, Bouguer, geoid and gravity gradients) and elevation of models by using different in-slab temperatures. For the purpose of comparison, the best fitting geophysical model with modified LAB (after insertion of slab) is taken the reference model (ΔT= 400 °C) as it predicts well the seismic velocities (Fig. 4.5). Fig. 4.7 illustrates that applying warmer slab degrades the fit of observables except for topography which stays the same (Table 4.2). The largest free-air residual anomaly belongs to the '100 °C colder slab' because of very low density of the slab compared to ambient asthenosphere (Figs. 4.7 and 4.8). For a higher thermal contrast between slab and the ambient asthenosphere, the standard deviation increased for the Bouguer anomaly field. The standard deviation of geoid residual improves while slab temperature decreases. In case of using 300 and 400 °C colder slab materials compared to asthenosphere, the geoid misfit in this test is dramatically large. As the deeper parts of model has a strong effect on the calculated geoid anomaly.

Fig. 4.7 illustrates a range of models which can fit observables that the model of 400 °C colder slab with modified LAB (Fig. 4.5) has the smallest misfit among others. Similarly, residual anomalies of gravity gradient components show a similar effect of in-slab temperature on fit of observables. As mentioned in chapter 3, the exception in the fit to observables is again the gravity gradient component G_{EU} which is originated from Makran area.

Table 4.2. Effects of different slab-mantle thermal contrast on geophysical residual anomalies (measured minus calculated). Std. stands for Standard deviation.

Residual	statistics	Slab 0 °C	Slab 100 °C	Slab 200 °C	Slab 300 °C	Slab 400 °C
Free-air	Std.	29.72	28.60	27.19	26.39	26.28
	Mean	-2.44	-4.89	-2.77	-2.37	-2.17
Bouguer	Std.	23.97	22.71	21.21	20.55	20.66
	Mean	-1.49	-1.49	-1.49	-1.49	-1.49
Geoid	Std.	9.05	8.24	6.99	5.71	4.9
	Mean	-1.20	-1.50	1.06	-3.19	8.39

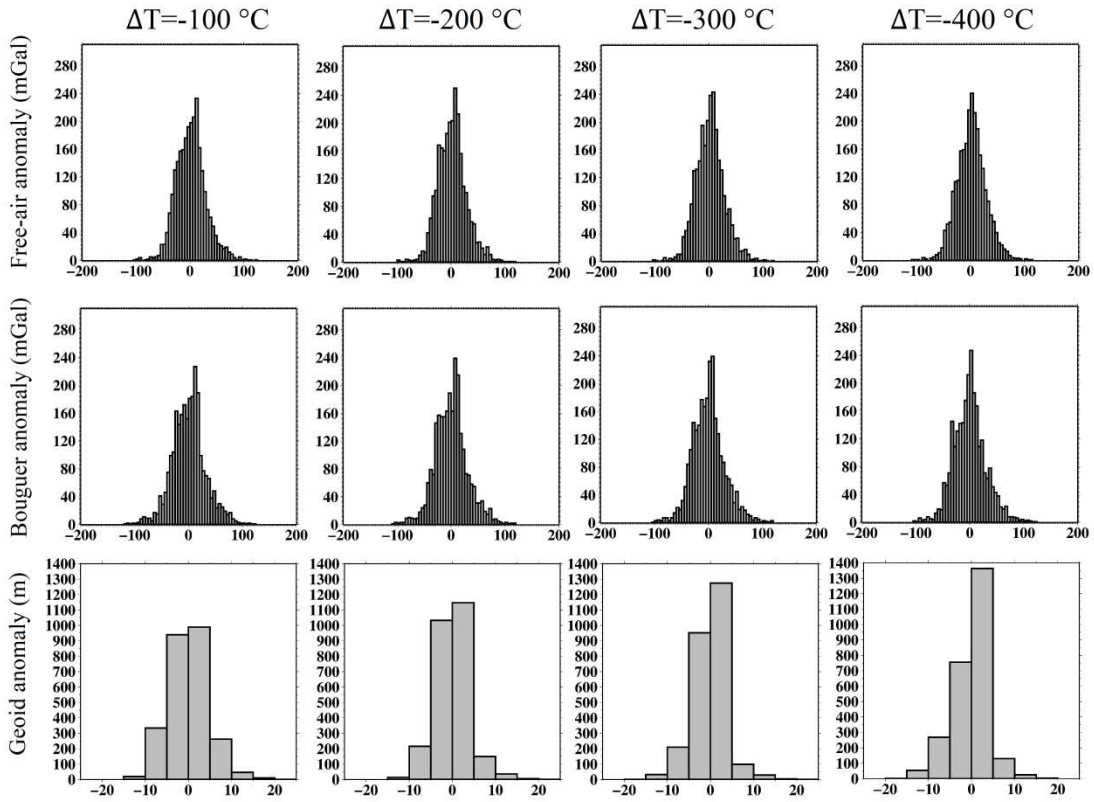

Figure 4.7. Histograms of residual (observed minus calculated) anomalies for tests with heterogeneous lithosphere and modified LAB after adding slab. Rows are: top) free-air, middle) Bouguer, bottom) geoid. Columns indicate models (from left to right) with different slab thermal decrease of ΔT= 100, 200, 300, and 400 °C compared to mantle. All vertical axes are number of points and horizontal axes are amplitude.

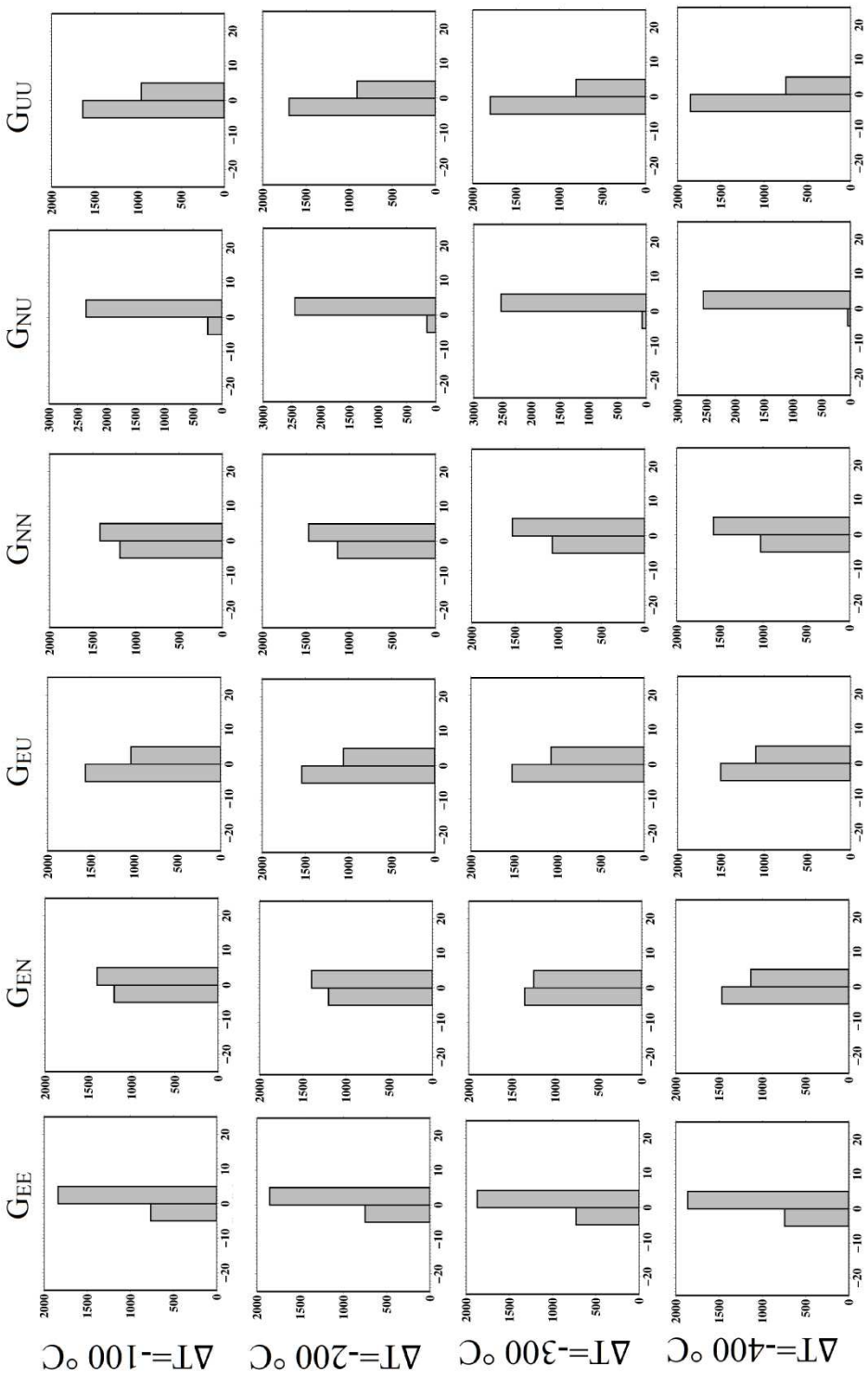

Figure 4.8. Histogram map of residual anomalies (observed minus calculated) of gravity gradient components sorted in columns belong to each of gradient tensor components from left to right: EE, EN, EU, NN, NU, UU; rows indicate models with different slab temperatures of (from above to below) first) 400 °C, second) 300 °C, third) 200 °C, and forth) 100 °C. All vertical and horizontal axes are number of points and amplitude of the gravity gradients (in Eotvös), respectively. I must note that gradient components are almost insensitive to sub-lithospheric structure in my model.

4.4 Discussion

For comparing different LABs and seismic predictions with referenced tomography I selected four cross sections of our preferred model including slab.

4.4.1 Comparison of different LABs

Figs. 4.9a to 4.9d represent cross-sections of the assumed thermal structure of the preferred model including slab. Along the profiles, Moho depth range between 40 and 65 km. Comparing the resulted Moho depth from this study with a global model CRUST1.0 (Laske et al., 2013) reveals some differences. Our Moho depth has local thickening associated with elevated areas. Whereas, CRUST1.0 is shallower than the present study Moho in all profiles 1 to 4 (Figs. 4.9a to 4.9d). The discrepancies of our LAB and global lithospheric thickness LITHO1.0 (Pasyanos et al., 2014) are more significant in terms of depth and shape. Despite some correlation between our LAB and LITHO1.0 depths, the depth of the obtained LAB in east of profile 1 and 3 is significantly larger than LITHO1.0 (Fig. 4.9d). In profile 2, the Central Iran lithosphere is thicker in our model than predictions by LITHO1.0. A large LAB depth in west of profile 4 associates with the Makran slab hanging part. This feature is visible in LITHO1.0 depth with shallower depth (Fig. 4.9d). In Profile 4, the obtained LAB is very shallower compared to a recent report of ~200 km by Entezar-Saadat et al. (2017), who reported a considerably thicker LAB beneath the east of Iranian Plateau (~200 km) due to lack of thermochemical effects in their study.

In conclusion, our LAB in all profiles follows the general trend of LITHO1.0 but with a shift in absolute depth. However, our Moho and LAB depths are still deeper than predictions from CRUST1.0 and LITHO1.0 global models, which predict lower values of ~10 km and ~100 km for Moho and LAB depths, respectively. Nevertheless, such a thin lithosphere (~60 km), similar to what is suggested by LITHO1.0, is a matter of debate to be representative of a continental lithosphere with Proterozoic composition beneath the Central Iran (e.g. Su et al., 2014).

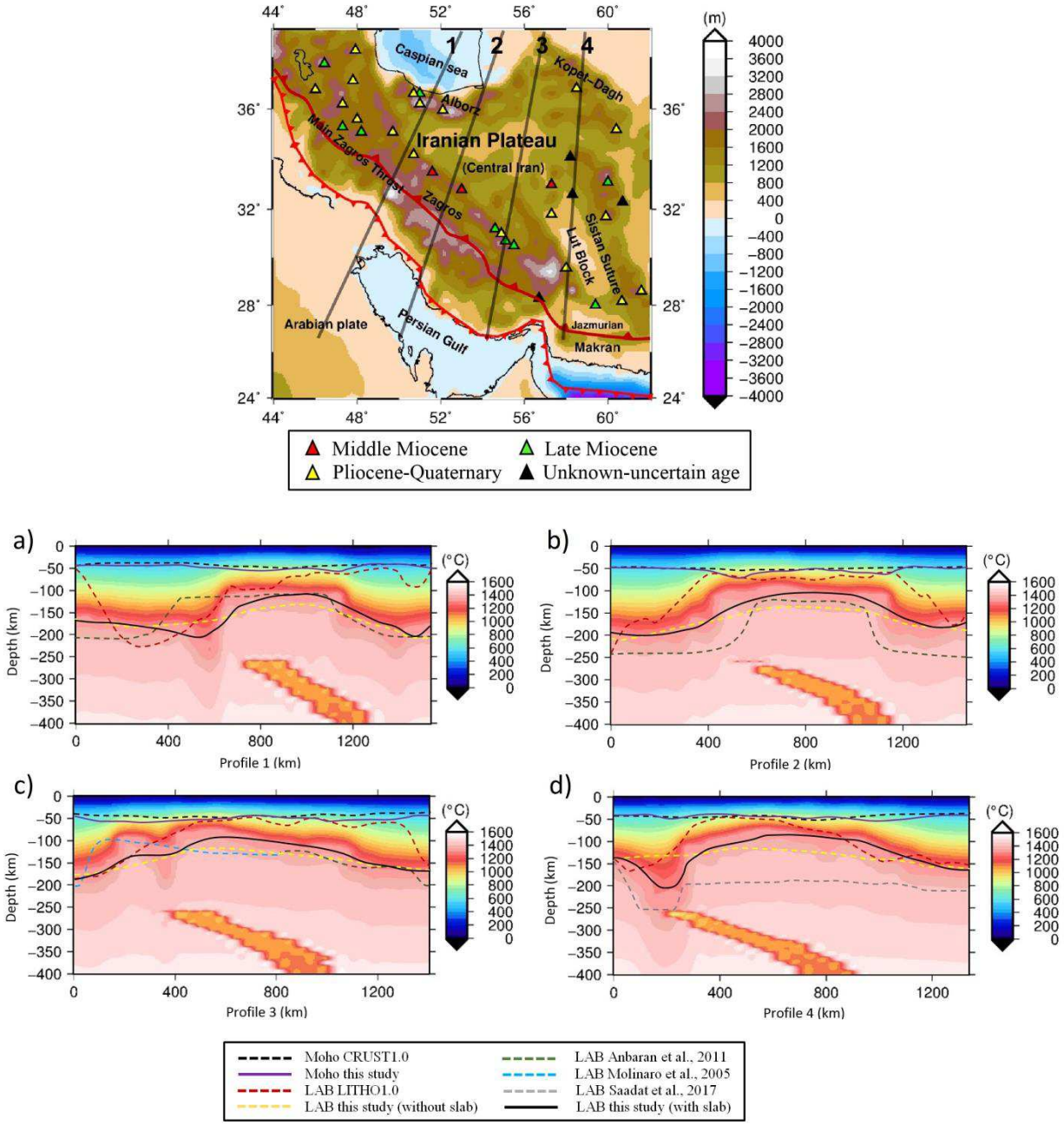

Figure 4.9. Topography map of the Iranian Plateau and adjacent areas including location of profiles. The legend shows the age of main volcanoes distributed over the area. Line with large triangles shown in topography map represent the Main Zagros Thrust (MZT) separating Arabian plate from the Eurasian overriding plate. MZT, which neighbours a narrow discrete belt of strongly tectonized ophiolitic-mélange and igneous assemblages, is known as the main location of Neo-Tethys ocean closure in the continuation of colliding plates. In a more local scale, MZT is dividing different rheological and seismological parts of the Zagros collision zone; e.g., metamorphic zone from the southern part of Zagros composed of the folded thrust belts (Takin, 1972; Berberian and King, 1981). In imaging the present-day slab location, I considered the higher probabilities for slab presence with respect to MZT. a-d) temperature distributions of the model along four profiles crossing the subducting slab.

4.4.2 Synthetic Vs velocities versus tomography model (SL2013sv)

To avoid overestimates on slab geometry, I apply a large-scale tomography model of S-wave tomography model SL2013sv (Schaeffer and Lebedev, 2013) to simulate the main organization of the subducting slab beneath the Iranian Plateau. Fig. 4.10 illustrate the subducting slab is strongly imaged in SL2013sv absolute and relative (referenced to mean depth) velocity cross sections. With some discrepancies, however, imaged in regional and global seismic tomography models (Alinaghi et al., 2007), a high velocity zone beneath Persian Gulf and Makaran (Fig. 4.10) moves northeastward towards Eurasia Plate equally interpreted as location of subducting slab. Bearing in mind, lateral uncertainty of SL2013sv model increases with depth and slab has only 100-150 km width. Therefore, I averaged the location of high velocity zone in absolute SL2013sv model to find the estimation of the slab location.

Fig. 4.10 shows that our model provides low-velocity zones beneath the Central Iran extended to a depth of ~200 km. As a similar trend in all cross sections, there is a high-velocity zone starting from ~260 km that extends to the bottom of model beneath Central Iran. However, comparing absolute and relative velocity anomalies shows that absolute velocities taken from global model SL2013sv are more suitable to visualize the deep structures while the relative velocity anomalies referenced to mean depth, are more useful for visualizing the shallower parts in the lithospheric mantle. I must note that thick areas of the modelled lithosphere are strongly in agreement with shallow high velocity zones in map (down to ~200 km) of relative SL2013sv model (Fig. 4.10 the rightest column).

Magma upwelling is traced by low-velocity zones in seismic tomography models (Lambert and Wyllie, 1970; Plasman et al., 2017). This magma assemblage naturally occurs below the thin parts of the lithosphere. Therefore, magma-upwelling and low-velocity zones are mixing with the pronounced lithospheric thinning. Nevertheless, magmatism is not just occurring over the thinned LAB (Allen et al., 2013). The left column of Fig. 4.10 shows how the magmatism correlates to slab break-off and correlates specially with the places where the volcanic chain (Fig. 4.1) is located at the surface.

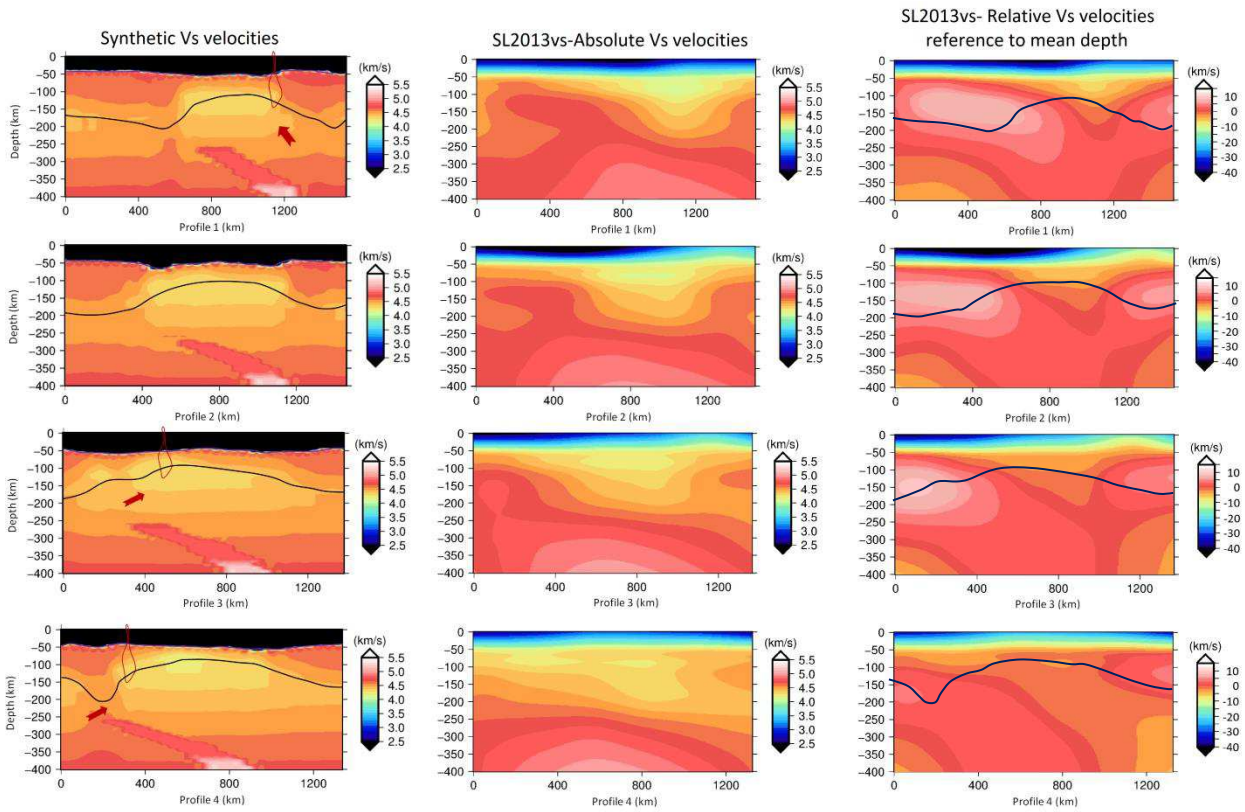

Figure 4.10. Cross sections of model along a) Profile 1, b) Profile 2, c) Profile 3 and d) Profile 4. For location of profiles see Fig. 4.9. The seismic velocities in different columns are as follows: left column: our synthetic Vs velocities, middle column: absolute Vs velocities from SL2013sv, right column: Vs velocities from SL2013sv relative to the mean depth (black line is the modified LAB after adding slab). Based on the dominant frequencies of the seismic tomography model (~50 s) and an average grain size of 5 cm the anelasticity effects (Afonso et al., 2008) are included in our synthetic anomalies. Red polygons and arrows are indicating the low velocity zones, which might relate to the location of magma chambers beneath volcano locations. Arrows show the probable magma feedback due to the small-scale convection.

4.4.3 Slab break-off: geodynamic implications

Implementing the current depleted Phanerozoic composition for slab leads to a minor density change in the shallow part of asthenosphere ($\Delta\rho \approx 30$ kg/m^3). However, the predicted seismic velocities both in shallow and deep areas are comparable to reference model SL2013sv. Figs. 4.11a to 4.11d illustrate that the density contrast between the shallower part of the slab (~260-370 km) and adiabatic mantle is not as big as that in the deepest part of the slab. Therefore, in the lack of high density contrast between slab and asthenosphere, the small-scale convection triggers the circulation of asthenospheric material through slab window, vice versa (Kiaslaniemi et al., 2014).

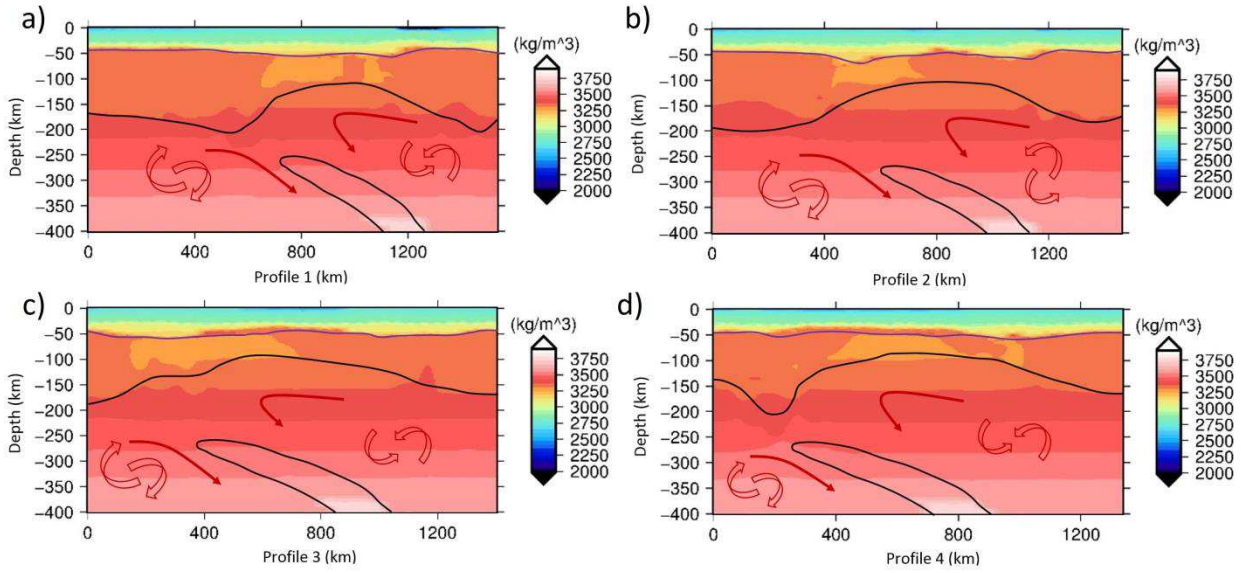

Figure 4.11. Density structure along four cross sections: a) Profile 1, b) Profile 2, c) Profile 3, and d) Profile 4; see Fig. 4.9 for location of profiles. Red solid arrows show the direction of sinking slab; circular arrows show the small-scale convection that also supports moving of slab and magma exhumation. I must note that this model is unable to show mantle convection. However, the proposed dynamic scenario for the area supports such circulations in line with subduction. The single arrows show the direction of sinking slab.

The resulted topography of Lithosphere-Asthenosphere Boundary (LAB) associates with the superposition of different geodynamic processes: i) the shortening of the Iranian Plateau and the Arabian-Eurasian thickening related to the Eurasia–Africa convergence lasting from Mid-Jurassic to present; ii) impingement of a small-scale convection beneath Central Iran commencing in the mid Eocene; and iii) the Neo-Tethys slab break-off in the mid Eocene suggested by volcanism and seismic tomography models. Estimates on the timing of the Neo-Tethys (Iran part) show closure of the NeoTethys Ocean floor at maximum in the Late Cretaceous after initial rifting phase starting in late Permian (Sengör et al., 1980; Koop and Stoneley, 1982; Stampfli et al., 1991; Ghasemi and Talbot, 2006). It is assumed that the subduction age is ~15-30 Myr after closure of Neo-Tethys Ocean (e.g. McQuarrie and van Hinsbergen, 2013). To estimate the present-day depth of the sinking slab, van der Meer et al. (2009) suggests a linear age-depth relation of Neo-Tethys slab suggesting the top of slab is at ~150-300 km depth.

Fig. 4.11 presents a schematic sketch of the 3D structure of the slab illustrating the break-off beneath Iranian Plateau. As shown in Fig. 4.11, the slab tearing has been triggered from the eastern side of Anatolia towards the Zagros Mountains. Based on the results of geodynamical modeling (van Hunen and Allen, 2011), the sinking slab has been potentially detached from the hanging part in the middle, associates with the concentration of Late Miocene to Quaternary magmatism in the southeast of Zagros (Fig. 4.1; 55°E, 30.5°N) (Agard et al., 2011; Ghasemi and Talbot, 2006). In the southwest of our study area, the Makran subduction zone, different studies argued about the dipping angle of the slab. The slab is proposed to have lower angles at shallow depths, increasing to ~45° at larger depth (Jacob and Quittmeyer, 1979; White, 1982; Harms et al., 1984; Byrne et al., 1992; Kopp et al., 2000;

Smith et al., 2013). Regardless the debates, a possible conclusion is that the Makran slab is migrating horizontally in time, which means it remains at a shallow depth after the initial subduction.

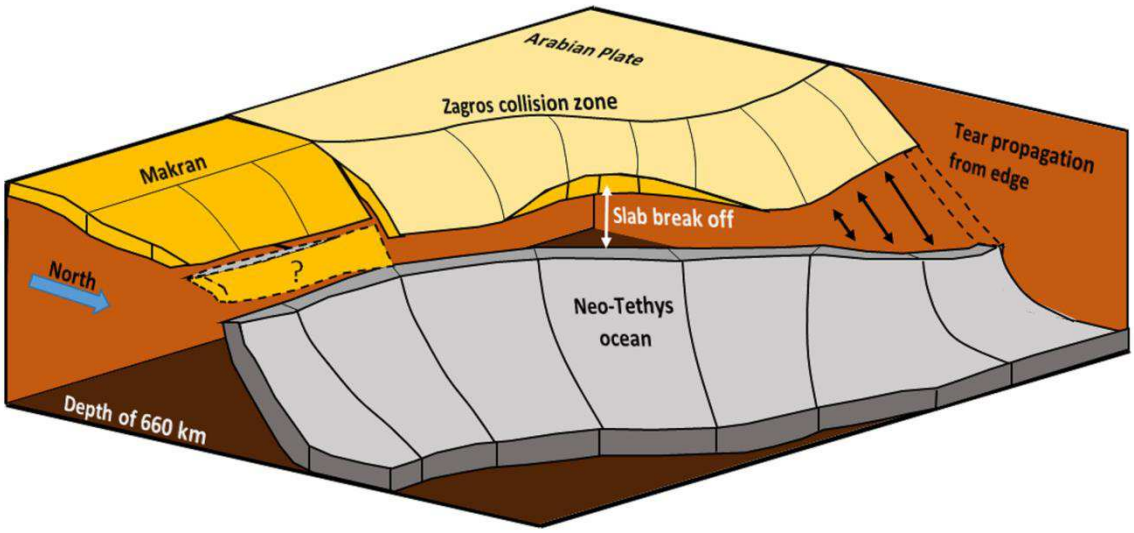

Figure 4.12. The 3D structure of subducting slab and break-off beneath Iranian Plateau based on the dynamic model (Ghasemi and Talbot, 2006; van Hunen and Allen, 2011), magmatism (Omrani et al., 2008; Agard et al., 2011) and seismic tomography (Alinaghi et al., 2007; Schaeffer and Lebedev, 2013). The figure shows the scenario of tear propagation from the edges to the middle of the sinking slab.

4.5 Conclusion

Following the recent slab break-off from geochronological and magmatism, geodynamical modeling and seismic tomography models, I simulated the shape of sub-lithospheric heterogeneities. Global and regional seismic tomography models illustrate the presence of positive velocity anomaly beneath Iranian Plateau interpreted as a remnant of NeoTethys slab. Synthetic seismic velocity can be reproduced using a cold and compositionally depleted body that is considered as the origin of the high seismic velocity zone. The disturbing effects of cold/dense sublithospheric body result in a decrease in the lithospheric thickness in order to fit geophysical observables. Therefore, the lithospheric models ignoring sub-lithospheric heterogeneities might be significantly biased. Because adding sub-lithospheric heterogeneities causes a maximum change of ~50 km in lithospheric thickness. Moreover, the results of this study reveal an important conclusion that shallow part of slab with intrinsic lithospheric composition should be cold enough if a very dense slab similar to the density of slab in the deep mantle is required. Otherwise, the effect of temperature causes faster velocity anomalies. It is still debated if the Makran slab has been detached from hanging part or not. Further studies are needed to address the organization of subduction in the Makran.

Chapter 5:

The structure of crust and upper mantle beneath Makran subduction zone

5.1. Introduction

The Makran subduction zone has an enigmatic architecture in lithospheric and sublithospheric scale due to lack of deep seismicity. On the one hand, seismic tomography models image the deep slab structure with some discrepancies regarding to depth, width and shape of the subducing slab (Bijwaard et al., 1998; Alinaghi et al., 2007; Koulakov, 2011; Schaeffer and Lebedev, 2013). On the other hand, earthquake locations enable us to depict only the shallower part of the Makran subducting slab up to ~85 km depth (Engadhal et al., 1988; Barnhart et al., 2014).

The active tectonic and geological setting of the Makran motivated me to conduct some numerical models to explore more on the subduction history. For this purpose, first I use geodynamic modeling to estimate the basic physical properties of subduction including density, temperature and geometry. I need physical property of crust, subducting plate and upper mantle to quantify the Makran subduction with respect geophysical modeling. Therefore, in the second step, I apply an integrated geophysical-petrological methodology to investigate the present-day thermochemical structure and physical parameters of the upper mantle using comprehensive datasets (mantle xenolith, potential field data and elevation). The best fitting geophysical model leads to the density structure. In crustal scale, I aim to figure out convergence characteristics. In (sub)lithospheric scale, the homogenous density model is perturbed by prescribing low temperature zone (suggested by high velocity zone in seismic tomography model e.g. SL2013sv (Schaeffer and Lebedev, 2013)) and mantle composition variations (mainly derived from mantle xenolith samples). The disturbing effect of cold and dense slab should be compensated by modifying the lithospheric geotherm and affect the density structure in crust of the final model.

5.2. Seismological studies

The available seismic tomography and present-day seismicity of the region image partially the present slab beneath the Oman-Makran-Sistan region (Fig. 5.1). The location of earthquakes (EHB catalogue, Engadhal et al., 1988) indicates the shallow and low angle dipping of subducting slab beneath the Oman Sea and the Makran accretionary prism (Fig. 5.1b). Previous works studied the horizontal migration (>600 km) of the western Makran slab (Jacob and Quittmeyer, 1979; Kopp et al., 2000; Engdahl et al., 2006; Smith et al., 2013; Penney et al., 2017).

Fig. 5.2 shows more details in tomography models in the Makran subduction zone including discrete high velocity zones and evidences of detachment in different cross sections. The main feature in seismic tomography of eastern Makran is a high velocity zone down to ~400 km associated with slab (Fig. 5.2a). The number of qualitative models for describing the present-day plate tectonic and subduction history is effectively done by using tomography model pictures (e.g. Hafkenscheid et al., 2006; Hatzfeld and Molnar, 2010).

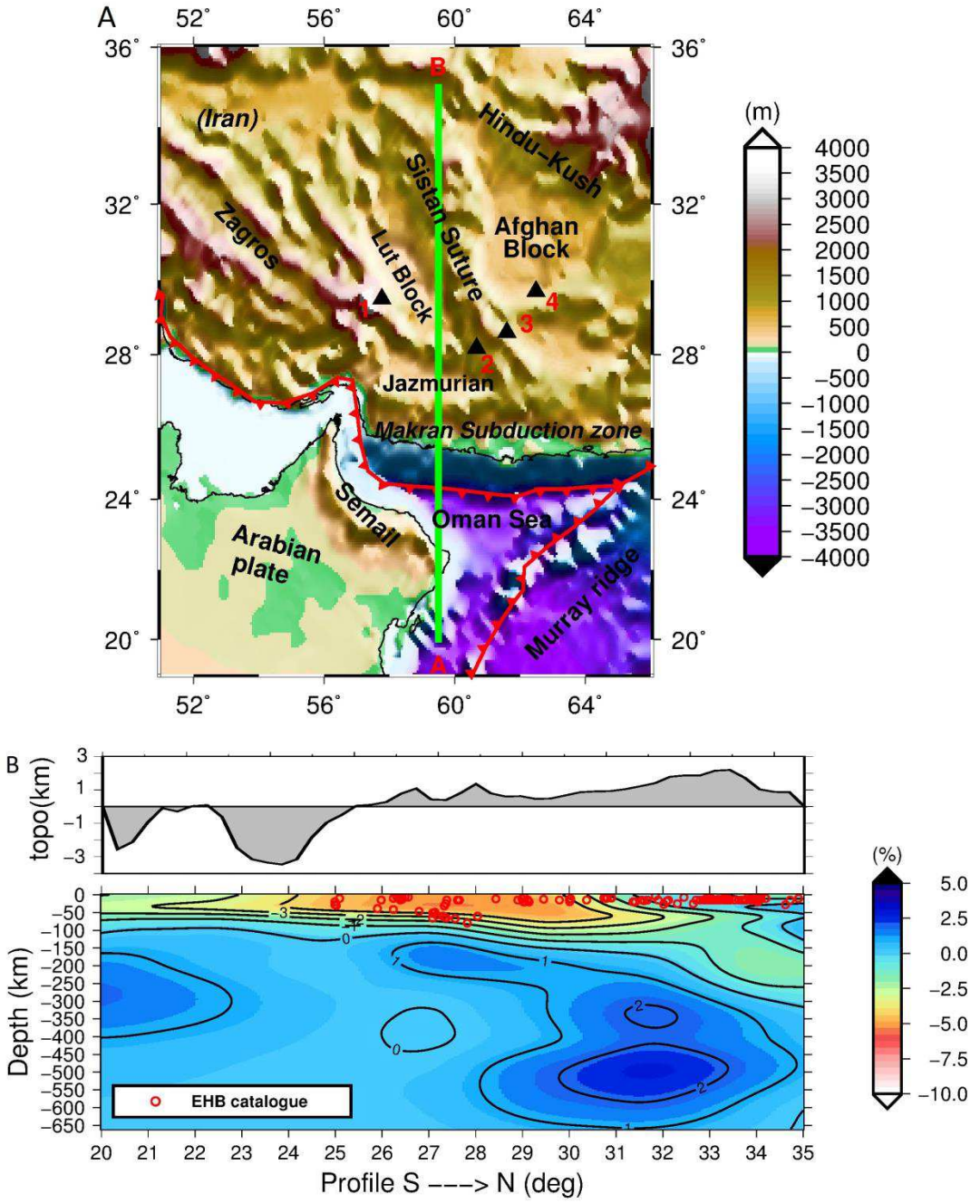

Figure 5.1. a) The map showing topography and main thrust (Bird, 2003) in Makran subduction zone. Profile AB shows the location of our study region. In the background, elevation data has been taken from 1×1 min-arc resolution ETOPO1 (Amante and Eakins, 2009). Numbers stands for 1: Ghale-Hassan, 2: Bazman, 3: Taftan and 4: Kuh-Soltan volcanoes. B) Cross section of Vs seismic velocity anomaly from global model SL2013sv (Schaeffer and Lebedev, 2013) referenced to AK135 model.

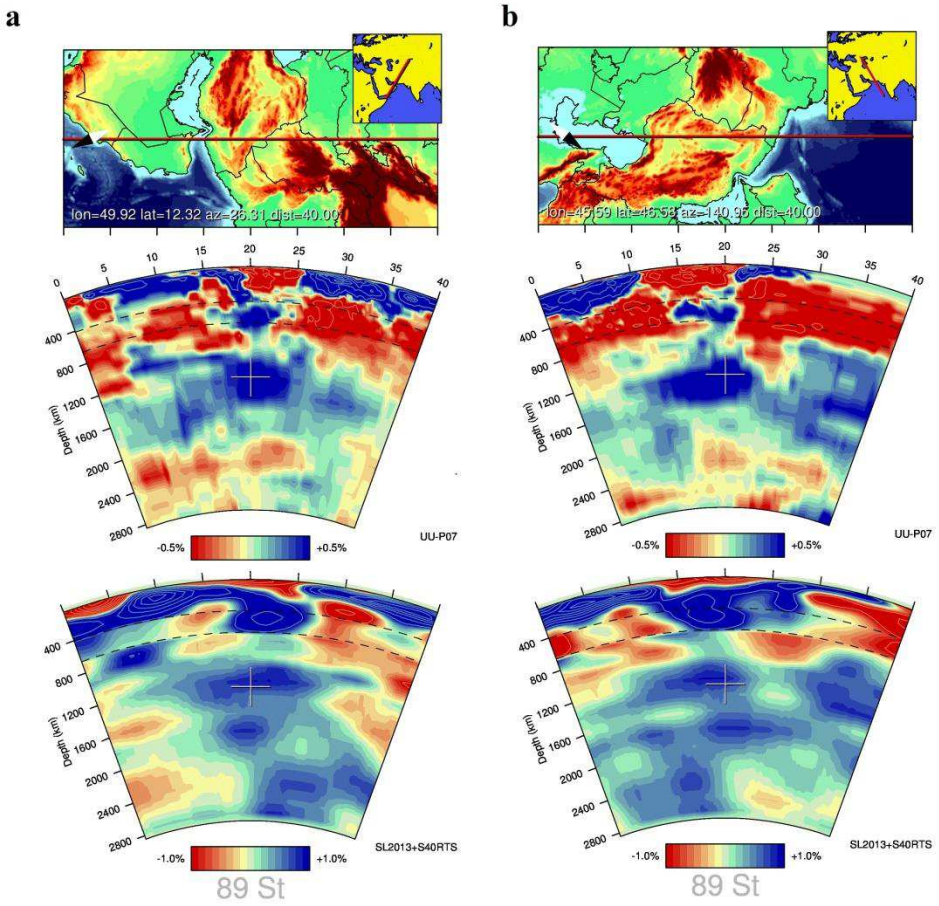

Figure 5.2. Tethyan realm and seismic tomography taken from van der Meer et al. (2017). In each of subfigures: top panel) red line shows the location of profile, middle panel) the combined SL2013sv and S40RTS S-wave and lower panel) the UUP07 P-wave tomographic models.

5.3 Tectonic setting

Marine geophysical data associated with formation of ocean basins shows a northward plate motion in the Makran subduction zone and adjacent area (e.g. Gaina et al., 2015). The plate reconstruction is taken as reference in subduction modeling showing the passage of an oceanic plate before subduction (Fig. 5.3).

Prior to subduction, the emplacement of Semail and Jazmurian ophiolite belts have been started in mid-Jurassic. The final ophiolite displacement most likely has been delayed until the late Cretaceous (Haynes and Reynolds, 1980) (Fig. 5.4). Rifting of Indian plate which might be triggered by sequential effects of subduction partial melting (mid Eocene), created potential weak zone for more decoupling, subduction and plate obductions (Fig. 5.4). Continuation of subduction and plate convergence caused the decollement in overriding crust and formation of the Makran accretionarry prism. Very young magmatism in Taftan and Bazman (Miocene-Quaternary) might originate from an active upper mantle beneath the Makran. Subduction might be paused in lack of further driving force from the south in the presence of the *locked* faults.

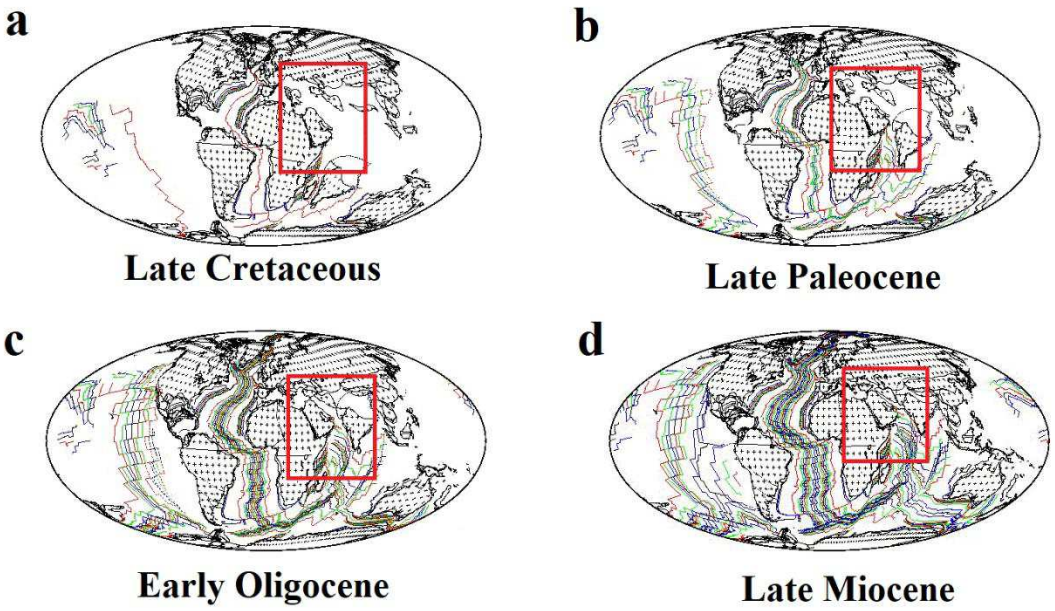

Figure 5.3. Late Cretaceous (~85 Myr to recent) plate reconstruction (Royer et al., 1992).

Extension of ocean floor was continued until the initiation of subduction (Gaina et al., 2015; van der Meer et al., 2009) and the extensive Eocene volcanism in Iranian Plateau and north of the Makran subduction zone (Agard et al., 2011). The Miocene-Quaternary volcanism in Taftan and Bazman (Fig. 5.4) was the latest activity related to subduction (Kheirkhah et al., 2015). To the north of Makran subduction zone, the Jazmurian and Lut depressions are spatially limited to Sistan suture zone (Fig. 5.4).

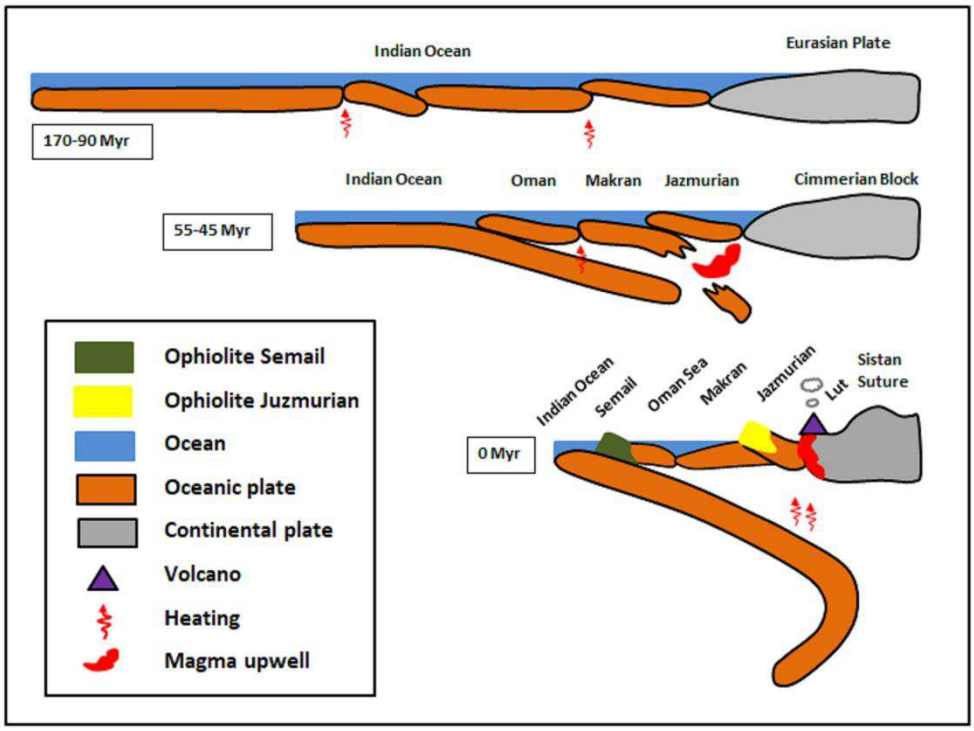

Figure 5.4. Cartoon shows the evolution of the Makran subduction zone region (Profile A–B shown on Fig. 5.1a) and so far tectonic activities since Mid-Jurassic (~170 Myr).

5.4 Methodology

5.4.1 Geodynamic modeling: the effects of prescribed surface plate motions on slab deformation

Local models are biased by underestimating the effect of regional disturbing sources on geophysical observable. Constraining the model with respect to the deep structure is highly uncertain due to the inherit uncertainty of the constraints. Geodynamic modeling will assist to estimate the present-day geometry of subduction in line with some estimates given for physical properties of subducting and overriding plates.

The Open Source code ASPECT (Advanced Solver for Problems in Earth's ConvecTion) (Kronbichler et al., 2012) was used to provide a dynamic model for Makran subduction. ASPECT solves the equation of viscosity, strain rate, stress, etc. using nonlinear scheme. I set the maximum to 100 iterations and misfit to 10^{-6}. It can provide high accuracy at a numerical cost unachievable with traditional methods. The results are more robust if I compare the dynamic modeling results and present-day static model derived from geophysical observables, mainly gravity data, and available lithospheric thickness maps.

5.4.2 Geophysical modeling: integrated geophysical-petrological modeling (LitMod)

The method used to derive the temperature, seismic velocity and density distributions within the lithosphere and sub-lithosphere is the integrated geophysical–petrological modeling (LitMod), which has been described in detail elsewhere (Fullea et al., 2009 and 2014). Here, I present a general overview of the fundamentals for completeness, with a special focus on the topics relevant to our study. In particular, I want to quantify the effects of lithospheric thermochemical heterogeneities on bulk density in the presence of cold and compositionally depleted slabs as imaged by seismic tomography (Fig. 5.1b). Integrated geophysical-petrological modeling enables us to define the thermochemical structure, shear wave seismic velocity and density model using comprehensive datasets: mantle xenolith, potential field data (free-air and Bouguer anomalies) and elevation.

I note that the lithospheric mantle and subducting slab is here defined: (i) thermally, as the portion of the mantle characterized by a conductive geotherm, and (ii) compositionally, as the portion of the mantle characterized by a relatively depleted composition with respect the fertile primary upper mantle composition in the sub-lithosphere (i.e., PUM composition, see Table 5.2). For more details regarding the formulas for the gravity anomalies and elevation the reader is referred to Fullea et al. (2009). The thermal conductivity in the lithospheric mantle is effectively calculated through solving thermal equations. The density in mantle part is a function of composition, temperature and pressure. In crust, I specify the density values based on the oceanic/continental affinities proposed by the geodynamical scenario of the region. The density in crust is linearly varying with depth through a user-defined compression coefficient.

5.5 Results

5.5.1 Geodynamic modeling

Different parameters characterize our 2D dynamic model. At the first step, I use incompressible material for the sake of simplicity. The model is composed of 80 km thick oceanic lithosphere at left sinking under continental lithosphere at the right side. The density of subducting plate and overriding plates are 3300 and 3250 kg/m^3 respectively.

The initial geometry is a box type with 2000 km length and 1000 km depth. The bottom boundary is no slip and vertical boundaries are free slip. Temperature is zero at the top and 1300 ºC at the bottom of plates. The temperature in mantle increases very slowly to avoid extra decreasing of density. Velocity at the top of model varies between our models (Fig. 5.5). First, I allow plates to move freely. In the next step, oceanic subducting plates move with 1.5 cm/yr speed and the overriding continental plate is slower with the speed of 0.35 cm/yr (Torsvik et al., 2010). Finally, I test a model with a fixed overriding plate and 0.85 cm/yr fast sinking plate.

Viscosity is one the key parameters in dynamic model. The final viscosity could be single or weighted average of different rheologies: dislocation, diffusion and plastic deformation. Each of viscosity type contributes to different characteristics of the model where temperature, pressure and stress should be dominant in viscous behaviour. I limit the viscosity range to 10^{19} and 10^{23} to avoid model will be time costly.

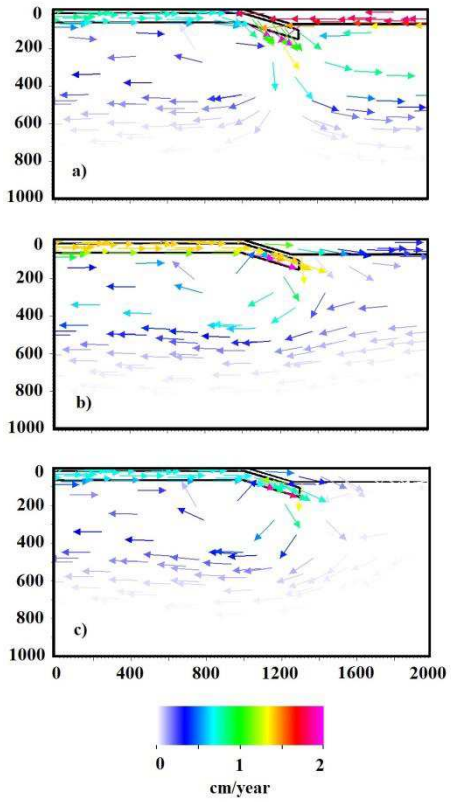

Figure 5.5. The model set-up: a square with free slip vertical and no slip lower boundaries. Oceanic lithosphere locates in left side and continental lithosphere is in the right side. a) top of the model is free slip, b) oceanic lithosphere moves with speed of 1.5 cm/year and continental lithosphere with the speed of 0.35 cm/year. c) Oceanic lithosphere sinks with the speed of 0.85 cm/year and continental lithosphere is fixed.

a)

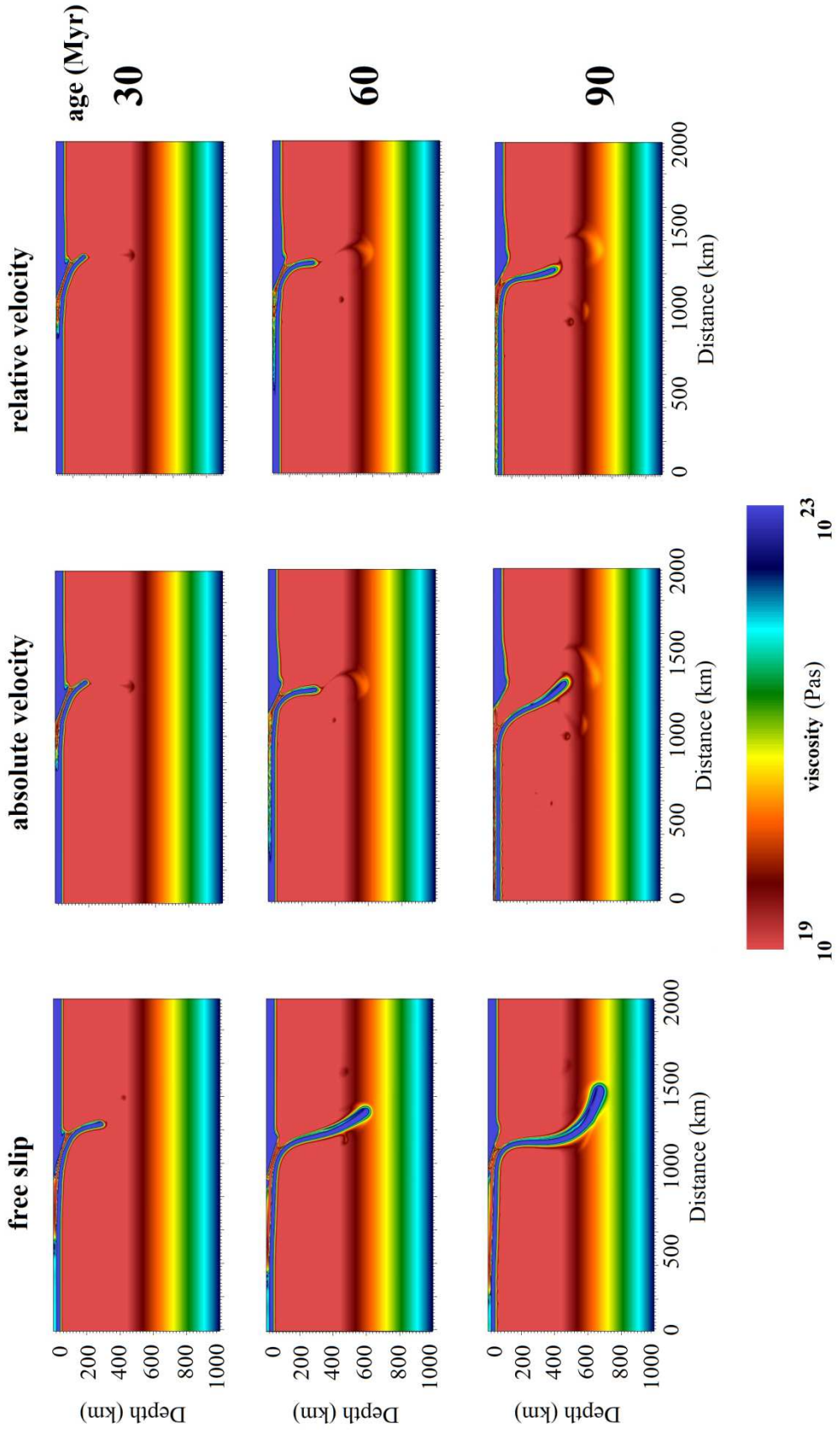
age (Myr)
30
60
90
relative velocity
absolute velocity
free slip
Depth (km)
Distance (km)
viscosity (Pas)
10^19
10^23

b)

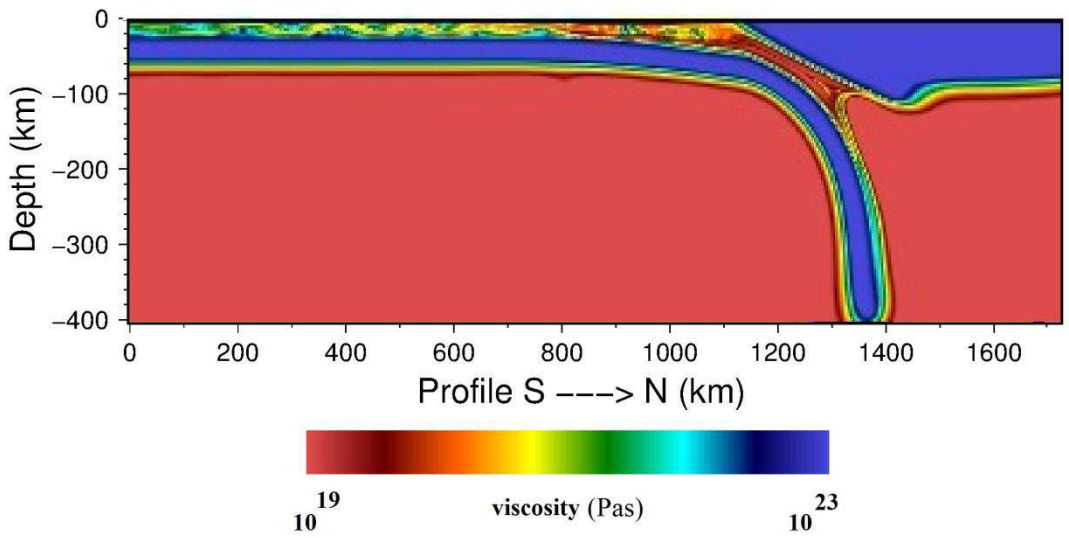

Figure 5.6. a) Snapshots of dynamic models at different ages: left) free slip, middle) absolute velocity and right) relative velocities. The slab is the fastest in free-slip top boundary and slows down using absolute velocity for plates. The slowest slab is achieved using relative velocity. b) Zoomed-in view of the modelled subduction around the trench and above ~ 410 km discontinuity. The figure shows the slab deformation at 60 Myrs considering absolute plate velocities (Torsvik et al., 2010).

5.5.2 Geophysical modeling

5.5.2.1 Lithospheric structure

The forward modeling scheme require an initial geometry model (Moho depth from CRUST1.0 (Laske et al., 2013) and Lithosphere-Asthenosphere Boundary (LAB) from LITHO1.0 (Pasyanos et al., 2014)) and physical parameters for the crust and upper mantle material. The physical parameters and chemical composition are detailed in Tables 5.1 and 5.2.

Crustal density and thermal parameters were set based on typical values for continental/oceanic crust in agreement with previous local studies (e.g. Entezar-Saadat et al., 2017). Further constraint is that the thermal conductivity slightly differs due to continental/oceanic affinity. Different tests were conducted on to find the best fitting geophysical observables.

Table 5.1. Physical properties used in this study: density, ρ (kg/m^3); thermal conductivity, K [W/(Km)]; volumetric heat production, H (μW/m^3); compression coefficient, β (mPa^{-1}). The heat production in the lithospheric mantle and asthenosphere is assumed 0.02 μW/m^3 while is ~25 times smaller than in crust overlain the Makran subduction zone (Smith et al., 2013). The heat production in the sublithosphere part is negligible (Fullea et al., 2009 and references therein).

No.	Material description	Density	Thermal conductivity	Compression coefficient
0	Water	1030	0	2
1	Indian Ocean (oceanic)	2690	2.3	12
2	Oman Gulf (oceanic)	2850	2.1	7.5
3	Makran (oceanic)	2810	2.0	6.5
4	Jazmurian (oceanic)	2800	2.2	6.5
5	Iran (upper crust)	2750	2.0	10
6	Iran (lower crust)	2900	2.0	15
c1, c2, c3, c4, slab, asthenosphere	(Sub)lithospheric mantle and slab	*	**	-
* Mantle densities are computed according to the corresponding temperature, pressure and bulk composition, see text for more details. ** The temperature-dependent thermal conductivity is computed iteratively while solving the thermal problem.				

In this study, geometry of Moho and LAB are according as much as possible to the global models which are seismological based on slab shape in our region (Fig. 5.7e). Average Moho depth of ~40 km characterizes continental crust in Iran. The largest Moho depth (~55 km) exists in topographic areas of Sistan suture (Fig. 5.7d) in order to fit observed gravity field data. However, I take CRUST1.0 as initial Moho depth. The thin crust of Oman Sea (~15 km) is limited between Semail Ophiolite in south and plate boundary (Bird, 2003) in north. To the north of Oman Sea, the crustal thickness beneath Makran increases gradually until Moho depth is ~40 km. Despite some discrepancies, the obtained Moho thickness is well consistent with the previous estimates of Moho depth in Makran (Kopp et al., 2000; Smith et al., 2013; Entezar-Saadat et al., 2017). Previous studies show a thin crust (up to ~20 km) beneath Lut Block and a deepening to ~55±15 km depth beneath the Makran onshore.

Fig. 5.5d shows the crustal domains 5 and 6 those represent upper and lower continental crustal layers beneath Iran with average thickness of ~20 km. From the left to the right of the profile, crustal parts are: the Indian Ocean, Oman Gulf, Makran, Jazmurian, and Iranian crust. The Indian ocean, the Oman Gulf, Jazmurian and the Makran crusts have been units representing oceanic crusts (Kopp et al., 2000; Smith et al., 2013; Entezar-Saadat et al., 2017) specified by higher densities (Table 5.1). I must note that the boundaries between crustal bodies are well-correlated with earthquake events (Fig. 5.7d).

5.5.2.2 Compositional setting

The lithospheric mantle composition is averagely Phanerozoic along profile (e.g. Artemieva, 2006; Griffin et al., 2009) with a slight variation to be constrained by two mantle xenolith samples (Nasir and Stern, 2012; Su et al., 2014). Neo-Proterozoic mantle of Arabian plate from 540–850 Ma (Nasir and Stern, 2012) is a compositional domain (mantle c1, Table 5.2; Fig. 5.7d) based on the mantle xenolith sample. Furthermore, I apply a more fertile mantle (low Mg# of mantle c2) with high Al_2O_3 content in the area above slab to reference the mantle composition related to dense/fertile subducting slab (Griffin et al., 2009). Underlying the Makran subduction zone, lithosphere is characterized by a low range of partial melting

rate (Kheirkhah et al., 2015) but the estimated composition (mantle c3, Table 5.2) is still considered to be fertile.

Geographically outside the modeling area, a recent study on mantle xenoliths of the northeast of Iran (Su et al., 2014) shows the upper mantle beneath NE of Iran is Proterozoic with a low rate of partial melt (Mg#=88.96) which characterizes the most fertile mantle composition (mantle c4) along our profile. In order to fit geophysical observables, I modified the model for lithosphere by modifying the Moho and LAB depths. An increase of 50 km to initial lithospheric thickness taken from LITHO.1.0 improved the fit to observed gravity data.

Table 5.2. Upper mantle chemical compositions (except mantle composition 4, referred to unpublished mantle xenolith data by B-X Su) used in this study

Oxides	Mant. c1[1]	Mant. c2	Mant. c3[3]	Slab[4]	Asthenosphere PUM[5]
SiO_2	45.4	45	45	44	45
Al_2O_3	3.7	3.9	3	2.3	4.5
FeO	8.3	8.1	7.9	8.4	8.1
MgO	39.3	38.7	42	41.4	37.8
CaO	3.2	3.2	1.9	2.2	3.6
Na_2O	0.26	0.28	0.13	0.24	0.36
Mg#=(100Mg/Mg+Fe)	89.93	89.5	90.45	89.8	89.3

1. based on mantle Peridotite (Nasir and Stern, 2012)
2. defined in Griffin et al. (2009)
3. between Proterozoic and Phanerozoic compositions (Tunini et al., 2015)
4. Spinel lherzolite defined in Griffin et al. (2009)
5. Primary Upper Mantle (McDonough and Sun, 1995)

5.5.2.3 Seismic velocities

Having applied 300˚C thermal contrasts between slab and ambient mantle (consistent with geodynamic modeling section 5.4) and using different composition compared to asthenosphere (shown in Fig. 5.7f), the model can predict the seismic velocity anomalies from SL2013sv. Vs seismic velocities decrease with depth until the LAB whereas it will increase in our model down to 400 km due to the effect of pressure. Positive velocity anomalies are particularly seen at depths of 200 and 400 km (Fig. 5.7f).

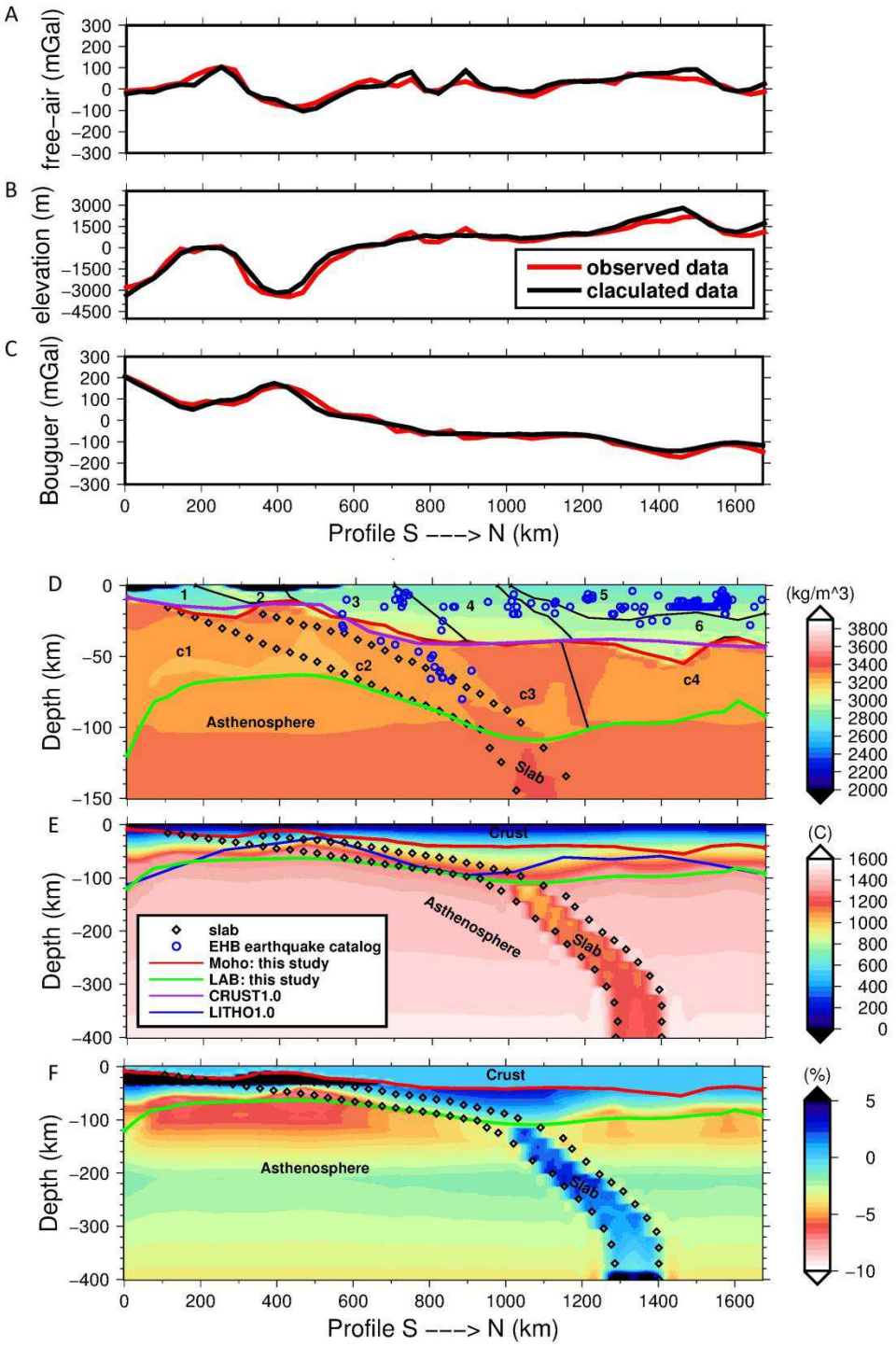

Figure 5.7. Geophysical observables vs. calculated data in Makran subduction zone and surrounding area. a) Free-air data from DTU10 (Anderson et al., 2010), b) Elevation data (Fig. 5.1 subtitle), c) Bouguer anomaly after applying Bouguer reduction (with a reduction density of 2670 kg/m^3) on Free-air data. d) Density cross section (zoomed in to upper 150 km) with signification of different crustal and lithospheric bodies, described in Tables 5.1 and 5.2. The resulted and referenced Moho are shown. e) Temperature cross section down to 400 km with the resulted and referenced LABs. f) Predicted shear wave velocity anomaly referenced to AK135 (Kennett et al., 1995).

5.6. Discussion

In order to find the best fitting model, I run different tests applying alternative in-slab temperatures. Large misfits of the medium cold slab (100-200 °C) and isotherm slab with ambient asthenosphere suggest the increase of thermal contrast to be efficient. Fig. 5.8 indicates the accuracy of this statement since in-slab density at 200 km depth returns to the asthenosphere value using at least 300 °C colder slab. The deeper part of the slab has always higher density compared to the ambient asthenosphere (by changing temperature and composition, we modify the depth at which some phase transitions take place (e.g. Olivine-Wadsleyite) (Fig. 5.8). Nonetheless, seismic velocities increase even without dramatic decrease of in-slab temperature.

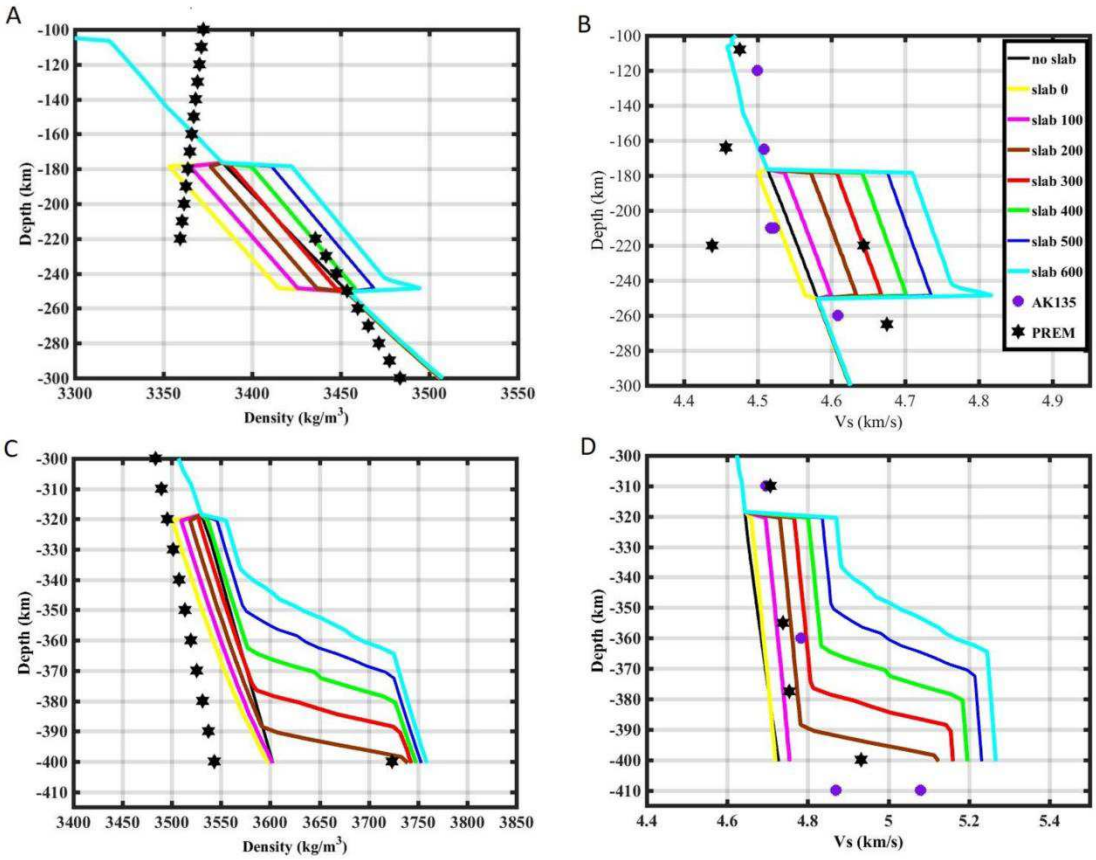

Figure 5.8. Comparison of in-slab densities and velocities at different depths (a and b zoomed-in to an average 200 km depth, and c and d are zoomed-in to an average 400 km depth). Graph colors show various in-slab thermal contrasts related to the ambient mantle (0, 100, 200, 300, 400, 500, 600 °C). 'slab 0' means slab and the ambient mantle are isotherm and slab is only distinguished by the compositional depletion. To note, in this study slab is compositionally depleted compared to asthenosphere. Therefore, the modelled slab density can be less than the one in asthenosphere considering a low thermal contrast between slab and asthenosphere. However, by decreasing temperature, the absolute slab density always increases.

Resulted from this test, deep slab is only faster than the ambient asthenosphere when is enough cold and compositionally depleted compared to ambient asthenosphere. Comparing seismic velocity and density values with global reference models (AK135 (Kennett et al., 1995) and PREM (Dziewonski and Anderson, 1981)) illustrate the harmony between present study results and documented predictions. Very cold slabs (>300 °C) provide still in the range but inacceptable large values of seismic velocity and densities compared to references.

5.7 Conclusions and outline

The present-day status of the subducting slab beneath the Makran subduction zone is revealed through seismic tomography models. However uncertainties are indicated by discrepancies between various seismic tomography models. This motivated me to model Neo-Tethys oceanic plate subduction over the past 90 Myrs based on plate reconstructions. In this way, I could assess the effects of both Africa-Eurasia plate convergence rate and the absolute plate motion reference frame on deformation of the subducting slab. I conducted a suite of numerical model set-ups with different boundary conditions to find a number of acceptable numerical solutions for the subduction. In present study, I assume the surface velocities of my model in the past 60 Myr reaches to only ~4 cm/yr.

The assumed boundary velocity condition imposes a certain geometry of the slab and a different range of deformation at the overriding plate. So far my results illustrate a strong correlation between slab deformation and plate velocities. Additionally, the large and small scale mantle convection controls the final location of slab beneath Sistan suture. Further, my dynamic model is still simple and basic. More parameters to make the model constrained will develop the robustness of the model.

Filling the gap between shallow structure from seismicity and deep features derived from seismic tomography and geodynamic models motivated me to model the present-day structure of the Makran subduction zone from surface down to 400 km depth. My lithospheric density distribution was derived from a slight change in the upper mantle composition constrained by mantle xenoliths. My model predicts the velocity features in seismic tomography models only when the slab body is added to sub-lithosphere. Once more, this study confirms the necessity of modifying the seismically defined Moho depth and subduction related lithospheric thickness after implementing petrological constraints on lithospheric and sub-lithospheric structure. In terms of amplitude, the obtained density model is comparable to predictions from global velocity and density models. Despite above mentioned advantages, a more complete and local database on crustal physical properties, seismicity and lithospheric composition can improve present results.

Chapter 6:
Conclusion and outlines
6.1 Conclusion

By crustal modeling, I gained first-order estimates of the basement structure from inversion of aeromagnetic data as initial geometry model to start forward modeling. Inverted geometry of basement is in one-by-one correlation with aeromagnetic data in terms of shape of signal. This can be interpreted that the medium to long wavelength contents of data has been projected to basement undulations. Further, our basement structure is modified to be well correlated with the most prominent magnetic features, e.g. most of igneous rocks, volcanoes and oceanic crust intrusions were modelled. Moreover, I considered the Curie depth as the base of magnetization while it resulted in introduction of Curie depth map of Iran for the first time. In this thesis, I developed the knowledge of intra-crustal structure beneath Iran. Likewise previous studies on crustal layers which are based on their density contrast, I used also susceptibility contrast between crustal layers down to Curie depth which enabled us to: i) distinguish between provinces of middle crust, ii) define magnetic/non-magnetic lower crust and upper mantle of the area where Curie depth is deeper and/or shallower than Moho depth. It is important that central Iran magnetic crust is shallower than Moho depth. This study is an example to indicate the high impact of combined gravity and magnetic modeling in modeling intra-crustal structure that is less constrained by using only gravity data modeling.

In lithospheric modeling, this thesis addresses for the first time the compositional distribution of lithospheric mantle beneath Iranian Plateau. Applying a varying range of fertility, constrained by mantle xenolith samples, leads to introduction of lithospheric mantle domains of Iran. Petrological studies are not capable to reveal regional distribution of mantle composition for entire area. Whereas, this study shows that geophysical modeling can approach to indirectly explore more on deep physical parameters of the Earth interior. However, I must note that I followed a trade-off strategy to decide on lithospheric domains as the solution of potential field modeling for composition is non-unique. In similar, I followed age, tectonic, xenolith sample to define the lithospheric composition. Of course, the geophysical residual anomalies were minimized in the preferred model. Our approach in modeling using multiple data sets assisted in reduction of uncertainties of the final model. In particular, using satellite gravity gradients constrain the model in the depths ranging 50-100 km.

In sub-lithospheric scale, this study addresses for the first time thermochemical structure of the slab beneath Iranian Plateau while the main features in tomography model were predicted. So, I found a more complete answer to the structure of lithosphere when deep structure beneath is not underestimated which is usually done by assuming a constant density for asthenosphere in the classic thermal modeling approach. I agree with the smaller effect of dense bodies in depth. Nevertheless, I must note that the presence of cold slab beneath lithosphere influences the geotherm of entire model. Therefore, the model with asthenosphere heterogeneity assumptions has two advantages: i) it is capable of fitting seismic features and ii) the LAB is modified to compensate the thermal/gravitational effect of slab. The second causes to increase the temperature of central Iran lithosphere. As the warmer material is lighter, the entire model's mass excess due to slab is compensated by lighter/warmer lithosphere above. More importantly, in chapter 2, I found a shallower depth of magnetization

than the Moho boundary in central Iran, literally means the deeper part of crust beneath central Iran is a transition between crustal and lithospheric material.

Based on seismological studies, the slab in Makran part is not that deep like in Zagros. Hence, I decided to model independently that area. From technical point of view, firstly, my model in Makran subduction zone addresses for the first time the geophysical model of a slab just under the lithosphere. Secondly, I applied the derived information from geodynamic modeling and applied them as a priori data in my static modeling. From the practical aspects, the crustal density and lithospheric composition was modified to compensating the extra density due to presence of shallow slab. In conclusion, my model supports the proposed crustal decollement and its main faulting system follows the convergence scenario. For the cause of this crustal characterization, the sequences of elevated chains in Iran possibly sharpened after initiation of continental plate subduction. Interestingly, the modelled lithospheric structure is consistence with the slab break-off, a dominant geodynamical scenario in the area. The thickening of lithosphere is well consisted with hanging parts of subducted oceanic plate. The crustal thickening follows the general subduction mechanism in our model, for instance is thicker in the trench where oceanic slab detaches from the surface. Nevertheless, our static model only allows to describe lithospheric structure of the present time by fitting geophysical observables and not to describe plate histories in detail.

6.2 Outlines

The next steps to this research are following as:

1) I have partially modelled the density structure beneath Makran using different data and methodologies. The next challenge is to estimate the density structure of both initial subducting slab and corresponding overriding plate.

2) In particular, plate reconstruction shows that the slab drives northward. I expect that slab starts to head toward north and sinks sluggishly because of its weight. This process will give a more complete image of slab beneath Makran in time.

3) Dynamic modeling needs the definition of mantle flows and its effects on the slab deformation. Despite limitations, the geodynamic model, in principle, enables us to see the possible location of slab through time unachievable by tomography or static models.

Bibliography

Abedi, M., Bahroudi, A., 2016. A geophysical potential field study to image the Makran subduction zone in SE of Iran, Tectonophysics, doi: 10.1016/j.tecto.2016.09.025.

Abu-Aljarayesh, I., Mahmood, S., Nasir, S., 1993. Magnetic study on lower crustal and upper mantle xenoliths from northeast Jordan. Abhath Al-Yarmouk, Pure Science and Engineering, 2, 41–54.

Afonso, J. C., Fernàndez, M., Ranalli, G., Griffin, W. L., Connolly, J. A. D., 2008. Integrated geophysical-petrological modeling of the lithosphere and sublithospheric upper mantle: methodology and applications, Geochem. Geophys. Geosyst., 9(5).

Afonso, J. C., Fullea, J., Griffin, W. L., Yang, Y., Jones, A. G., Connolly, J. A. D., O'Reilly, S. Y., 2013a. 3-D multi-observable probabilistic inversion for the compositional and thermal structure of the lithosphere and upper mantle, I: a priori petrological information and geophysical observables, J. geophys. Res., 118, 2586–2617.

Afonso, J. C., Fullea, J., Yang, Y., Connolly, J. A. D., Jones, A. G., 2013b. 3-D multi-observable probabilistic inversion for the compositional and thermal structure of the lithosphere and upper mantle, II: general methodology and resolution analysis, J. geophys. Res., 118, 1650–1676.

Afonso, J. C., Ranalli, G., Fernàndez, M., 2007. Density structure and buoyancy of the oceanic lithosphere revisited, Geophys. Res. Lett., 34, L10302, doi:10.1029/ 2007GL029515.

Agard, P. et al. 2011. Zagros orogeny: a subduction-dominated process, Geol. Mag., 148(5–6), 692–725.

Aghanabati, A., 2004. Geology of Iran, Geological Survey of Iran Press, Tehran.

Alavi, M., 1994. Tectonics of the Zagros orogenic belt of Iran: new data and interpretations, Tectonophysics, 229, 211–238.

Alinaghi, A., Kolakov, I., Thybo, H., 2007. Seismic tomographic imaging of P- and S-waves velocity perturbations in the upper mantle beneath Iran, Geophys. J. Int., 169, 1089–1102.

Allen, M. B., Ghassemi, M. R., Shahrabi, M., Qorashi, M., 2003. Accommodation of late Cenozoic oblique shortening in the Alborz range, northern Iran, Journal of Structural Geology, 25, 659–672.

Allen, M.B., Kheirkhah, M., Neill, I., Emami, M.H., McLeod, C.L., 2013. Generation of arc and within-plate chemical signatures in collision zone magmatism: Quaternary lavas from Kurdistan Province, Iran, J. of Petrology, 54, 887–911 doi:10.1093/petrology/egs090.

Alvers, M.R., Barrio-Alvers, L., Bodor, C., Götze, H.-J., Lahmeyer, B., Plonka, C., Schmidt, S., 2015. Quo vadis inversion? Constraining interactive inversion, First Break, 33, 65-73.

Alvers, M.R., Götze, H.-J., Barrio-Alvers, L., Plonka, C., Schmidt, S., Lahmeyer, B., 2014. EM and Potential Methods: A novel warped-space-concept for interactive 3D-geometry-inversion to improve seismic imaging, First Break, 32(4), 81-87.

Amante, C., Eakins, B.W., 2009. ETOPO1 arc-minute global relief model: procedures, data sources and analysis, NOAA Technical Memorandum NESDIS NGDC-24, 19 pp.

Andersen, O. B., Knudsen, P., Berry, P., 2010. The DNSC08GRA global marine gravity field from double retracked satellite altimetry, J. of Geodesy, 84(3), doi: 10.1007/s00190-009-0355-9.

Artemieva, I. M, 2006. Global 1 × 1 thermal model TC1 for the continental lithosphere: implications for lithosphere secular evolution, Tectonophysics, 426, 245–277.

Aubourg, C., Smith, B., Eshraghi, A., Lacombe, O., Authemayou, C., Amrouch, K., Bellier, O., Mouthereau, F., 2010. Implications markers in the Western Fars Arc (Zagros, Iran): tectonic new magnetic fabric data and their comparison with palaeostress, Geological Society, London, Special Publications, 330, 97-120, doi:10.1144/SP330.6.

Aubourg, C., Robion, P., 2002. Composite ferromagnetic fabrics (magnetite, greigite) measured by AMS and partial AARM in weakly strained sandstones from western Makran, Iran, Geophys. J. Int., 151, 729–737.

Austermann, J., Iaffaldano, G., 2013. The role of the Zagros orogeny in slowing down Arabia-Eurasia convergence since ~5 Ma, Tectonics, 32, 351–363, doi:10.1002/tect.20027.

Ballato, P., Uba, C. E., Landgraf, A., Strecker, M. R., Sudo, M., Stockli, D. F., Friedrich, A., Tabatabaei, S. H., 2011. Arabia–Eurasia continental collision: insights from late tertiary foreland-basin evolution in the Alborz Mountains, Northern Iran, Bull. geol. Soc. Am., 123(1–2), 106– 131.

Barnhart, W. D., Hayes, G. P., Samsonov, S. V., Fielding, E. J., Seidman, L. E., 2014. Breaking the oceanic lithosphere of a subducting slab: The 2013 Khash, Iran earthquake, Geophysical Research letters, 41, 32–36, doi:10.1002/2013GL058096.

Berberian, M., 1983. The southern Caspian: A compressional depression floored by trapped, modified oceanic crust, Can. J. Earth Sci., 20, 163–183, doi:10.1139/e83-015.

Berberian, M., King, G. C. P., 1981. Towards a paleogeography and tectonic evolution of Iran, Can. J. Earth Sci., 18, 210–265.

Berberian, M., 1995. Master 'blind' thrust faults hidden under the Zagros folds: active basement tectonics and surface morphotectonics, Tectonophysics, 241, 193–224.

Bijwaard, H., et al. 1998. Closing the gap between regional and global travel time tomography, J. Geophys. Res., 103 (B12), 30, 055–30, 078. doi:10.1029/98jb02467.

Bird, P., 2003. An updated digital model of plate boundaries, Geochemistry Geophysics Geosystems, 4(3), 1027, doi:10.1029/2001GC000252.

Bouman J., Ebbing J., Fuchs M., Sebera J., Lieb V., Szwillus W., Haagmans R., Novak P., 2016. Satellite gravity gradient grids for geophysics, Nature Scientific Reports, 6, 21050, doi; 10.1038/srep21050.

Bouman, J., et al. 2013. GOCE gravity gradient data for lithospheric modeling, Int. J. Appl. Earth Observ. Geoinf., http://dx.doi.org/10.1016/j.jag.2013.11.001.

Bowin, C., 2000. Mass anomalies and the structure of the Earth, Physics and Chemistry of the Earth, 25 (4), 343-353.

Brunet, M. F., Korotaev, M. V., Ershov, A. V., Nikishin, A. M., 2003. The South Caspian Basin: A review of its evolution from subsidence modeling, Sediment Geol., 156(1–4), 119–148, doi:10.1016/S0037- 0738(02)00285-3.

Burg, J. -P., Bernoulli, D., Smit, J., Dolati, A., Bahroudi, A., 2008. A giant catastrophic mud-and-debris flow in the Miocene Makran, Terra Nova, 20(3), 188–193.

Byrne, D. E., et al., 1992. Great thrust earthquakes and aseismic slip along the plate boundary of the Makran subduction zone, J. Geophys. Res. Solid Earth, 97(B1), 449–478.

Casciello, E., Verges, J., Saura, E., Casini, G., Fernàndez, N., Blanc, E., Homke, S., Hunt, D., 2009. Fold patterns and multilayer rheology of the Lurestan Province, Zagros Simply Folded Belt (Iran), Geol. Soc. Lond., 166, 1–13.

Clark, D. A., Emerson, D. W., 1991. Notes on rock magnetization characteristics in applied geophysical studies, Exploration geophysics, 22, 547-555.

Connolly, J., 2005. Computation of phase equilibria by linear programming: a tool for geodynamic modeling and an application to subduction zone decarbonation, Earth planet. Sci. Lett., 236, 524–541.

Connolly, J. A. D., 2009. The geodynamic equation of state: What and how, Geochem. Geophys. Geosys., 10, Q10014, doi:10.1029/ 2009GC002540.

Connolly, J. A. D., Kerrick, M., 2002. Metamorphic controls on seismic velocity of subducted oceanic crust at 100–250 km depth, Earth and Planet. Sci. Let., 204 (1-2), 61-74.

Davies, J. H., von Blanckenburg, F., 1995. Slab break-off: A model of lithosphere detachment and its test in the magmatism and deformation of collisional orogens, Earth and Planetary Science Letters, 129, 85–102, doi:10.1016/0012-821X(94)00237-S.

Davoudzadeh, M., Schmidt, K., 1984. A review of the Mesozoic paleogeography and paleotectonic evolution of Iran, Neues Jahrb. Geol. Palaeontol. Abh., 168, 182–207.

Dehghani, G., Makris, J., 1984. The gravity field and crustal structure of Iran, Neues Jahrb. Geol. Palaeontol. Abh., 168, 215–229.

Doin, M. P., Fleitout, L., 1996. Thermal evolution of the oceanic lithosphere: an alternative view, Earth and Planet. Sci. Let., 142, 121-136.

Doin, M. P., Fleitout, L., 1996. Thermal evolution of the oceanic lithosphere: an alternative view, Earth and Planet. Sci. Let., 142, 121-136.

Dziewonski, A. M., Anderson, D. L., 1981. Preliminary reference Earth model, Physics of the Earth and Planetary Interiors, 25, 297-356.

Ebbing, J., Bouman, J., Fuchs, M., Lieb, V., Haagmans, R., Meekes J. A. C., Abdul Fattah, R., 2013. Advancements in satellite gravity gradient data for crustal studies, The leading edge, 936-941.

Egan, S. S., Mosar, J., Brunet, M. F., Kangarli, T., 2009. Subsidence and uplift mechanisms within the South Caspian Basin: Insights from the onshore and offshore Azerbaijan region, Geol. Soc. Spec. Publ., 312, 219–240, doi:10.1144/SP312.11.

Emami, H., Verges, J., Nalpas, T., Gillespie, P., Sharp, I., Karpuz, R., Blanc, E. J. -P., Goodarzi, M. G. H., 2010. Structure of the Mountain Front Flexure along the Anaran anticline in the Pusht-e Kuh Arc (NW Zagros, Iran): insights from sand box models, in Tectonic and Stratigraphic Evolution of Zagros and Makran during the Mesozoic-Cenozoic, pp. 155–78, eds Leturmy, P. and Robin, C., Geol. Soc. London Spec. Pub. no. 330.

Engdahl, E. R., Jackson, J. A., Myers, S. C., Bergman, E. A., Priestley, K., 2006. Relocation and assessment of seismicity in the Iran region, Geophys. J. Int., 167, 761–778 doi: 10.1111/j.1365-246X.2006.03127.x.

Entezar-Saadat, V., Motavalli-Anbaran, S. H., Zeyen, H., 2017. Lithospheric structure of the Eastern Iranian plateau from integrated geophysical modeling: A transect from Makran to the Turan platform, Journal of Asian Earth Sciences, 138, 357–366.

Floberghagen, R., Fehringer, M., Lamarre, D., Muzi, D., Frommknecht, B., Steiger, C., Piñeiro, J., da Costa, A., 2011. Mission design, operation and exploitation of the gravity field and steady state ocean circulation explorer mission, J. of Geodesy, http://dx.doi.org/10.1007/s00190-011-0498-3.

Fullea, J., Fernàndez, M., Zeyen, H., Vergés, J., 2007. A rapid method to map the crustal and lithospheric thickness using elevation, geoid anomaly and thermal analysis. Application to the Gibraltar Arc System, Atlas Mountains and adjacent zones, Tectonophysics, 430, 97–117.

Fullea, J., Afonso, J. C., Connolly, J. A. D., Fernàndez, M., García-Castellanos, D., Zeyen, H., 2009. LitMod3D: an interactive 3-D software to model the thermal, compositional, density, seismological, and rheological structure of the lithosphere and sublithospheric upper mantle, Geochem. Geophys. Geosyst., 10(8), doi: 10.129/2009GC002391.

Fullea, J., Fernàndez, M., Afonso, J. C., Vergés, J., Zeyen, H., 2010. The structure and evolution of the lithosphere–asthenosphere boundary beneath the Atlantic–Mediterranean Transition Region, Lithos, doi:10.1016/j.lithos.2010.03.003.

Fullea, J., Muller, M. R., Jones, A. G., Afonso, J. C., 2014. The lithosphere–asthenosphere system beneath Ireland from integrated geophysical–petrological modeling II: 3D thermal and compositional structure, Lithos, 189, 49-64.

Gaina, C., van Hinsbergen, D. J. J., Spakman, W., 2015. Tectonic interactions between India and Arabia since the Jurassic reconstructed from marine geophysics, ophiolite geology, and seismic tomography, Tectonics, 34, doi:10.1002/2014TC003780.

Geosoft, 2015. Oasis Montaj MAGMAP filtering, defining and applying filters and inverse FFT in MAGMAP, Geosoft Incorporated, p. 25.

Ghasemi, A., Talbot, C. J., 2006. A new tectonic scenario for the Sanandaj Sirjan Zone (Iran), J. Asian Earth Sci., 26, 683–693.

Ghorbani, M., 2013. The Economic Geology of Iran: Mineral Deposits and Natural Resources. 1st Ed. Springer, New York (569 P.).

Glennie, K.W., Hughes Clarke, M.W., Boeuf, M. G. A., Pilaar, W. F. H., Reinhardt, B. M., 1990. Inter-relationship of Makran-Oman Mountains belts of convergence, Geol. Soc., Lond., Special Publications, 49, 773– 786, doi:10.1144/GSL.SP.1992.049.01.47.

Golonka, J., 2007. Geodynamic evolution of the South Caspian Basin, in Oil and Gas of the Greater Caspian Area, edited by P. O. Yilmaz and G. H. Isaksen, AAPG Stud. Geol., 55, 17–41.

Götze, H. J., Lahmeyer, B., 1988. Application of 3-dimensional interactive modeling in gravity and magnetics, Geophysics, 53(8), 1096–1108.

Götze, H.-J., 2015. Potential Methods and Geoinformation Systems. In: Freeden, W., Nashed, M.Z., Sonar, T. (Eds.): Handbook of Geo-Mathematics. Berlin, Heidelberg, Springer Verlag, 1 – 21, doi:10.1007/978-3-642-27793-1_52-2.

Gök, R., Mahdi, H., al-Shukri, H., Rodgers, A., 2008. Crustal structure of Iraq from receiver functions and surface wave dispersion; implications for understanding the deformation history of the Arabian-Eurasian collision, Geophys. J. Int., 172, 1179–1187.

Gradmann, S., Ebbing, J., Fullea, J., 2013. Integrated Geophysical Modeling of Lateral Transition Zone in Lithospheric Mantle under Norway and Sweden: Geophys. J. Int., 194, 1358-1373.

Green, T., Abdullayev, N., Hossac, J., Riley, G., Roberts, A. M., 2009. Sedimentation and subsidence in the South Caspian Basin, Azerbaijan, Geol. Soc. Spec. Publ., 312, 241–260, doi:10.1144/SP312.12.

Grégoire, M., Langlade, J.A., Delpech, G., Dantas, C., Ceuleneer, G., 2009. Nature and evolution of the lithospheric mantle beneath the passive margin of East Oman: evidence from mantle xenoliths sampled by Cenozoic alkaline lavas, Lithos, 112, 203–216.

Griffin, W. L., O'Reilly, S.Y., Afonso, J. C., Begg, G., 2009. The composition and evolution of lithospheric mantle: a re-evaluation and its tectonic implications, J. Petrol., 50, 1185–1204.

Gritto, R., et al. 2008. Crustal structure of North Iraq from receiver function analyses, Monitoring Research Review, Ground-Based Nuclear Explosion Monitoring Technologies, 298, 80–86.

Guest, B., Axen, G. J., Lam, P. S., Hassanzadeh, J., 2006. Late Cenozoic shortening in the west-central Alborz Mountains, northern Iran, by combined conjugate strike-slip and thin-skinned deformation, Geosphere, 2(1), 35–52.

Guest, B., Guest, A., Axen, G., 2007. Late Tertiary tectonic evolution of northern Iran: A case for simple crustal folding, Global Planet. Change, 58(1–4), 435–453, doi:10.1016/j.gloplacha.2007.02.014.

Hafkenscheid, E., Wortel, M. J. R., Spakman, W., 2006. Subduction history of the Tethyan region derived from seismic tomography and tectonic reconstructions, J. Geophys. Res., 111, B08401, doi:10.1029/2005JB003791.

Harms, J. C., Cappel, H. N., Francis, D. C., 1984. The Makran coast of Pakistan: its stratigraphy and hydrocarbon potential, Mar. Geol. Oceanogr. Arab. Sea Coastal Pakistan, 3, 27.

Hatzfeld, D., Molnar, P., 2010. Comparisons of the kinematics and deep structures of the Zagros and Himalaya and of the Iranian and Tibetan Plateaus and geodynamic implications, Rev. Geophys., 48, RG2005, doi:10.1029/2009RG000304.

Hatzfeld, D., Tatar, M., Priestley, K., Ghafory-Ashtyany, M., 2003. Seismological constraints on the crustal structure beneath the Zagros Mountain belt (Iran), Geophys. J. Int. 155, 403–410.

Haynes, S. J., Reynolds, P. H., 1980. Early development of Tethys and Jurassic ophiolite displacement: Nature, v. 283, p. 561-563.

Holland, T., Powell, R., 1998. An internally consistent thermodynamic data set for phases of petrological interest, J. Metamorph. Geol., 16, 309– 343.

Holzrichter, N., 2013. Processing and interpretation of satellite and ground based gravity data at different lithospheric scales, PhD thesis, Kiel University.

Jackson, J. A., Fitch, T., 1981. Basement faulting and the focal depths of the larger earthquakes in the Zagros Mountains (Iran), Geophys. J. R. Astron. Soc., 64, 561–586.

Jacob, K.H., Quittmeyer, R.C., 1979. The Makran region of Pakistan and Iran: trench-arc system with active plate subduction, in Geodynamics of Pakistan, pp. 305–318, eds Farah, A. and de Jong, A., Geol. Surv. Pakistan, Quetta.

Jiménez-Munt, I., Fernàndez, M., Saura, E., Vergés, J., Garcia-Castellanos, D., 2012. 3-D lithospheric structure and regional/residual Bouguer anomalies in the Arabia–Eurasia collision (Iran), Geophys. J. Int., 190, 1311–1324.

Kaislaniemi, L., van Hunen, J., Allen, M.B., Neill, I., 2014. Sublithospheric small-scale convection—A mechanism for collision zone magmatism, Geology, 42(4), 291–294.

Kaviani, A., Paul, A., Bourova, E., Hatzfeld, D., Pedersen, H., Mokhtari, M., 2007. A strong seismic velocity contrast in the shallow mantle across the Zagros collision zone (Iran), Geophys. J. Int., 171, 399–410.

Kennett, B. L. N., Engdahl, E. R., Buland, R., 1995. Constraints on seismic velocities in the Earth from travel times, Geophys. J. Int., 122(1), 108–124.

Keskin, M., Pearce, J.A., Mitchell, J.G., 1998. Volcano-stratigraphy and geochemistry of collision-related volcanism on the Erzurum-Kars Plateau, northeastern Turkey, Journal of Volcanology and Geothermal Research, 85, 355–404, doi:10.1016/S0377-0273(98)00063-8.

Kheirkhah, M., Neill, I., Allen, M. B., 2015. Petrogenesis of OIB-like basaltic volcanic rocks in a continental collision zone: Late Cenozoic magmatism of Eastern Iran, Journal of Asian Earth Sciences, 106, 19–33.

Knapp, C. C., Knapp, J. H., Connor, J. A., 2004. Crustal-scale structure of the South Caspian Basin revealed by deep seismic reflection profiling, Mar. Pet. Geol., 21(8), 1073–1081, doi:10.1016/j.marpetgeo.2003.04.002.

Kopp, C., Fruehn, J., Flueh, E. R., Reichert, C., Kukowski, N., Bialas, J., Klaeschen, D., 2000. Structure of the Makran subduction zone from wide-angle and reflection seismic data, Tectonophysics, 329, 1, 171–191.

Koulakov, I., 2011. High-frequency P and S velocity anomalies in the upper mantle beneath Asia from inversion of worldwide travel time data, Journal of Geophysical Research, Solid Earth, 116(B4).

Kronbichler, M., Heister, T., Bangerth, W., 2012. High accuracy mantle convection simulation through modern numerical methods, Geophys. J. Int., 191, 12–29, doi: 10.1111/j.1365-246X.2012.05609.x.

Lambert, I. B., Wyllie, P. J., 1970. Low-Velocity Zone of the Earth's Mantle: Incipient Melting Caused by Water, Science, 169 (3947), 764-766, doi: 10.1126/science.169.3947.764.

Laske, G., Masters., G., Ma, Z., Pasyanos, M., 2013. Update on CRUST1.0 - A 1-degree Global Model of Earth's Crust, Geophys. Res. Abstracts, 15, Abstract EGU2013-2658.

Maggi, A., Priestley, K., 2005. Surface waveform tomography of the Turkish–Iranian plateau, Geophys. J. Int., 160, 1068–1080.

McCall, G. J., 1997. The geotectonic history of the Makran and adjacent areas of Southern Iran, J. Asian earth sci., 15, 517–531.

McCall, G. J. H., Kidd, R. G. W., 1982. The Makran, Southeastern Iran: the anatomy of a convergent plate margin active from Cretaceous to Present, Geol. Soc., Lond., Special Publications, 10(1), 387–397, doi:10.1144/GSL.SP.1982.010.01.26.

McDonough, W.F., Sun, S., 1995. The composition of the Earth, Chem. Geol., 120, 223–253.

McQuarrie, N., van Hinsbergen, D. J. J., 2013. Retro-deforming the Arabia Eurasia collision zone: age of collision versus magnitude of continental subduction, Geology, 41, 315–318.

Mohammadi, N., Sodoudi, F., Mohammadi, E., Sadidkhouy, A., 2013. New constraints on lithospheric thickness of the Iranian plateau using converted waves, J. of Seismol., 17, 883–895.

Mokhtari, M., Farahbod, A. M., Lindholm, C., Alahyarkhani, M., Bungum, H., 2004. An approach to a comprehensive Moho depth map and crust and upper mantle velocity model for Iran, Iranian Int. J. Sci., 5 (2), 223–244.

Molinaro, M., H. Zeyen, Laurencin, X., 2005. Lithospheric structure beneath the south-eastern Zagros Mountains, Iran: Recent slab break off?, Terra Nova, 17(1), 1–6.

Molinaro, M., Leturmy, P., Guezou, J.-C., Frizon de Lamotte, D., Eshraghi, S. A., 2005. The structure and kinematics of the southeastern Zagros fold thrust belt, Iran: from thin-skinned to thick-skinned tectonics, Tectonics, 24(3), doi:10.1029/2004TC001633.

Monsef, I., Rahgoshay, M., Mohajjel, M., Shafaii-Moghadam, H., 2010. Peridotites from the Khoy Ophiolitic Complex, NW Iran: Evidence of mantle dynamics in a supra-subduction-zone context, Journal of Asian Earth Sciences, 38, 105–120.

Morley, C. K., Kongwung, B., Julapour, A. A., Abdolghafourian, M., Hajian, M., Waples, D., Warren, J., Otterdoom, H., Srisuriyon, K., Kazemi, H., 2009. Structural development of a major late Cenozoic basin and transpressional belt in central Iran: the Central Basin in the Qom-Saveh area, Geosphere, 5(4), 325–362.

Motavalli-Anbaran, S. H., Zeyen, H., Brunet, M. F., Ardestani, V. E., 2011. Crustal and lithospheric structure of the Alborz Mountains, Iran, and surrounding areas from integrated geophysical modeling, Tectonics, 30, TC5012, doi:10.1029/2011TC002934.

Mousavi, N., Ardestani, V.E., Ebbing, J., Fullea, J., 2016. 3D Integrated geophysical-petrological modeling of the Iranian lithosphere. In EGU General Assembly Conference Abstracts, Vol. 18, p. 10601.

Mousavi, N., Ebbing, J., Ardestani, V. E., 2017. Interpretation of structure of lithosphere and crust in Zagros region using modeling of topography, geoid and potential field data (gravity and magnetic). Geosciences, 26 (103), 119-128, doi: 10.22071/gsj.2017.46771.

Mousavi, N., Ebbing, J., 2017, magnetic basement and crustal structure in the Arabia–Eurasia collision zone from a combined gravity and magnetic model. EGU2017, Austria.

Mousavi, N., Ebbing, J., 2018. Basement characterization and crustal structure beneath the Arabia–Eurasia collision (Iran): a combined gravity and magnetic study, Tectonophysics, 731-732, 155-171, doi:10.1016/j.tecto.2018.03.018.

Mousavi, N., Ebbing, J., Fullea, J., 2018a, the effects of slab breakoff on the present-day (sub)lithospheric architecture beneath the Iranian plateau, EGU2018, Austria.

Mousavi, N., Ebbing, J., Steinberger, B., 2018b, the effects of prescribed surface plate motions on slab deformation in the Makran subduction zone, German-Swiss geodynamics workshop.

Mouthereau, F., Lacombe, O., Vérges, J., 2012. Building the Zagros collisional orogen: timing, strain distribution and the dynamics of Arabia/Eurasia plate convergence, Tectonophysics, 532–535, 27–60.

Nabavi, M., 1976. An introduction to Geology of Iran, Geological Survey of Iran, Tehran.

Namaki, L., Gholami, A., Hafizi, M. A., 2011. Edge-preserved 2-D inversion of magnetic data: an application to the Makran arc-trench complex, Geophys. J. Int., 184, 1058–1068, doi: 10.1111/j.1365-246X.2010.04877.x.

Nasir, S., 1992. The lithosphere beneath the northwestern part of the Arabian Plate Jordan. Evidence from xenoliths and geophysics, Tectonophysics, 201, 357–370.

Nasir, S., Stern, R. J., 2012. Lithospheric petrology of the eastern Arabian Plate: Constraints from Al-Ashkhara (Oman) xenoliths, Lithos, 132–133, 98–112.

Nasrabadi, A., Tatar, M., Priestley, K., Sepahvand, M.R., 2008. Continental lithosphere structure beneath the Iranian plateau, from analysis of receiver functions and surface waves dispersion, in Proceedings of the 14th World Conference on Earthquake Engineering, Beijing, China.

Neill, I., Meliksetian, K., Allen, M.B., Navarsardyan, G., Karapetyan, S., 2013. Pliocene–Quaternary volcanic rocks of NW Armenia: Magmatism and lithospheric dynamics within an active orogenic plateau, Lithos, 180–181, 200–215, doi:10.1016/j.lithos.2013.05.005.

Nowrouzi, G., Ghafoury, M., Ashtiany, M., Javan Doley, G., 2007. Crustal velocity structure of northeast of central Iran and Binalud zone, using teleseismic receiver functions, J. Earth Space Phys., 33, 1205– 8647.

Omrani, J., Agard, P., Whitechurch, H., Benoit, M., Prouteau, G., Jolivet, L., 2008. Arcmagmatism and subduction history beneath the Zagros Mountains, Iran: a new report of adakites and geodynamic consequences, Lithos, 106 (3–4), 380–398.

Oskooi, B., Abedi, M., 2015. An airborne magnetometry study across Zagros collision zone along Ahvaz-Isfahan route in Iran, Journal of Applied Geophysics, 123, 112-122.

Parker, R.L., 1972. The rapid calculation of potential anomalies, Geophys. J. R. Astron. Soc., 31, 447–455.

Pasyanos, M. E., T. G., Masters, Laske, G., Ma, Z., 2014. LITHO1.0: An updated crust and lithospheric model of the Earth, J. Geophys. Res. Solid Earth, 119, 2153–2173, doi:10.1002/2013JB010626.

Paul, A., Kaviani, A., Hatzfeld, D., Vergne, J., Mokhtari, M., 2006. Seismological evidence for crustal-scale thrusting in the Zagros mountain belt (Iran), Geophys. J. Int., 166, 227–237.

Paul, A., Hatzfeld, D., Kaviani, A., Tatar, M., Pequegnat, C., 2010. Seismic imaging of the lithospheric structure of the Zagros mountain belt (Iran), Geol. Soc. Lond., Spec. Pub., 330, 5–18.

Pavlis, N. K., Holmes, S. A., Kenyon, S. C., Factor, J. K., 2008. An earth gravitational model to degree 2160: EGM2008, in Proceedings of the 2008 General Assembly of the European Geosciences Union, Vienna, Austria, 2008 April 13–18, EGU2008-A-01891.

Pazirandeh, M., 1973. distribution of volcanic rocks in Iran and a preliminary discussion of their relationship to tectonics. Geol. Sur. of Iran report, presented at the geological symposium of the national Iranian oil company in 1973.

Pearce, J. A., Lippard, S. J., Roberts, S., 1986. Characteristics and tectonic significance of supra-subduction zone ophiolites, Geological Society, London Special Publication, 16, 77–94.

Penney, C., Tavakoli, F., Saadat, A., Nankali, H., Sedighi, M., Khorrami, F., Sobouti, F., Rafi, Z., Copley, A., Jackson, J., Priestley, K., 2017. Megathrust and accretionary wedge properties and behavior in the Makran subduction zone, Geophys. J. Int., 209, 1800–1830.

Plasman, M., et al., 2017. Lithospheric low-velocity zones associated with a magmatic segment of the Tanzanian Rift, East Africa, Geophys. J. Int., 210, 465–481, doi: 10.1093/gji/ggx177.

Pollack, H. N., Hurter, S. J., Johnson, J. R., 1993. Heat flow from the Earth's interior: Analysis of the global data set, Rev. Geophys., 31(3), 267–280, doi:10.1029/93RG01249.

Popowski, T., Connard, G., Tull, S., Bashilov, V., 2006. GMSYS-3D Gravity and Magnetic Modeling for Oasis Montaj—User Guide. Northwest Geophysical Associates, Corvallis Oregon.

Priestley, K., McKenzie, D., Barron, J., Tatar, M., Debayle, E., 2012. The Zagros core: Deformation of the continental lithospheric mantle, Geochem. Geophys. Geosyst., 13, Q11014, doi:10.1029/2012GC004435.

Radjaee, A., Rham, D., Mokhtari, M., Tatar, M., Priestley, K., Hatzfeld, D., 2010. Variation of Moho depth in the central part of the Alborz Mountains, northern Iran, Geophys. J. Int., 181, 173–184.

Rezaeian, M., Carter, A., Hovius, N., Allen, M. B., 2012. Cenozoic exhumation history of the Alborz Mountains, Iran: new constraints from low-temperature chronometry, Tectonics, 31(2), 1–20.

Rochette, P., Jackson, J., Aubourg, C., 1992. Rock magnetism and the interpretation of ansisotropy of magnetic susceptibility, Review of Geophysics, 30, 209–226.

Rolandone, F., Lucazeau, F., Leroy, S., Mareschal, J.-C., Jorand, R., Goutorbe, B., Bouquerel, H., 2013. New heat flow measurements in Oman and the thermal state of the Arabian Shield and Platform, Tectonophysics, 589, 77-89.

Royer, J.-Y., Müller, R.D., Gahagan, L.M., Lawver, L.A., Mayes, C.L., Nürnberg, D., Sclater, J.G., 1992. A GLOBAL ISOCHRON CHART, University of Texas, Institute for Geophysics, Technical Report No. 117, https://perso-sdt.univ-brest.fr/~jroyer/Agegrid/utig_report.html#color_im.

Schaeffer, A. J., Lebedev, S., 2013. Global shear-speed structure of the upper mantle and transition zone, Geophys. J. Int., 194, 417–449.

Schmidt, S., Götze, H. J., 1999. Integration of data constraints and potential field modeling—an example from southern lower Saxony, Germany. Phys. Chem. Earth, 24(3), 191–196.

Sepehr, M., Cosgrove, J.W., 2004. Structural framework of the Zagros fold-thrust belt, Iran, Mar. Petrol. Geol., 21(7), 829–843.

Shad-Manaman, N. S., Shomali, H., 2010. Upper mantle S-velocity structure and Moho depth variations across Zagros belt, Arabian–Eurasian plate boundary, Phys. Earth planet. Int., 180, 92–103.

Shad-Manaman, N., Shomali, H., Koyi, H., 2011. New constraints on upper-mantle S-velocity structure and crustal thickness of the Iranian plateau using partitioned waveform inversion, Geophys. J. Int., 184, 247-267.

Shahabpour, J., 2010. Tectonic implications of the geochemical data from the Makran igneous rocks in Iran. Island Arc, 19(4), 676–689.

Sherkati, S., Letouzey, Y., Frizon de Lamotte, D., 2006. Central Zagros fold-thrust belt (Iran): new insights from seismic data, field observation and sandbox modeling, Tectonics, 25, TC4007, doi:10.1029/2004TC001766.

Smith, G. L., McNeill, L. C., Wang, K., He, J., Henstock, T. J., 2013. Thermal structure and megathrust seismogenic potential of the Makran subduction zone, Geophys. Res. Lett., 40 (8), 1528–1533.

Stern, R.J., Johnson, P., 2010. Continental lithosphere of the Arabian Plate: a geologic, petrologic, and geophysical synthesis, Earth-Science Rev., 101, 29–67.

Stixrude, L., Lithgow-Bertelloni, C., 2005. Mineralogy and elasticity of oceanic upper mantle: origin of the low velocity zone, Journal of Geophysical Research, 110, doi:10.1029/2004JB002965.

Stöcklin, J., 1968. Structural history and tectonics of Iran: a review. Am. Assoc. Petrol. Geol. Bull., 52, 1229–1258.

Su, B.-X., Chung, S.-L., Zarrinkoub, M. H., Pang, K.-N., Chen, L., Ji, W.-Q., Brewer, A., Ying, J.-F., Khatib, M. M., 2014. Composition and structure of the lithospheric mantle beneath NE-Iran: constraints from mantle xenoliths, Lithos, 202–203, 267–282.

Taghizadeh-Farahmand, F., Sodoudi, F., Afsari, N., Mohammadi, N., 2013. A detailed receiver function image of the lithosphere beneath the Kopet-Dagh (Northeast Iran), J. Seismol., 17 (4), 1207–1221.

Takin, M., 1972. Iranian geology and continental drift in the Middle East, Nature, 235, 147–150.

Talebian, M., Jackson, J., 2004. A reappraisal of earthquake focal mechanisms and active shortening in the Zagros Mountains of Iran, Geophys. J. Int., 156, 506–526.

Tavakoli-shirazi, S., 2012. The Geology of the High Zagros (Iran): tectonic and thermal evolution during the Paleozoic. PhD thesis, Department of Earth Sciences, Université de Cergy Pontoise, English.

Teknik, V., Ghods, A., 2017. Depth of magnetic basement in Iran based on fractal spectral analysis of aeromagnetic data, Geophys. J. Int., 209, 1878–1891.

Thomas, J. C., Grasso, J. R., Bossu, R., Martinod, J., Nurtaev, B., 1999. Recent deformation in the Turan and South Kazakh platforms, western central Asia, and its relation to Arabia–Asia and India–Asia collisions, Tectonics, 18, 201–214, doi:10.1029/1998TC900027.

Torsvik, T. H., Steinberger, B., Gurnis, M., Gaina, C., 2010. Plate tectonics and net lithosphere rotation over the past 150 My, Earth and Planetary Science Letters, 291, 106–112.

Tunini, L., Jiménez-Munt, I., Fernàndez, M., Vergés, J., Villaseñor, A., 2015. Lithospheric mantle heterogeneities beneath the Zagros Mountains and the Iranian Plateau: a petrological-geophysical study, Geophys. J. Int., 200, 596–614.

van der Meer, D. G., Spakman, W., van Hinsbergen, D. J. J., Amaru, M. L., Torsvik, T. H., 2009. Towards absolute plate motions constrained by lower-mantle slab remnants, nature Geosciences, 3, 36-40.

van der Meer, D. G., van Hinsbergen, D. J. J., Spakman, W., 2017. Atlas of the underworld: Slab remnants in the mantle, their sinking history, and a new outlook on lower mantle viscosity, Tectonophysics, doi:10.1016/j.tecto.2017.10.004.

van Hunen, J., Allen, M.B., 2011. Continental collision and slab break-off: A comparison of 3-D numerical models with observations, Earth and Planetary Science Letters, 302, 27–37, doi:10.1016/j.epsl.2010.11.035.

Vergés, J., Saura, E., Casciello, E., Fernández, M., Villaseñor, A., Jiménez-Munt, I., García-Castellanos, D., 2011. Crustal-scale cross-section across the NW Zagros Belt: implications for the Arabian Margin reconstruction, Geol. Mag., 148, 739–761.

Vernant, P., Nilforoushan, F., Hatzfeld, D., Abbassi, M. R., Vigny, C., Masson, F., Nankali, H., Martinod, J., Ashtiani, A., Bayer, R., Tavakoli, F., Chéry, J., 2004. Present-day crustal deformation and plate kinematics in the Middle East constrained by GPS measurements in Iran and northern Oman, Geophys. J. Int., 157(1), 381–398.

Villaseñor, A., Ritzwoller, M.H., Levshin, A.L., Barmin, M.P., Engdahl, E.R., Spakman, W. Trampert, J., 2001. Shear velocity structure of central Eurasia from inversion of surface wave velocities, Phys. Earth planet. Int., 123, 169–184.

White, R.S., 1982. Deformation of the Makran accretionary sediment prism in the Gulf of Oman (north-west Indian Ocean), Geol. Soc., London, Special Publ., 10 (1), 357–372.

White, R.S., Louden, K. E., 1982. The Makran Continental Margin: Structure of a Thickly Sedimented Convergent Plate Boundary. Convergent Margins: Field Investigations of Margin Structure and Stratigraphy.

Yousefi, E., Friedberg, J. L., 1977. Aeromagnetic Map of Iran. Quaderangle F5., Tehran, Geological Survey of Iran.

Zamani, B., Angelier, J., Zamani, A., 2008. State of stress induced by plate convergence and stress partitioning in northeastern Iran, as indicated by focal mechanisms of earthquakes, J. Geodyn., 45, 120–132.

Acknowledgements

To whom kicked me when I was down,
and
to all who gave me hand when I was low.

Erklärung

Diese Arbeit ist, abgesehen von der Beratung durch meinen Betreuer und die Zuhilfenahme der angegebenen Mittel, nach Inhalt und Form meine eigene. Die Arbeit hat weder ganz noch zum Teil bereits an anderer Stelle im Rahmen eines Prüfungsverfahren vorgelegen. Die Arbeit ist unter Einhaltung der Regeln guter wissenschaftlicher Praxis der Deutschen Forschungsgemeinschaft enstanden.

(Ort) ---------- (Datum) ---------- (Naeim Mousavi)